Universidade de Aveiro Departamento de Química
2022

DIANA GASPAR

Análise metabolómica de neurónios privados de oxigénio-glucose como modelo de encefalopatia hipóxico-isquémica para recém-nascidos

Metabolomics screening of oxygen-glucose deprived neurons as a model of hypoxic-ischemic encephalopathy for newborns

Universidade de Aveiro Departamento de Química
2022

DIANA GASPAR

Análise metabolómica de neurónios privados de oxigénio-glucose como modelo de encefalopatia hipóxico-isquémica para recém-nascidos

Metabolomics screening of oxygen-glucose deprived neurons as a model of hypoxic-ischemic encephalopathy for newborns

Dissertação apresentada à Universidade de Aveiro para cumprimento dos requisitos necessários à obtenção do grau de Mestre em Bioquímica, Especialização em Bioquímica Clínica, realizada sob a orientação científica do Doutor Bruno José Fernandes Oliveira Manadas, Investigador Principal do Centro de Neurociências e Biologia Celular da Universidade de Coimbra e da Doutora Ana Maria Pissara Coelho Gil, Professora Associada com Agregação do Departamento de Química e membro do CICECO – Instituto de Materiais de Aveiro da Universidade de Aveiro.

Apoio do projecto do CICECO – Instituto de Materiais de Aveiro, UIDB/50011/2020 & UIDP/50011/2020, no âmbito de FCT/MEC e FEDER (PT2020).

Este trabalho foi financiado pelo Fundo Europeu de Desenvolvimento Regional (FEDER), através do COMPETE 2020 – Programa Operacional para a Competitividade e Internacionalização e fundos nacionais Portugueses através da FCT – Fundação para a Ciência e a Tecnologia, no âmbito dos projetos POCI-01-0145-FEDER-029311, POCI-01-0247-FEDER-045311, UIDB/04539/2020 e UIDP/04539/2020.

Dedico esta dissertação à minha avó Maria que mesmo estando longe, esteve sempre perto.

O júri

Presidente

Prof. Doutor Brian James Goodfellow
Professor auxiliar do Departamento de Química da Universidade de Aveiro

Vogais

Prof. Doutora Rita Maria Pinho Ferreira
Professora auxiliar do Departamento de Química da Universidade de Aveiro

Prof. Doutora Ana Maria Pissara Coelho Gil
Professora associada com agregação do Departamento de Química e membro do CICECO da Universidade de Aveiro

Agradecimentos

Em primeiro lugar, gostaria de agradecer aos meus orientadores. Ao meu orientador de estágio curricular, Doutor Bruno Manadas, pela oportunidade que me deu de fazer parte da sua equipa e de desenvolver este projeto, por todo o conhecimento transmitido, pelos conselhos, pela dedicação e pelo apoio. À minha orientadora institucional, Doutora Ana Gil, por toda a dedicação, preocupação, ajuda e apoio demonstrados.

Em segundo lugar, um agradecimento muito especial à Inês Caramelo e à Margarida Coelho, que foram as duas pessoas fundamentais nesta jornada. Sem elas não teria sido possível realizar este trabalho. Muito obrigada por tudo o que me ensinaram, pela preocupação com o meu trabalho, pela paciência, pela compreensão, pela disponibilidade, pelo carinho, pela ajuda essencial na parte prática e na análise de dados, e por me terem acompanhado ao longo de toda esta etapa. Não me esquecerei de vocês.

Gostaria também de agradecer à Vera Mendes pela ajuda na realização da aquisição de dados, pela disponibilidade e pelo carinho.

Agradeço também ao Laboratório de Biologia Celular por ter disponibilizado a sala de cultura, o que permitiu a preparação das culturas primárias de neurónios cerebrocorticais e a realização de ambos os modelos de morte neuronal.

Quero também agradecer ao grupo do professor Carlos Duarte da Universidade de Coimbra por ter cedido os córtices cerebrais usados na preparação das culturas primárias.

Um agradecimento especial à minha amiga Maria que sempre caminhou ao meu lado e sempre que eu precisei esteve lá para mim, tanto nos momentos bons e felizes, como nos momentos mais difíceis. Como se diz, “o que Aveiro uniu, ninguém separa”.

Por último, um obrigada muito especial às pessoas mais importantes da minha vida, o meu avô, a minha mãe, o meu irmão e o meu namorado, obrigada por sempre terem estado ao meu lado, por serem o meu aconchego, por me ampararem, por me ouvirem e por acreditarem em mim (às vezes mais do que eu). Obrigada do coração.

Palavras-chave

Encefalopatia Hipóxico-Isquémica, Lesão Cerebral, Privação de Oxigénio e Glucose, Espectrometria de Massa, Metabolómica, Potenciais Biomarcadores.

Resumo

A encefalopatia hipóxico-isquémica (HIE) é considerada uma das mais frequentes causas de lesão cerebral em recém-nascidos. Esta lesão resulta de um evento de asfixia que pode ocorrer antes, durante ou após o nascimento. A HIE é um episódio devastador que afeta 1 a 8 crianças por 1000 nascimentos em países desenvolvidos, sendo esta incidência maior em países subdesenvolvidos. A paralisia cerebral é uma das condições mais frequentemente associada a HIE. Atualmente, o diagnóstico de HIE é baseado em critérios clínicos que o tornam pouco preciso, lento e inacessível em várias unidades hospitalares e países. Em relação ao tratamento, a hipotermia terapêutica é considerada o padrão de tratamento para recém-nascidos com HIE, mas apresenta um janela terapêutica pequena, até 6 horas após o nascimento. Assim, é fundamental e urgente proceder à descoberta de biomarcadores para ajudar no diagnóstico de HIE. Deste modo, o objetivo deste estudo foi proceder à realização do perfil metabolómico de culturas primárias de neurónios cerebrocorticais submetidas a dois modelos de morte neuronal, um modelo celular de HIE (privação de oxigénio e glucose (OGD)) e um modelo baseado em glutamato, para identificar potenciais biomarcadores que possam vir a ser usados no diagnóstico clínico de HIE. Para tal, inicialmente, foram preparadas culturas primárias de neurónios isolados do córtex cerebral de embriões de ratos Wistar (E17-18) e ao dia *in vitro* 9, as células foram submetidas a um insulto de OGD (2 horas) e a um estímulo de glutamato (20 minutos). Após 24 horas (para o insulto de OGD) e após 6 horas (para o estímulo de glutamato), procedeu-se à extração do proteoma e do metaboloma celulares, seguida de precipitação das proteínas com metanol. Uma vez preparadas as amostras, foi realizada uma análise metabolómica por cromatografia líquida acoplada à espectrometria de massa tandem/híbrida, de modo a identificar potenciais metabolitos de interesse. Neste estudo foram realizadas duas análises: uma análise metabolómica não direcionada e uma análise metabolómica direcionada. Após processamento e análise dos dados, os metabolitos triptofano, β-NAD, FAD, e esfinganina foram identificados como sendo potenciais biomarcadores e o metabolismo dos esfingolípidos como sendo uma via metabólica possivelmente alterada. Estes resultados podem contribuir para a realização de um perfil de biomarcadores translacionais para HIE. No futuro, uma vez que os resultados foram obtidos de modelos *in vitro*, é necessário proceder à sua posterior validação no modelo animal de HIE e, de seguida, em humanos. A análise metabolómica dos secretomas permitirá inferir sobre biomarcadores circulantes.

Keywords

Hypoxic-Ischemic Encephalopathy, Brain Injury, Oxygen-Glucose Deprivation, Mass Spectrometry, Metabolomics, Potential Biomarkers.

Abstract

Hypoxic-ischemic encephalopathy (HIE) is considered one of the most frequent causes of brain injury in newborns. This injury results from an event of asphyxia that can occur before, during, or after birth. HIE is a devastating episode that affects 1 to 8 infants per 1000 live births in developed countries, and this incidence is higher in underdeveloped countries. Cerebral palsy is one of the conditions most frequently associated with HIE. Currently, the diagnosis of HIE is based on clinical criteria that make it inaccurate, slow and inaccessible in several hospital units and countries. Regarding treatment, therapeutic hypothermia is considered the standard of care for newborns with HIE, but it has a small therapeutic window, within 6 hours after birth. Thus, it is essential and urgent to proceed to the discovery of biomarkers to help in the diagnosis of HIE. In this way, the aim of this study was to perform a metabolomics profiling of primary cultures of cerebrocortical neurons submitted to two models of neuronal death, a cellular model of HIE (oxygen and glucose deprivation (OGD)) and a glutamate-based model, to identify potential biomarkers that may be used in the clinical diagnosis of HIE. For this purpose, initially, primary cultures of neurons isolated from the cerebral cortex of Wistar rat embryos (E17-18) were prepared and at day *in vitro* 9, the cells were submitted to an OGD insult (2 hours) and a glutamate stimulus (20 minutes). After 24 hours (for the OGD insult) and after 6 hours (for the glutamate stimulus), the cellular proteome and metabolome were extracted, followed by precipitation of the proteins with methanol. Once the samples were prepared, a metabolomics analysis was performed by liquid chromatography coupled to tandem/hybrid mass spectrometry, in order to identify potential metabolites of interest. In this study, two analyses were performed: an untargeted metabolomics analysis and a targeted metabolomics analysis. After data processing and analysis, the metabolites tryptophan, β-NAD, FAD, and sphinganine were identified as potential biomarkers and sphingolipid metabolism as a possible altered metabolic pathway. These results may contribute to translational biomarker profiling for HIE. In the future, since the results were obtained from *in vitro* models, it is necessary to further validate them in the animal model of HIE and then in humans. The metabolomics analysis of the secretomes will allow to infer on circulating biomarkers.

TABLE of CONTENTS

ABBREVIATIONS LIST

5-FDU – 5-Fluoro-2'-Deoxyuridine

A

ACN – Acetonitrile
Acetyl-CoA – Acetyl Coenzyme A
aEEG – Amplitude-Integrated Electroencephalogram
AIF – Apoptosis Inducing Factor / All Ion Fragmentation
AMPA – 2-(aminomethyl)phenylacetic Acid
ANOVA – Analysis of Variance
APCI – Atmospheric Pressure Chemical Ionization
API – Atmospheric Pressure Ionization
APPI – Atmospheric Pressure Photo-Ionization
Ar – Argon
ATP – Adenosine Triphosphate

C

CDP-choline – Cytidine 5-Diphosphocholine
CE – Collision Energy
CES – Collision Energy Spread
CI – Chemical Ionization
CID – Collision-Induced Dissociation
CNS – Central Nervous System
CUR – Curtain Gas

D

DC – Direct Current
DDA – Data Dependent Acquisition
DIA – Data Independent Acquisition
DIV – Day *in vitro*
DNA - Deoxyribonucleic Acid
DP – Declustering Potential

E

E – Embryonic Day
EI – Electron Ionization
EIC(s) – Extracted Ion Chromatogram(s)
EPO – Erythropoietin
ESI – Electrospray Ionization
ESI-TOF – Electrospray Ionization Time-of-Flight

F

FA – Formic Acid
FAD – Flavin Adenine Dinucleotide
FC – Fold Change
Full-scan MS – Full-scan Mass Spectra

G

g – Gravity Force
GC – Gas Chromatography
GFAP – Glial Fibrillary Acidic Protein
GS1 – Nebulizer Gas 1
GS2 – Nebulizer Gas 2

H

HBSS – Hank's Balanced Salt Solution

HEPES – 2-[4-(2-hydroxyethyl)piperazin-1-yl]ethanesulfonic Acid

HI – Hypoxia-Ischemia / Hypoxic-Ischemic

HIE – Hypoxic-Ischemic Encephalopathy

HILIC - Hydrophilic Liquid Interaction Chromatography

HPLC – High-Performance (or High-Pressure) Liquid Chromatography

I

IDA – Information-Dependent Acquisition

IL-1β – Interleukin-1β

IS – Internal Standard

K

KEGG – Kyoto Encyclopedia of Genes and Genomes

L

LC – Liquid Chromatography

LC-MS – Liquid Chromatography-Mass Spectrometry

LC-MS/MS – Liquid Chromatography coupled to Tandem/Hybrid Mass Spectrometry

LDH – Lactate Dehydrogenase

LINAC – Linear Accelerator

LOD – Limit of Detection

LOQ – Limit of Quantification

log – Logarithm

M

M – Analyte Molecule

M + Na – Sodium Adduct

MALDI - Matrix-Assisted Laser Desorption/Ionization

MAP2 – Microtubule Associated Protein 2

MCP – Microchannel Plate

MeOH – Methanol

miRNAs – MicroRNAs

MR – Magnetic Resonance

MRI – Magnetic Resonance Imaging

MRM – Multiple-Reaction Monitoring

mRNA – Messenger Ribonucleic Acid

MRS – Magnetic Resonance Spectroscopy

MS – Mass Spectrometry

MSCs – Mesenchymal Stem Cells

MS/MS – Tandem/Hybrid Mass Spectrometry / Fragmentation Spectra

m/z – Mass-to-Charge Ratio

$[M + H]^+$ – Protonated Molecule

$[M - H]^-$ – Deprotonated Molecule

N

n - Biological Replicates

N/A – Not Applicable

NAA – *N*-acetyl Aspartate

NAC – *N*-acetylcysteine

NAD/NAD(H) – Nicotinamide Adenine Dinucleotide
NCDase – Neutral Ceramidase
NDD – Neurodevelopmental Delay
NGF – Nerve Growth Factor
NICU – Neonatal Intensive Care Units
NMDA – *N*-methyl-D-aspartate
NMR – Nuclear Magnetic Resonance
NO – Nitric Oxide
NOS – Nitric Oxide Synthase

O

OGD – Oxygen and Glucose Deprivation

P

***p* –** *p*-value
PARP1 – Poly (ADP-Ribose) Polymerase 1
PBS – Phosphate-Buffered Saline
PCA – Principal Component Analysis
PCs – Principal Components
PDL – Poly-D-Lysine
PLS-DA – Partial Least Squares-Discriminant Analysis

Q

q2 – Collision Cell
Q – Quadrupole
Q1 – First Quadrupole
Q3 – Third Quadrupole
QqQ – Triple Quadrupole
QTOF – Quadrupole Time-of-Flight

R

RF – Radio Frequency
RNA – Ribonucleic Acid
ROS – Reactive Oxygen Species
rRNA – Ribosomal Ribonucleic Acid
RT – Retention Time

S

S1P – Sphingosine 1-Phosphate
S100B – S100 Calcium-Binding Protein B
SB – Sample Buffer
Sham – OGD Control
SIRT1 – Sirtuin 1
SM1 – STEMCELL Modified-1
S/N – Signal-to-Noise Ratio
SOD – Superoxide Dismutase
SphK2 – Sphingosine Kinase 2
SRM – Selected-Reaction Monitoring
SWATH-MS – Sequential Window Acquisition of all Theoretical Mass Spectra

T

TBI – Traumatic Brain Injury
TC – Tissue Culture
TDC – Time-to-Digital Converter
TEM – Temperature
TNF-α – Tumor Necrosis Factor Alpha
TOF – Time-of-Flight
tRNA – Ribonucleic Acid Transporter

U

UCHL1 – Ubiquitin C-terminal Hydrolase L1

UC-MSCs – Umbilical Cord-Mesenchymal Stem Cells

UCPs – Uncoupling Proteins

V

VIP – Variable Importance in Projection

vs – Versus

X

XIC(s) – Extracted Ion Chromatogram(s)

SYMBOLS LIST

D

Da – Dalton

E

eV – Electron-Volt

K

kV – Kilovolt

L

L/l – Liter

M

ms – Millisecond

P

ppm – Parts Per Million
psi – Pound Force per Square Inch

R

rpm – Rotations Per Minute

S

s – Second

V

V – Volt

Chapter 1
Introduction

1. INTRODUCTION

1.1. Hypoxic-Ischemic Encephalopathy

Hypoxic-ischemic encephalopathy (HIE) is a disease associated to complex physiological, cellular, and molecular changes resulting from a severe anoxic brain insult during the neonatal period [1-3]. It is estimated that worldwide, approximately 0.7 million newborns die each year, and 1.15 million develop sequelae due to HIE [4]. The HIE incidence ranges from 1 to 8 infants per 1000 live births in developed countries and is as high as 26 infants per 1000 live births in underdeveloped countries [5]. Hypoxic-ischemic encephalopathy can cause premature mortality, since about 24% of these patients usually die in neonatal intensive care units (NICU) [6], or a variety of life-long morbidities/disabilities, including acute symptoms such as seizures, alteration of consciousness, weak breathing, poor muscle tone or metabolic derangement, visual and auditory problems (about 40%), chronic conditions such as cerebral palsy (about 10-20%), epilepsy, intellectual disability, and behavioral disorders [1,7,8]. Therefore, it is critical to develop an accurate and fast diagnosis as well as therapeutic strategies to improve the quality of life in newborns suffering from HIE [9].

1.1.1. HIE Etiology – Perinatal Asphyxia

The most frequent cause of HIE is perinatal asphyxia. Asphyxia of the umbilical cord, through the suppression of blood circulation, leads to a deprivation of oxygen and nutrients in the brain, triggering a cascade of biochemical events that result in brain injury. [10] In preterm infants, the main brain injury patterns includes periventricular white matter injury, while in term infants includes basal ganglia and thalamus lesions [11-13].

The adequate cerebral blood flow assures oxygen and glucose needs in the fetal brain. A variety of conditions can interrupte the umbilical cord blood flow, such as placental abruption, uterine rupture, and prolapse or occlusion of the umbilical cord [14]. The impaired cerebral blood flow causes responses at the systemic and cellular level. At the systemic level, asphyxia causes a redistribution of the cardiac output to preserve the perfusion of the Central Nervous System (CNS), heart, and other vital organs. However, if the hypoxia-ischemia (HI) is too prolonged, these organs also suffer from hypoperfusion. At the cellular level,

specifically in the brain, due to its high demands of energy, the lack of oxygen and glucose initiates a cascade of events that may lead to cell dysfunction and death. [10,15,16]

1.1.2. HIE Pathophysiology

Hypoxic-ischemic encephalopathy pathophysiology results from the brain injury caused by HI and could last for weeks [10]. Hypoxia-ischemia develops acutely or chronically during the perinatal period and the duration of the insult and the timing of medical intervention play important roles [6,17].

The decrease in cerebral blood flow due to HI insult reduces the delivery of oxygen and glucose to the brain starting a cascade of events. First, the first energy failure determines the acute phase. After reperfusion, the blood flow and the cerebral energy metabolism are restored, and there is a partial recovery during the first 30 to 60 minutes after the insult. Although there may be neuronal death in the primary phase, many neurons are able to recover, at least partially. [18-20] This event is then followed by the latent phase, which may last from 1 to 6 hours and is characterized by events of oxidative stress, inflammation, excitotoxicity, and activation of apoptotic cascades [18,21]. Next, the secondary phase (delayed neuronal death) lasts for approximately 6 to 15/24 hours after the HI injury. The secondary phase is characterized by seizures, cytotoxic edema (cell swelling), excitotoxicity, impaired cerebral oxidative balance, and secondary energy failure with a nearly complete failure of mitochondrial activity, leading to cell death. [21-23] Finally, the tertiary phase can last for months after the acute insult and involves late cell death, repair and remodeling of the injured brain, and astrogliosis (**Figure 1**) [24].

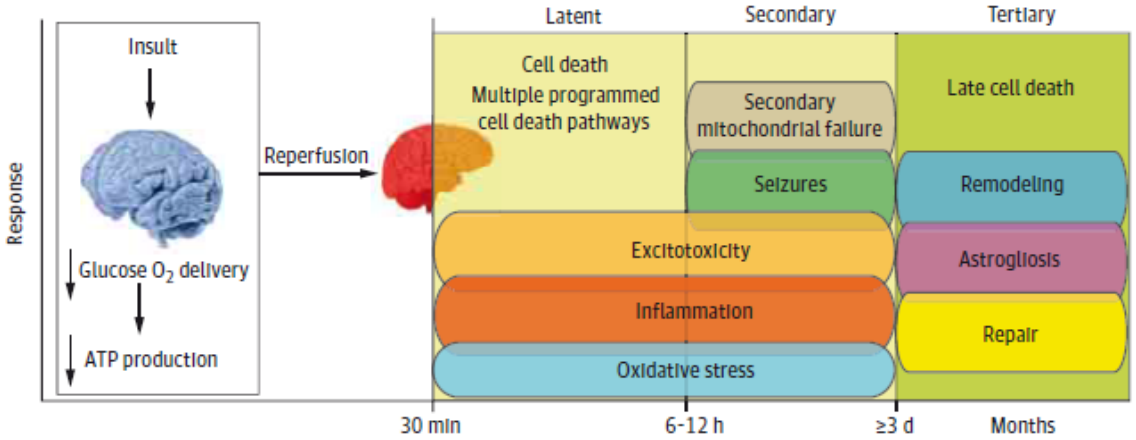

Figure 1. Schematic overview of the pathophysiological features of hypoxic-ischemic encephalopathy. The hypoxic-ischemic insult causes decreased delivery of oxygen (O_2) and glucose to the brain, resulting in decreased production of adenosine triphosphate (ATP). In the primary phase (30-60 minutes), partial neuronal recovery occurs after reperfusion. Excitotoxicity, inflammation and oxidative stress continue during the latent (1-6 hours) and secondary (6-15/24 hours) phases. However, seizures and failure of mitochondrial activity occur only in the secondary phase. The tertiary phase (months) is characterized by late cell death, remodeling, astrogliosis, and repair. From Douglas-Escobar & Weiss, 2015 [17].

The pathophysiology of HIE encompasses the interconnection of five processes, namely, excitotoxicity, intracellular calcium (Ca^{2+}) accumulation, oxidative stress, mitochondrial dysfunction, and inflammation [25]. Initially, the primary energy failure initiates a cascade of biochemical events that can end in brain injury [16]. First, there is a decrease in adenosine triphosphate (ATP) production, which results in a switch to anaerobic glycolysis in the intracellular metabolism, and consequently, in an increase in intracellular lactate levels. The increased lactate levels in cytosol leads to lactic acidosis in the cells. [26] Another consequence of the depletion in ATP production is the failure of the ATP-dependent pumps, such as the sodium (Na^+) and potassium (K^+) pumps (Na^+/K^+ ATPase), which causes an imbalance of the cellular homeostasis due to the incapacity to maintain the ionic gradients. The failure of ATP-dependent pumps results in the intracellular accumulation of Na^+, chloride (Cl^-) and water, causing cell swelling/lysis (known as cytotoxic edema). The events mentioned above lead to depolarization of the neuron membranes with the production of multiple nervous impulses, which results in an excessive release of the excitatory neurotransmitter glutamate into the synaptic cleft, with consequent accumulation. The excessive extracellular glutamate is also due to the decreased activity of the ATP-dependent pumps present in astrocytes (glial cells), since these pumps help keep glutamate levels low

in the synaptic cleft. [26,27] Membrane depolarization and high levels of glutamate in the extracellular space cause over-stimulation of the extracellular glutamate ionotropic receptors (*N*-methyl-D-aspartate (NMDA) and 2-(aminomethyl)phenylacetic acid (AMPA)) located in the postsynaptic neuron, triggering the excitotoxic cascade. The opening of the glutamate receptor channels and other voltage-dependent Ca^{2+} channels allows the influx of Ca^{2+} into the neurons, increasing Ca^{2+} levels in the cytosol. [26,28] High intracellular Ca^{2+} levels activate nitric oxide synthase (NOS) enzyme and Ca^{2+}-dependent enzymes, such as phospholipases, proteases, and nucleases. The activation of NOS results in the production of reactive oxygen species (ROS), such as nitric oxide (NO) and NO free radicals, while the activation of Ca^{2+}-dependent enzymes causes oxidative modifications in lipids and proteins, and deoxyribonucleic acid (DNA) degradation. [29-31] Nitric oxide has multiple adverse neuronal effects, since it increases the expression of apoptotic proteins and by reacting with superoxide gives raise to peroxynitrite, a toxic free radical [32,33].

Under HI conditions, there is an excessive accumulation of ROS, mainly in the mitochondria, leading to mitochondrial energy failure [26,34,35]. Consequently, the decreased ATP production, results in a failure of the ATP-dependent pumps with consequent depolarization of the neuronal membranes, as previously decribed, creating a vicious cycle [28]. Regarding mitochondria dysfunction, the alteration of its outer membrane permeability is triggered by excitatory amino acids (glutamate), intracellular Ca^{2+}, ROS (NO), inflammation, and increase of pro-apoptotic proteins, which allows the release of apoptotic factors, which can activate intrinsic apoptotic pathways, like caspase-dependent pathways [15,36].

In the immature brain, the HI insult triggers an inflammatory response. Microglia, astrocytes, and neutrophils are types of cells present in the CNS that mediate inflammation. There are two different types of microglial cells phenotypes, M1 phenotype (secretes pro-inflammatory cytokines) and M2 phenotype (secretes predominantly anti-inflammatory cytokines). Also, activated microglia promote phagocytosis, which contributes to the restoration of tissue homeostasis, since it helps to eliminate necrotic cells and cellular debris. [37] Regarding astrocytes, they can play opposite functions in HI: on one hand, they release superoxide dismutase (SOD) and glutathione (important for antioxidant defense) and enhance extra-synaptic glutamate uptake [38,39]; on the other hand, they release pro-inflammatory cytokines that increase NO levels and induce neuronal death by apoptosis [40].

The mechanisms previously described are schematized on **Figure 2**.

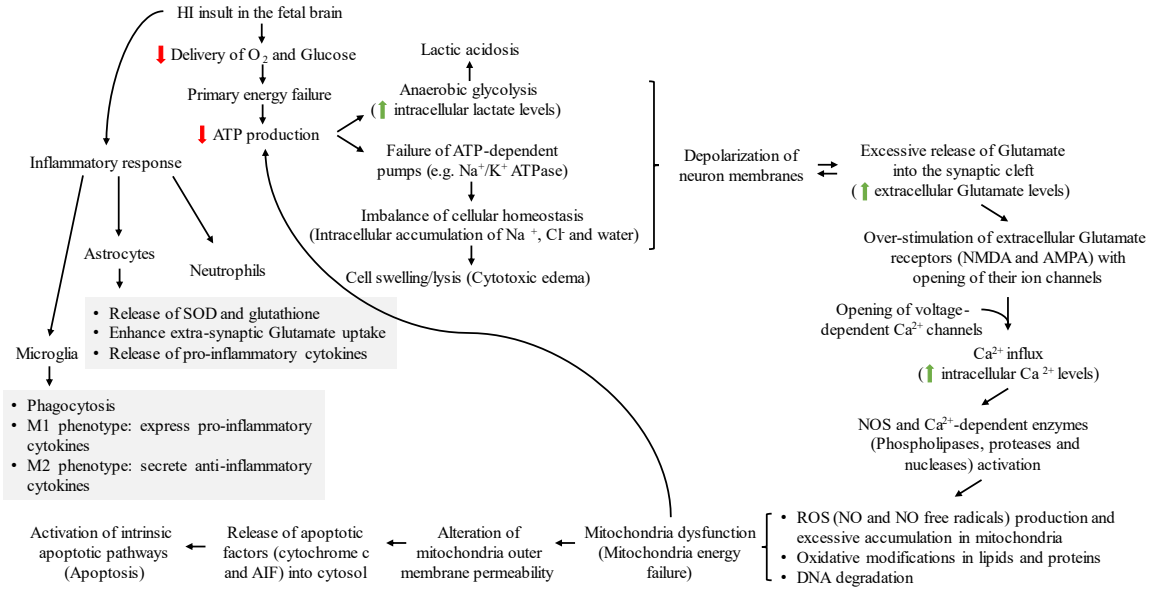

Figure 2. Pathophysiology of hypoxic-ischemic encephalopathy. After HI insult in the brain, an energy failure occurs because of the decreased delivery of oxygen (O_2) and glucose, with consequent decreased production of adenosine triphosphate (ATP). The ATP depletion results in an increase of the intracellular lactate levels due to the anaerobic glycolysis and in an imbalance of the cellular homeostasis due to the failure of the ATP-dependent pumps, which can cause cell swelling and/or lysis. Increased levels of lactate, electrolytes, and water inside neurons lead to the depolarization of their membranes, triggering the excessive release of glutamate into the synaptic cleft, with consequent over-stimulation of its receptors. The accumulation of glutamate in the extracellular space also leads to the depolarization of neuron membranes. The opening of glutamate receptors ion channels and calcium (Ca^{2+})-dependent channels allows calcium to flow inside neurons, activating nitric oxide synthase (NOS) and calcium-dependent enzymes. These enzymes lead to reactive oxygen species (ROS) production, lipid and protein oxidation, and deoxyribonucleic acid (DNA) degradation, resulting in mitochondrial dysfunction and energy failure. This energy (ATP) failure triggers a new cycle. The mitochondria dysfunction includes the alteration of its outer membrane permeability, which leads to the release of apoptotic factors in the cytosol and, consequently, to the activation of apoptotic pathways. In the inflammatory response triggered by HI insult, microglia cells develop phagocytosis and release pro- and anti-inflammatory cytokines, phenotype M1 and M2, respectively, while astrocytes release superoxide dismutase (SOD), glutathione and only pro-inflammatory cytokines, and help in glutamate uptake. Neutrophils contribute to ROS production. Na^+: sodium; K^+: potassium; Cl^-: chloride; NMDA: *N*-methyl-D-aspartate; AMPA: 2-(aminomethyl)phenylacetic acid; NO: nitric oxide; AIF: apoptosis inducing factor.

1.1.3. Current Diagnostic Methods

Nowadays, there is still no accurate, fast and accessible methodology for all countries and/or in hospital units to diagnose HIE. The initial diagnosis of HIE is based on the presence of neurological dysfunction, often accompanied by difficulty in initiating and maintaining respiration, abnormality of muscle tone and power, and seizures [41]. Currently, the HIE diagnosis criteria of the American Academy of Pediatrics are: (1) Apgar score of less than 5 at 5 and 10 minutes; (2) fetal umbilical artery acidemia (fetal umbilical artery pH less than 7.0, or base deficit greater than or equal to 12 mmol/L, or both); (3) presence of multisystem organ failure; and (4) neuroimaging evidence of acute brain injury seen on brain magnetic resonance imaging (MRI) and/or magnetic resonance spectroscopy (MRS) [42]. The more criteria matched, the more likely a HI event has occurred.

The Apgar score is a rapid qualitative method performed on newborns immediately after birth to assess the newborn health or the need for further diagnosis [43]. The Apgar score includes 5 components: color (appearance), heart rate (pulse), reflexes (grimace), muscle tone (activity), and respiration. To each of these components is assigned a sore of 0, 1, or 2. The score is reported at 1 and 5 minutes after birth for all infants and at 5-minute intervals up to 20 minutes for infants with a score less than 7. An Apgar score between 7 and 10 at 5 minutes is considered reassuring, while a score between 0 and 3 is considered low in the term infant and late-preterm infant. [44]

Multisystem organ failure can comprise renal, hepatic, and gastrointestinal injuries, hematologic abnormalities, cardiac dysfunction, metabolic derangements, or a combination of these [42].

Despite not all hospital units have access to a MRI facility, this technique provides insightful information about the pathophysiological state of the newborn. Magnetic resonance imaging is a non-invasive technique that uses strong magnetic fields and radio waves to produce highly detailed images of the anatomy and function of the body. [45] When performed between the first and fourth days of life provides information about the progression of brain injury, while a MRI obtained at 10 days of life provides information about the full extent of the injury [42].

Recently, innovative approaches are emerging as complementary diagnostic tools, such as MRS. Magnetic resonance spectroscopy is performed on the same machine as MRI and measures the concentrations of selected metabolites present in the brain, including

creatine, glutamate, *N*-acetyl aspartate (NAA), and lactate [46]. Lactate is a marker of the anaerobic metabolism, which may be seen in cases of acute HI insults or in metabolic disorders, so after an HI insult, the magnetic resonance (MR) spectrum may show a lactate peak or low NAA (indicating loss of neuronal integrity) [47,48]. Elevated and prolonged lactate levels are due to the persistent abnormality of the brain's energy metabolism during HIE [49].

The Sarnat and Sarnat classification (**Table 1**), which evaluates the level of consciousness, neuromuscular control, complex reflexes, autonomic function, seizures, and electroencephalogram findings, classifies HIE into three stages (mild, moderate and severe), according to its clinical features [50].

Table 1. Clinical features of the three stages of hypoxic-ischemic encephalopathy according to Sarnat and Sarnat. From Sarnat & Sarnat, 1976 [50].

	Stage 1 (Mild)	**Stage 2 (Moderate)**	**Stage 3 (Severe)**
Level of consciousness	Hyperalert	Lethargic or obtunded	Stupor or coma
Neuromuscular control			
Muscle tone	Normal	Mild hypotonia	Flaccid
Posture	Mild distal flexion	Strong distal flexion	Intermittent decerebration
Stretch reflexes	Overactive	Overactive	Decreased or absent
Myoclonus	Present	Present	Absent
Complex reflexes			
Suck	Weak	Weak or absent	Absent
Moro	Strong	Weak	Absent
Oculovestibular	Normal	Overactive	Weak or absent
Tonic neck	Slight	Strong	Absent
Autonomic function			
Pupils	Mydriasis	Miosis	Variable
Heart rate	Tachycardia	Bradycardia	Variable
Bronchial and salivary secretions	Sparse	Profuse	Variable
Gastrointestinal motility	Normal or decreased	Increased (diarrhea)	Variable
Seizures	None	Common	Uncommon
Electroencephalogram	Normal	Early: low voltage Later: periodic	Early: periodic Later: isoelectric

Seizure activity can be assessed by an amplitude-integrated electroencephalogram (aEEG) for at least 20 minutes, and it can be useful to complement diagnostic and help during therapeutic choices [51,52].

Furthermore, several molecular biomarkers for HIE are being investigated as potential diagnostic biomarkers. S100 calcium-binding protein B (S100B) is a cytosolic protein synthesized and released by astrocytes after an astroglial injury, which was described to be elevated at 6 hours after delivery on moderate and severe HIE newborns [49,53]. Glial fibrillary acidic protein (GFAP) is an intermediate filament protein that supports the cytoskeleton of the astroglial cells. Term infants with HIE and abnormal brain MRI scans at 1 week of life, have shown elevated serum GFAP levels at the time of birth and during the first week of life. [49,54] Ubiquitin C-terminal hydrolase L1 (UCHL1) is an important protein present in the neuronal cytoplasm and was described to be elevated in the umbilical cord blood from newborns with HIE [55]. Interestingly, microRNAs (miRNAs) have also been identified as potential diagnostic biomarkers. It has been shown that the miR-374a levels are downregulated in the umbilical cord blood of HIE newborns [56].

The metabolic state of asphyxiated newborns has also been investigated. During anaerobic metabolism, lactate is produced by reduction of pyruvate (reaction catalyzed by the enzyme lactate dehydrogenase (LDH)). Although most infants with HIE have high serum lactate levels, the degree of lactic acidosis does not accurately predict the severity of the grade of the subsequent encephalopathy. [49] However, a recent study describes salivary and serum LDH as a promising early diagnostic biomarker of HIE among newborns with perinatal asphyxia, since it was higher in the HIE group when compared with the control group [57]. Together, the data shown reinforce the need to identify new biomarkers for HIE.

1.1.4. Treatments – Therapeutic Hypothermia Applied in the Clinic and Neuroprotective Agents in Development

1.1.4.1. Therapeutic Hypothermia

Therapeutic hypothermia is the standard of care for infants with moderate-to-severe encephalopathy. It is important to act before the secondary phase, during the therapeutic window, to decrease neuronal death extension. [58] The latent phase is considered the therapeutic window for neuroprotective intervention [59]. Only infants born at or beyond 36 weeks of gestation and who meet the aforementioned criteria for the diagnosis of HIE within 6 hours after birth can be considered to hypothermia [42,51]. Thus, it is very important that infants are diagnosed correctly and in a timely manner.

Two methods of cooling have been used in the treatment of infants with HIE: selective head cooling and whole-body cooling. The selective head cooling can be achieved with cooling caps placed around the infant's head, while the whole-body cooling can be achieved with passive cooling, cool packs and/or cooling blankets. In the selective head cooling is used a servo-controlled radiant heater to maintain the rectal temperature at 34 °C ± 0.5 °C, and in the whole-body cooling the rectal temperature is maintained at 33.5 °C ± 0.5 °C. [60] Temperatures below 32 °C show a smaller neuroprotective effect and temperatures below 30 °C can cause severe systemic adverse effects and increased mortality [61]. Therapeutic hypothermia should last for 72 hours [62] and recent studies suggest a greater neuroprotection in newborns who were submitted to the whole-body cooling method [52].

The neuroprotective effect of therapeutic hypothermia involves the modulation of some irreversible injury mechanisms, such as inhibition of the inflammatory cascade, reduced production of ROS, reduction in the metabolic rate by the reduction of oxygen consumption and carbon dioxide production, decelarating brain damage [18,63,64]. However, in cases of severe HIE, this neuroprotective action is less effective, since the latent phase (the therapeutic window) presents a greater energy failure, with consequent rapid neuronal death by necrosis [65]. Currently, hypothermia is the only therapy to be applied to infants diagnosed with HIE, and it is known to effectively decrease mortality or moderate-to-severe neurodevelopmental delay (NDD) at 18 to 24 months and to increase survival without NDD [66-69].

1.1.4.2. Neuroprotective Agents in Development

Nowadays, a series of ongoing clinical trials are trying to identify potential new treatments to be applied in HIE. In the last years, different potential neuroprotective agents have been studied to prevent the cascade of injurious effects that occurs after HI. Examples of these potential neuroprotective agents are erythropoietin (EPO) [70,71], melatonin [72], allopurinol [73,74], *N*-acetylcysteine (NAC) [75], magnesium sulfate ($MgSO_4$) [76], and stem cells. They act in the different stages of the disease and may be very promising as adjuvant therapies for hypothermia in the treatment of HIE.

Erythropoietin is a glycoprotein that has recognized neuroprotective effects in the CNS, which can be early and late beneficial effects. Early benefits include anti-apoptotic [77], anti-inflammatory [78], neurotrophic [79], and antioxidant [80] effects, whereas later effects (long-

term effects) include increased neurogenesis, angiogenesis [81] and oligodendrogenesis [82]. The acute effects may promote improved cell survival and the long-term effects may promote brain repair [83].

The neuroprotective property of melatonin and allopurinol relies mainly on their antioxidant action against oxidative stress resulting from a HI event. Melatonin acts as a scavenger of ROS, is able to up-regulate the expression of antioxidant enzymes, such as glutathione peroxidase and SOD, stimulates gene expression, and improves mitochondrial efficiency and integrity [84,85], while allopurinol has the ability to inhibit the enzyme xanthine oxidase, which is responsible for the reaction that converts hypoxanthine into xanthine and then uric acid, during reperfusion [86]. *N*-acetylcysteine also exhibits a neuroprotective antioxidant effect, since it also scavenges ROS, restores glutathione levels and reduces NO production [87].

Finally, $MgSO_4$ decreases the flow of Ca^{2+} into the cells due to its ability to inhibit NMDA glutamate receptors, which prevents the pathophysiological mechanisms associated with brain injury caused by intracellular Ca^{2+} accumulation from being triggered [88], and reduces the risk of cerebral palsy [89].

1.1.4.2.1. Mesenchymal Stem Cells

The therapeutic application of stem cells has been investigated as a promising option for neuroprotective treatment in newborns with HIE. Stem cell therapy is thought to modulate inflammation, apoptosis, and oxidative stress and enhance regeneration, immune regulation, and anti-inflammatory effect [90].

Stem cells are cells with the capacity to auto-renew and to differentiate into many different lineages of specialized cells that make up the human body's tissues and organs [91]. Mesenchymal stem cells (MSCs) can be isolated from biological tissues, such as umbilical cord and placenta, and they have been proved to have potential utility in reducing the inflammatory and apoptotic processes resulting from brain injury, since they have a strong immunomodulatory effect that protects against neuroinflammatory cascades triggered by HIE [92-95]. One of the advantages of MSCs is their capability to proliferate *in vitro*, since the number of MSCs obtained after isolation from biological sources is scarce, but an elevated number of MSCs is often required in clinical settings [96]. The trophic function of MSCs could

be attributed to the production of growth factors, chemokines, interleukins, and extracellular matrix molecules [97-100].

Nowadays, there are studies investigating the safety and efficacy of stem cell therapy, namely MSCs therapy, as a potential treatment for HIE. One study evaluated the capacity of umbilical cord-derived mesenchymal stem cells (UC-MSCs) to help in the recovery of injured neurons using an *in vitro* model and an *in vivo* model of HIE [101]. This study demonstrated that: UC-MSCs are able to inhibit the apopototic death in injured neurons *in vitro*; intraventricular administration of UC-MSCs decreases lesion volume; and, UC-MSCs inhibit the secretion of inflammatory factors, such as tumor necrosis factor alpha (TNF-α) and interleukin-1β (IL-1β). Another study performed using allogeneic umbilical cord tissue-derived MSCs showed that the infusion of these cells is safe in newborns with HIE treated with hypothermia [102]. Both studies have been shown to be safe and effective based on neurological and functional exams, electroencephalographies, and MRI [103,104].

1.1.5. HIE Models

To study HIE pathophysiology and to test innovative neuroprotective therapeutic strategies, the most used experimental models are the oxygen and glucose deprivation (OGD) cellular model and the modified Vannucci rat animal model.

1.1.5.1. Oxygen and Glucose Deprivation Cellular Model

The OGD cellular model is the most practiced *in vitro* cellular model of HIE in immature animals, where brain slices (hippocampal [105] or forebrain slices [106]) and neuronal cultures can be used [107]. In this model, in order to mimic the HI insult, the brain slices or the neuronal cultures are incubated in a glucose-free deoxygenated buffer medium (OGD medium), inside an anaerobic chamber (OGD chamber) at 37 °C [108-110].

Many studies have been developed in primary cultures of hippocampal neurons using the OGD cellular model [108,110]. However, in this project, the *in vitro* cellular model of OGD is applied to primary cultures of cerebrocortical neurons from Wistar rat embryos.

1.1.5.2. Modified Vannucci Rat Animal Model

The modified Vannucci rat model was introduced by Vannucci's group, in 1981, to study the HI brain damage in the immature rats. This model is based on that described by Levine in the adult rats, in 1960, and consists of unilateral occlusion of the common carotid

artery (ischemia), after anesthesia, in 7-day-old rats, followed by systemic hypoxia produced by the inhalation of 8% of oxygen (O_2) for 3.5 hours. [7,111-113] These hypoxic conditions were selected as they demonstrated low mortality and capacity to survive at least 48 hours, following the hypoxic period, allowing assessment during recovery of reflex and behavioral status and recognition of microscopic brain damage, if present [112]. This model uses 7-day-old rats, since at this age the animal's brain development is similar to that of a human fetus with 32-34 weeks of gestation or to that of a newborn with complete cerebrocortical neuronal layer and poor myelination of the white matter) [7]. The HI brain injury is limited to the cerebral hemisphere ipsilateral to the common carotid artery occlusion and is mainly observed in cerebral cortex, subcortical and periventricular white matter, striatum (basal ganglia), and hippocampus [113].

1.2. Mass Spectrometry – The Mass Spectrometer, its Components, and Some Definitions

Mass spectrometry (MS) is defined as the measurement of the molecular masses and fragment masses obtained from distinct chemical species [114]. A mass spectrometer is an analytical instrument that produces a beam of gas phase ions from analytes in samples, then separates the ions according to their mass-to-charge ratios (*m/z*) by applying electrical and/or magnetic fields, and provides analog or digital output signals, called peaks, from which the *m/z* and the intensity (abundance) of each detected ion may be determined [115].

The main components of a mass spectrometer are sample introduction system, ionization source, mass analyzer, ion detector, vacuum system, and computers. At the ionization source, the analytes are vaporized and ions are produced. Next, in the mass analyzer, these ions are separated according to their *m/z* and the signal intensities of each *m/z* value are determined in the ion detector. The vacuum system prevents the loss of ions through collisions with neutral gas molecules and with the walls of the mass analyzer and the detector. Finally, the computers are necessary to record and process the data produced. [115,116]

An example of a mass spectrometer is the TripleTOF 6600 system from AB Sciex, represented in **Figure 3**.

Figure 3. TripleTOF 6600 system from AB Sciex [117].

The TripleTOF 6600 system consists of five components, namely, DuoSpray Turbo V Source (**Figure 4.A**), QJet Ion Guide, High frequency LINAC (Linear Accelerator) Collision Cell, Accelerator TOF (Time-of-flight) Analyzer, and Detection system, which are schematized in **Figures 4.B** and **C** [117,118]. The DuoSpray Turbo V Source combines two ionization methods, electrospray ionization (ESI) and atmospheric pressure chemical ionization (APCI) in a single source [119]. In this project, ESI will be used, since this ionization method is most commonly used for the analysis of polar compounds and it is suitable for a wide range of compounds (from small to large molecules), while APCI is more commonly used for less polar compounds [115].

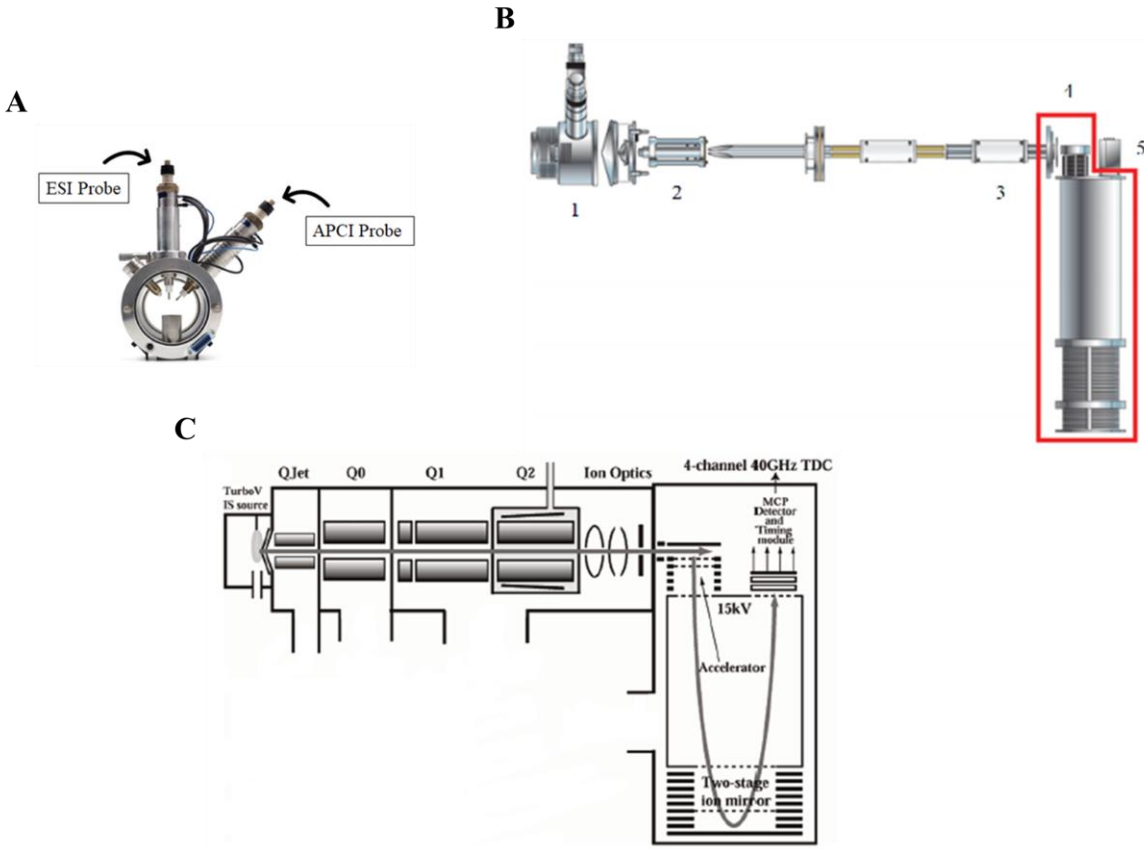

Figure 4. The TripleTOF 6600 system. (A) DuoSpray Turbo V Source [119]. (B) Representation of the instrument platform [117]. (1) DuoSpray Turbo V Source; (2) QJet Ion Guide; (3) High frequency LINAC Collision Cell; (4) Accelerator TOF Analyzer; (5) Detection system. (C) Schematic diagram of the components [118]. ESI: electrospray ionization; APCI: atmospheric pressure chemical ionization; Q: quadrupole; TDC: time-to-digital converter; MCP: microchannel plate.

As mentioned before, gas phase ions of analytes present in samples are produced in the ionization source. Ions are atoms, molecules, or fragments of molecules with one or more positive or negative electrical charges. There are different methods to create ions that can be classified as hard and soft. Hard ionization generates more energy than that required for the formation of the molecular ions, and the excess of energy causes the dissociation of bonds within the analyte molecules. This dissociation promotes extensive fragmentation of the molecules. On the other hand, soft ionization, such as electrospray ionization, does not lead to fragmentation of the analyte molecules. [115]

The *m/z* of an ion corresponds to the ratio between the mass (*m*) of the ion and the number of electrical charges (*z*) that the sample acquires upon ionization. The unit of mass

used in mass spectrometry is dalton (Da). A single electrical charge is the electromagnetic force associated with a proton (+1) or an electron (–1). [115]

The mass spectrum is a two-dimensional representation of the distribution and intensity (abundance) of the ions introduced into the mass analyzer, according to their *m/z* values (**Figure 5**) [115]. A mass spectrum has four basic elements: molecular ion, base peak, fragment ions, and isotope peaks. The molecular ion ($[M]^{+\bullet}$) or a related species, such as the protonated or desprotonated molecule, are represented by the peak with the highest *m/z* value, while the base peak corresponds to the most intense peak in the spectrum. Fragment ions can correspond to different *m/z* values that are always lower than the *m/z* value corresponding to the molecular ion. Isotope peaks are presented if the analyte includes elements with isotopic forms. [115]

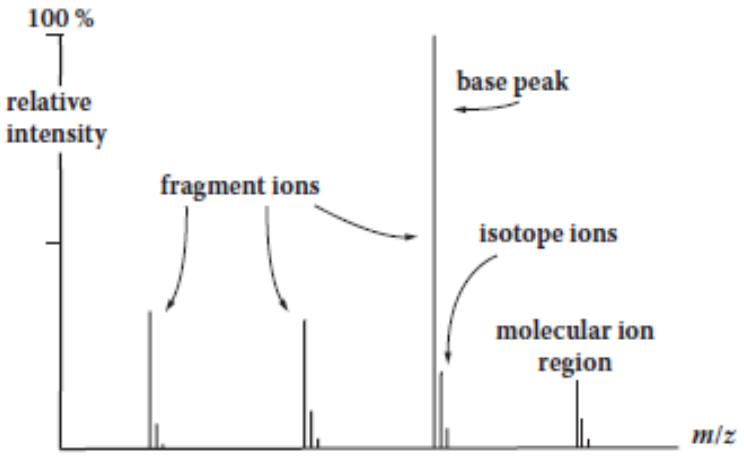

Figure 5. Mass spectrum, where the *y*-axis represents the intensity (abundance) of the ions, and the *x*-axis represents the mass-to-charge ratio (*m/z*), and its elements. From Greaves & Roboz, 2014 [115].

1.2.1. Sample Introduction System of a Mass Spectrometer – Liquid Chromatography

The interface between liquid chromatography (LC) and MS was fundamental to the expansion of MS into biological applications. The analysis of biological samples by MS can include the separation of the sample components by gas chromatography (GC) or LC followed by their introduction into the ionization source [115]. Before the development of the ESI ionization method, a limiting factor for MS was that samples had to be in the vapor phase to be analyzed. Since the vaporization of an analyte depends on its molecular mass and polarity, small polar molecules (< 1 kDa) when heated are decomposed before entering

the vapor phase. In order to allow the analysis of polar compounds by MS, a process called chemical derivatization was used. Chemical derivatization allows the polarity to decrease and thus the volatility of the analytes to increase. The development of ESI facilitated the coupling of LC with MS, becoming a key technique for the profiling and analysis of metabolites in complex biological samples, since in ESI the vapor formation and ionization occur simultaneously preventing sample decomposition. [115,120] A high-performance (or high-pressure) liquid chromatography (HPLC) system is an example of a sample introduction system of a mass spectrometer and forms the combined technique known as liquid chromatography-mass spectrometry (LC-MS). Liquid chromatography-mass spectrometry is an analytical technique that combines the physical separation capabilities of HPLC with the mass analysis capabilities of MS. [114] High-performance liquid chromatography is a chromatographic technique used to separate, identify and quantify components of a mixture. First, the sample to be analyzed is introduced into a stream of mobile phase and then, the analyte molecules present in the mobile phase move along the column and are retarded (adsorbed) by chemical or physical interactions with the stationary phase. The amount of retardation and the sequential release of analyte molecules into the mobile phase depend on the nature of the analyte, stationary phase, and mobile phase composition and gradient. The retention time (RT) corresponds to the time that a specific analyte takes to pass through the column . [114,121]

The polarity of biological compounds led to the development of reversed-phase LC. In this type of chromatography, the polarities of the stationary and mobile phases are opposite to each other. In reversed-phase LC, the stationary phase is non-polar (hydrophobic) in contrast to what happens in normal-phase chromatography (where the stationary phase is polar), while the mobile phase is polar (aqueous). The most common stationary phase used for the analysis of molecules of less than 5 kDa is the C_{18} hydrocarbon chain. On the other hand, hydrophilic liquid interaction chromatography (HILIC) can be used to analyze the very polar compounds that are not retained on C_{18} columns. [115,122]

In reversed-phase LC, the hydrophobic or less polar molecules present in the polar mobile phase will adsorb preferentially to the hydrophobic stationary phase, and the hydrophilic or more polar molecules in the mobile phase will pass through the column. The compounds are eluted, successively, using an elution gradient in which the mobile phase composition is progressively altered, from a polar (such as water) to a non-polar (such as

acetonitrile (ACN)) solvent, thus compounds elute in order of their polarity (the most hydrophilic compounds are eluted first, and the least hydrophilic and the hydrophobic compounds are eluted last). [115,122]

1.2.2. Ionization Sources – Electrospray Ionization

In the ionization sources, the analyte molecules are vaporized and ionized and then, the ions obtained are transferred into the mass analyzer [115]. The amount of energy added to the analyte molecule during the ionization process and its structure determine what happens to the ions formed, whether they remain intact or fragment. Electron ionization is considered the most energetic ionization method, since it is the method that delivers the greatest amount of energy to the analyte, and therefore the most likely to cause fragmentation. On the other hand, ESI is classified as a soft ionization method, since it is the least energetic ionization method, that is, in ESI the amount of energy added to the analyte is less and insufficient to cause the fragmentation. [115]

The choice of the ionization method is often related to the polarity of the analytes, as depicted in **Figure 6**. Eletrospray ionization is considered the main ionization method for polar compounds, from small molecules to biopolymers, and imparts little energy to the ions formed. [115]

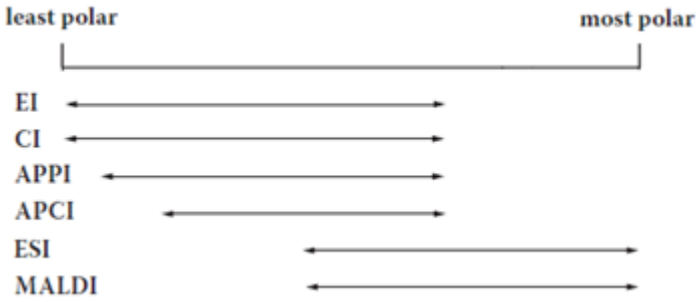

Figure 6. Relationship between the ionization method to be chosen and the polarity of the analytes to be studied. EI: electron ionization; CI: chemical ionization; APPI: atmospheric pressure photo-ionization; APCI: atmospheric pressure chemical ionization; ESI: electrospray ionization; MALDI: matrix-assisted laser desorption/ionization. Adapted from Greaves & Roboz, 2014 [115].

In ESI, the analytes are dissolved in an electrically conductive liquid medium, such as acetonitrile/water and methanol/water mixtures, and flow through a narrow steel tube, also called capillary, where they are subjected to a strong electric field, under atmospheric

pressure, which is obtained by applying a high voltage, typically in the range from 2 to 5 kV (positive or negative). The high voltage allows to obtain a solution with only one charge type, which is essential for the ionization process. Then, the liquid containing the analytes is nebulized by a sheath gas (a nitrogen (N_2) flow) located in a tube external to the capillary, obtaining a spray of charged droplets. [114,115,120] These charged droplets are dried (desolvated) with a second flow of gas, for example, a flow of heated N_2, which is called the drying gas. As the nebulization/evaporation process occurs, smaller and smaller droplets are formed to the point at which the droplets are no longer stable and disintegration occurs, releasing ions of the analytes into the vapor phase. When the droplets disintegrate to release ions, an extension with concave surfaces is formed, called Taylor cone. Finally, the ions enter in the mass analyzer (**Figure 7**). [114,115]

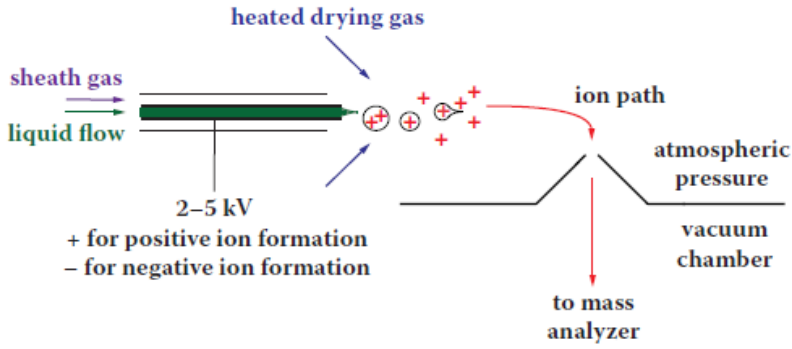

Figure 7. Electrospray ionization source. kV: kilovolts. From Greaves & Roboz, 2014 [115].

In positive ESI (positive ion mode), the main process of ion formation is the association of the neutral analyte molecules (M) with an ionizing agent, usually a proton (H^+), yielding protonated molecules ($[M + H]^+$), but there are other species, like alkali metal cations (particularly Na^+ and K^+), that can be added onto the analyte molecules to form $[M + Na]^+$ and $[M + K]^+$ ions, respectively [115].

In negative ESI (negative ion mode), ions are formed by deprotonation or anion attachment. Through deprotonation, carboxylic acids are often the target analyte molecules, obtaining deprotonated molecules ($[M - H]^-$). Through anion attachment, the addition of a halogen (like chloride) or an acetate anion can result in $[M + Cl]^-$ and $[M + CH_3COO]^-$ ions, respectively. [115]

1.2.3. Mass Analyzers – Quadrupole, Time-of-Flight and Quadrupole Time-of-Flight Analyzers

The mass analyzer is considered the heart of mass spectrometers. The function of the mass analyzer is to separate ions according to their *m/z* and to direct and transfer these ions onto a detector or into a collision cell. The quadrupole (Q) analyzers and the time-of-flight (TOF) analyzers are two types of mass analyzers. [114,115] The Q analyzers are *in-time* systems, since the ions are collected successively over a period of time (milliseconds to seconds), and are considered scanning instruments, that is, their electric field must be changed progressively over time, in order to obtain spectra. The TOF analyzers are *in-space* systems, since all ions are detected almost simultaneously (microseconds), and are considered nonscanning instruments, since spectra are obtained without having to change the operational parameters. [115]

In liquid chromatography coupled to tandem/hybrid mass spectrometry (LC-MS/MS), two or more analyzers can be combined into a single instrument, in order to improve the analytical capabilities. Tandem instruments involve similar analyzers, as the triple quadrupole (QqQ) systems, whereas hybrid instruments combine different analyzers, for example, the quadrupole time-of-flight (QTOF) systems. [115]

1.2.3.1. Quadrupole Analyzers

Quadrupole analyzers (**Figure 8**) consist of four 10-20 cm rods that must be aligned in order to create a symmetrical electric field, which is necessary to separate ions with different *m/z* values. Combinations of radio frequency (RF) voltages and direct current (DC) voltages applied on the rods generate fields that enable the transmission of ions from one end of the analyzer to the other. For any of these fields, only ions with a specific *m/z* value display a stable oscillatory trajectory through the quadrupole enabling them to reach the detector, whereas ions that have an unstable oscillation are discharged and lost by collision with the rods or the pre-filters (**Figure 9**). The progressive change of the DC and RF voltages allows the scanning of a mass range obtaining a spectra composed of different *m/z* values. [114,115,123]

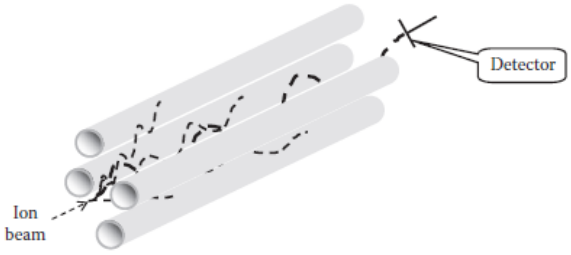

Figure 8. Schematic representation of a quadrupole mass analyzer. From Shrader, 2014 [114].

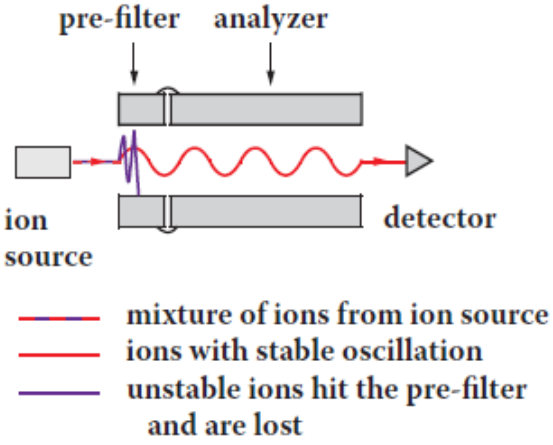

Figure 9. Separation of the ions according to their *m/z* value based on the stability of their flight trajectories through the electric field applied in the quadrupole analyzer. From Greaves & Roboz, 2014 [115].

An important configuration of quadrupoles is the QqQ system, which consists of two analytical quadrupole mass analyzers (Q1 and Q3) separated by a central section called collision cell (q2) (**Figure 10**). The q2 consists of RF voltages only. In QqQ, precursor ions are selected by the Q1 mass analyzer and then fragmented in the q2 by a process called collision-induced dissociation (CID). Collision-induced dissociation results from collisions between the analyte of interest and an inert gas, such as nitrogen or argon. The specific product ions produced by CID process are analyzed in the Q3 mass analyzer, and then passed to the detector. By keeping the electric fields of the Q1 and Q3 mass analyzers and the collision energy in q2 constant, only analyte ions with a specific mass transition (precursor/product ion pair) are able to reach the detector. This data acquisition mode is known as selected-ion monitoring or selected-reaction monitoring (SRM). In contrast, when the electric fields and collision energy must be changed progressively over time (scanning mode) to obtain spectra, the data acquisition mode is called multiple-reaction monitoring (MRM) (**Figure 11**). [115,123]

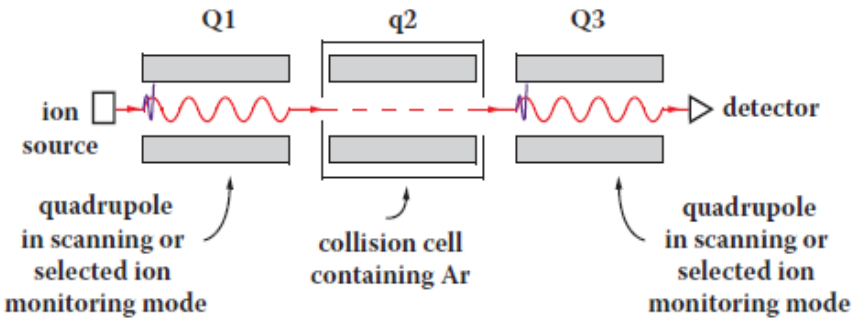

Figure 10. Representative scheme of a triple quadrupole system. Q1: first quadrupole; q2: collision cell; Q3: third quadrupole; Ar: argon. From Greaves & Roboz, 2014 [115].

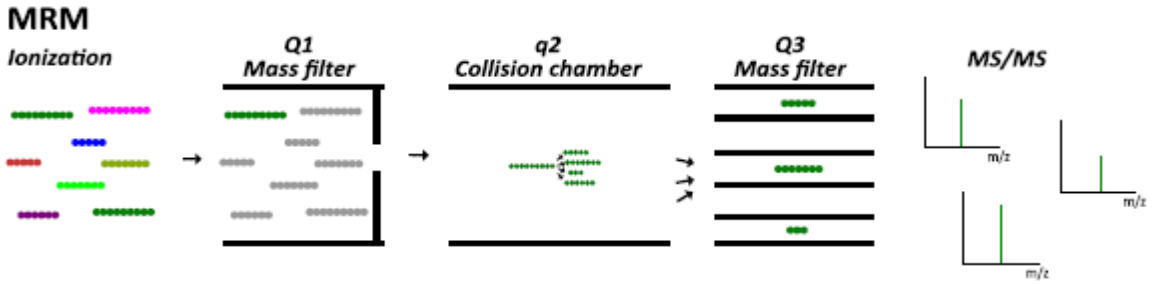

Figure 11. Schematic representation of the data acquisition mode multiple-reaction monitoring (MRM) performed in a triple quadrupole instrument. In MRM, the first quadrupole (Q1) selects the mass-to-charge ratio (*m/z*) of the precursor ion that is fragmented in the collision cell (q2). Then, one or more fragments ions are selected by the third quadrupole (Q3) towards the detector, obtaining a fragmentation spectrum (MS/MS) for each of the fragments. Adapted from Anjo, Santa, & Manadas, 2017 [124].

1.2.3.2. Time-of-Flight Analyzers

Time-of-flight analyzers separate ions based on their flight times over a specific distance or flight path, that is, after the ion formation in the ionization source, an electric field is used to accelerate them into the analyzer tube (flight tube) and for each ion, the travel/flight time from the source of the ion pulse through the flight tube of the analyzer to the detector is measured. The flight time of an ion is a function of its momentum (kinetic energy), and therefore its *m/z*. Since the acceleration voltage and the kinetic energy are the same for all ions, the lower the *m/z* of an ion, the greater its velocity and shorter its flight time, arriving at the detector first. [115,123]

The use of a single TOF analyzer with an ESI source or other API source is more difficult, because in these methods the production of ions is continuous. To overcome this

problem, orthogonal TOF analyzers have been developed, in which the analyzer is placed at a right angle (orthogonal) to the ion beam that emerges from the ionization source and the ion packets are created in a pusher region that uses a pulsed voltage. The ion packets are accelerated orthogonally into the analyzer tube where occurs the separation of ions with different *m/z* values. The ions entering the analyzer may present two types of trajectories: a horizontal trajectory (ions that arise from the ionization source direction) and vertical trajectory (ions that arise from the pusher that acts orthogonally, at 90°). Since the extracted ion packet must pass through the analyzer before another set of ions is introduced, only part of the continuous ion beam can be analyzed, which limits the duty cycle of the orthogonal injection process, and therefore the sensitivity of the orthogonal TOF analyzers. [115] The ion injection into an orthogonal TOF analyzer is schematized in **Figure 12**.

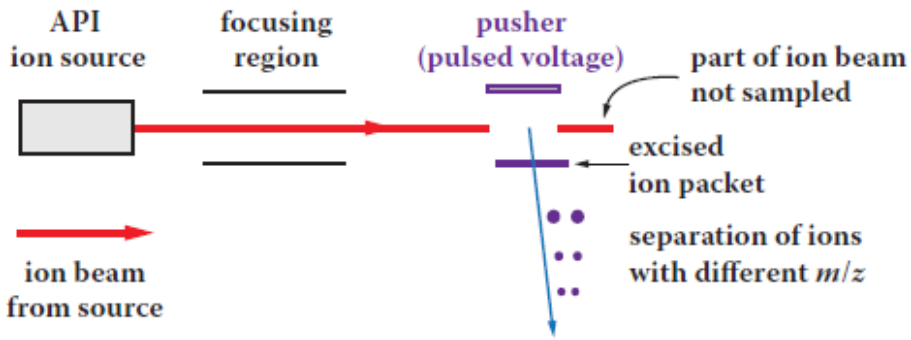

Figure 12. Injection of ions into an orthogonal TOF analyzer. The blue arrow represents the direction of the ions injected into the analyzer. API: atmospheric pressure ionization; *m/z*: mass-to-charge ratio. From Greaves & Roboz, 2014 [115].

One way to increase the resolution of a TOF analyzer is to increase the length of its flight path. To do this, the ion path (flight path) through the orthogonal TOF analyzer can include the passage through a reflectron (ion mirror), which results in a V-shaped (V geometry) ion path or can include the additional passage through a second reflectron, giving the ion path a W geometry (**Figure 13**). The V geometry is characteristic of electrospray ionization time-of-flight (ESI-TOF) instruments. [115]

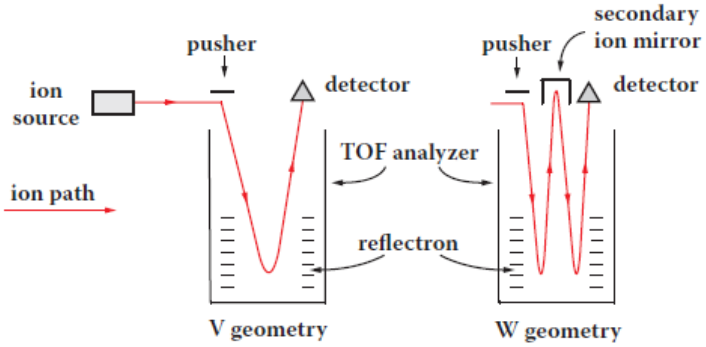

Figure 13. V (left) and W (right) geometries of the ion path in an orthogonal time-of-flight (TOF) analyzer. From Greaves & Roboz, 2014 [115].

1.2.3.3. Quadrupole Time-of-Flight Analyzers

Quadrupole time-of-flight systems (also called QqTOF) have high sensitivity, resolution and accurate mass measurement, where Q corresponds to a mass-resolving quadrupole that may be used in wide (all ions pass) or narrow (only an ion with a specific *m/z* passes) band pass mode to select which ions pass into the collision cell (q2), and TOF corresponds to a time-of-flight analyzer [115,125]. In the common QTOF configuration, an additional Q with RF voltages, designated Q0, is added to provide collisional cooling and to focus the ions entering the instrument [125]. This is the case in the TripleTOF 6600 system, which consists of three quadrupoles (Q0, Q1 and q2) followed by an orthogonal TOF analyzer (see **Figure 4**).

In QTOF analyzers, the full-scan MS data are obtained when the Q or Q1 analyzer is operating in the wide band pass mode (only RF voltages are applied to the Q or Q1), there is no gas in the q2, and all ions are transferred to the TOF analyzer, that is, in full-scan mode, the mass spectrometer measures the *m/z* values and abundances for all the features. For MS/MS data, the Q or Q1 analyzer operates in narrow band pass mode (combinations of DC and RF voltages are applied to the Q or Q1), which allows the specific selection of ions for fragmentation in q2 due to the ability to rapidly switch the analyzer's electric field. [115,125,126]

1.3. Metabolomics

In the last few years, advances in technology in the area of life sciences have led to the development of systems biology. The “omics cascade” comprises a set of levels of systems biology, such as genomics, transcriptomics, proteomics, and metabolomics (**Figure 14**). Metabolomics is an important field to characterize the phenotype changes caused by

environmental influences, disease, or changes in genotype. Metabolomics is defined as the qualitative and quantitative analysis of all small-molecule (50-1500 Da) metabolites (metabolome) present intracellularly or extracellularly in a given biological system, such as a cell, tissue, or organism. [115,127,128] The metabolome includes a huge variety of compound classes, such as amino acids, peptides, carbohydrates, lipids, organic acids, and nucleotides, thus its analysis is difficult by its great complexity. In complex systems, the biochemical and biological mechanisms are studied and understood through the analysis of an organism's response to a perturbation at the transcriptome, proteome, and metabolome levels. The metabolomics analysis requires the measurement of metabolites using sensitive and accurate techniques. Metabolomics studies have been applied in many research areas, such as environmental and biological stress studies and biomarker discovery for the diagnosis of diseases. [127-129]

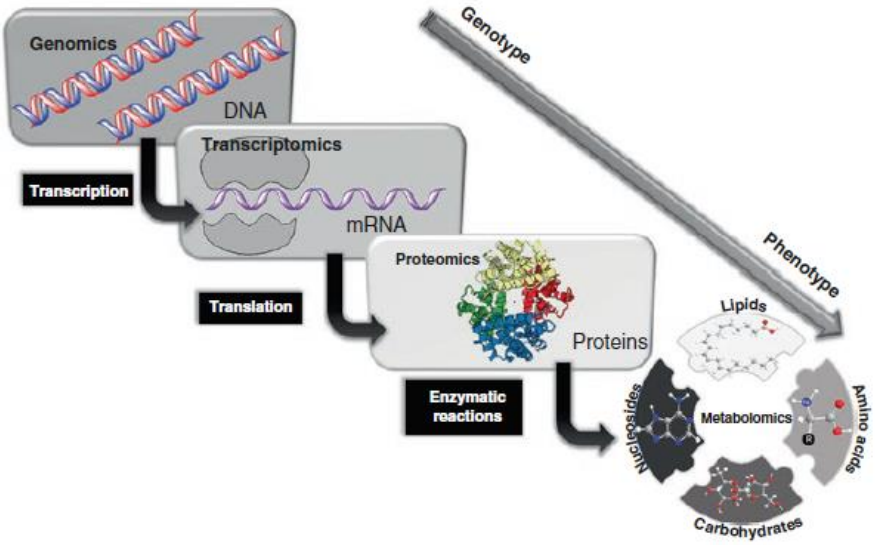

Figure 14. The "omics cascade". The genome is all the genetic information of an individual or a species that is encoded in its DNA. The transcriptome refers to the complete set of all RNA molecules (mRNA, rRNA, and tRNA). The proteome is the set of proteins synthesized by a cell or an organism. The metabolome is the entire set of small-molecule metabolites present, at a given moment, in a cell, tissue, organ, biofluid, or organism. The metabolome is the most predictive of phenotype. From Klassen *et al*., 2017 [130].

In metabolomics, nuclear magnetic resonance (NMR) and MS are widely used analytical techniques, especially MS when it is coupled with GC or LC to separate chemically diverse metabolite mixtures before the MS measurement [127]. Liquid chromatography-mass spectrometry stands out due to its high sensitivity, throughput and

wide metabolome coverage [126]. Liquid chromatography separates the metabolites according to their chemical properties, in order to reduce the sample complexity. Following separation, MS is used to detect the metabolic signal intensities, which are proportional to the metabolite concentrations for quantitative assessments. [131] Metabolomics can utilize many different types of mass analyzers, such as single Q or QqQ, TOF and QTOF [127].

A typical metabolomics workflow using LC-MS (or LC-MS/MS) (**Figure 15**) aims to compare various biological groups to identify metabolites that are significantly altered and requires several key steps, such as sample preparation, data acquisition and data processing, statistical analysis, metabolite identification and quantification, and further interpretation at the functional and biological level [127,129]. Sample preparation involves experimental design, sample collection and handling, and metabolite extraction. The experimental design includes considerations on experimental type, experimental factors and experimental comparisons, while sample collection and handling are of critical influence on experimental reproducibility. In metabolite extraction, the protocols are optimized to maintain the balance between the minimal matrix interference and maximum sample recovery. [129]

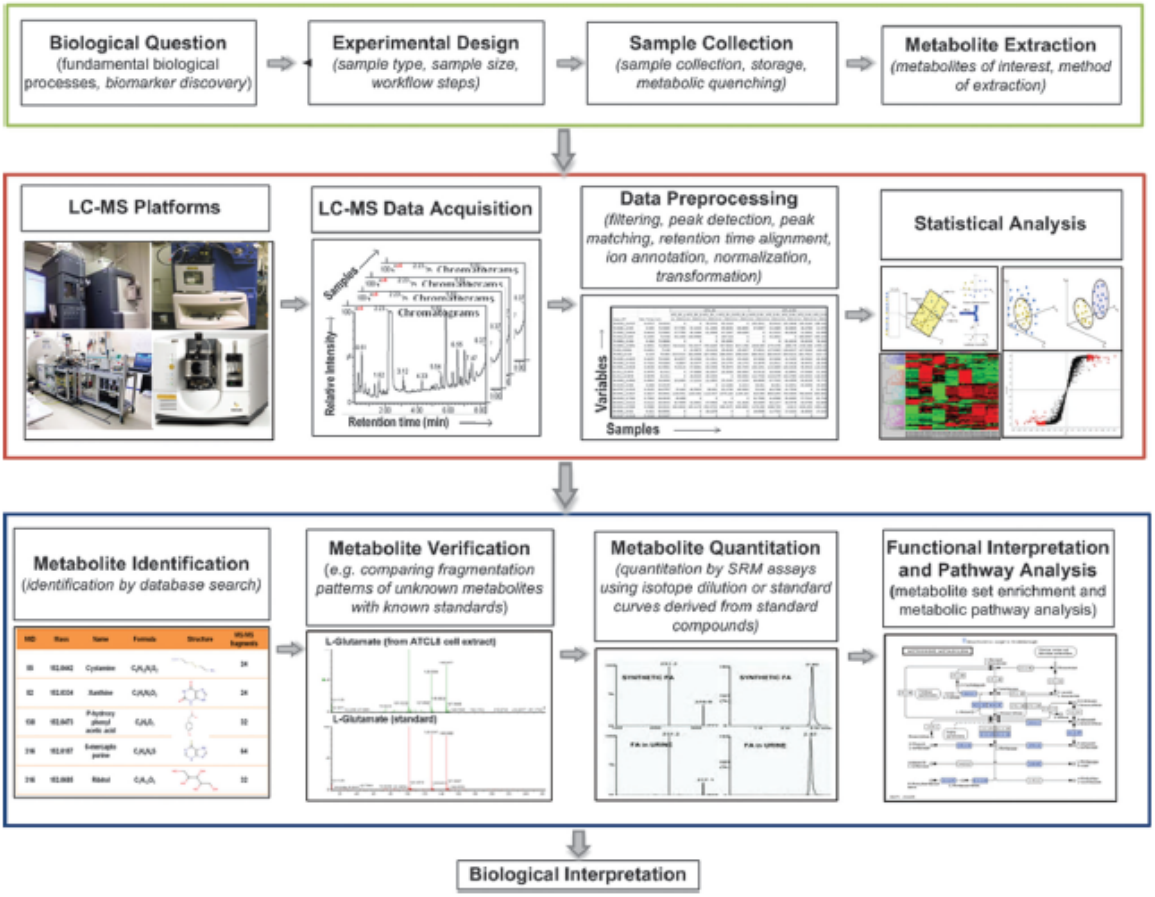

Figure 15. A metabolomics study workflow using liquid chromatography-mass spectrometry (LC-MS). From Zhou, Xiao, Tuli, & Ressom, 2012 [129].

1.3.1. Metabolomics Data Acquisition

Once the metabolites are extracted, metabolomics data must be acquired. In LC-MS, there are several data acquisition modes, namely SRM and MRM (mentioned in subchapter 1.2.3.1.), data dependent acquisition (DDA, also called information-dependent acquisition – IDA) and data independent acquisition (DIA). The DDA and DIA modes are explained and discussed in the following subchapters.

1.3.1.1. Data Dependent Acquisition

In DDA mode, the MS instrument acquires full-scan MS (full-scan mass spectra) followed by MS/MS analysis on a list of selected precursor ions from the full-scan spectrum based on their intensities (**Figure 16**) [132]. In full-scan MS the intensity (abundance) and *m/z* of all ions (precursor ions) eluting at a given time from a chromatographic separation are measured, while in MS/MS scan some or all detected ions are fragmented, and the intensities

(abundances) and *m/z*'s of the fragments are measured and recorded [133]. In this way, quantitative (obtained from the full-scan MS) and structural (obtained from the MS/MS spectra) informations can be acquired in the same sample analysis. Since the selection of the precursor ions for fragmentation in consecutive MS/MS scans is based on the intensity of the signal, usually selecting the most intense (abundant) ions, a potential limitation of DDA mode is that metabolic features of interest with low intensity or that are co-eluted with more intense species may never be selected for fragmentation and, consequently, will have no MS/MS data associated with them, making their detection and quantification impossible. [126,131] The MS/MS spectral information obtained from DDA can be directly used for metabolite annotation by matching against spectral library [126].

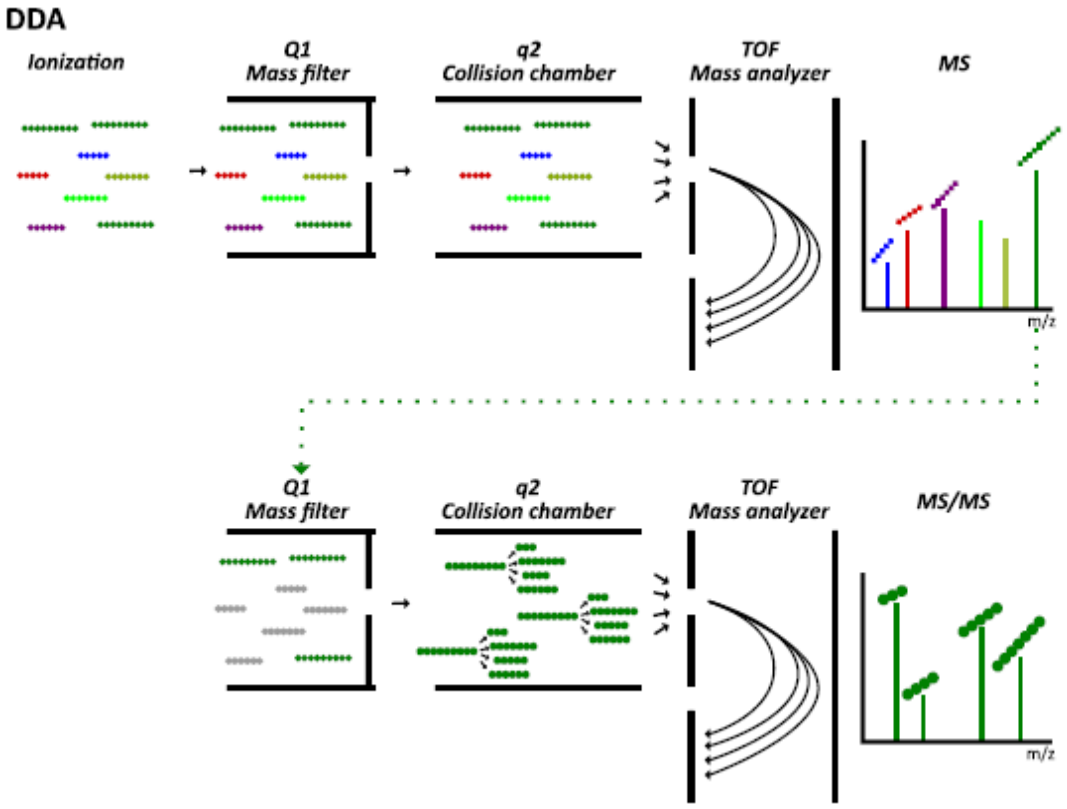

Figure 16. Scheme of the data dependent acquisition (DDA) mode used in liquid chromatography-mass spectrometry. Q1: first quadrupole; q2: collision cell; TOF: time-of-flight; MS: full-scan mass spectrum; MS/MS: fragmentation spectrum; *m/z*: mass-to-charge ratio. Adapted from Anjo, Santa, & Manadas, 2017 [124].

In DDA, the scan times for full-scan MS and MS/MS acquisitions should be selected carefully to obtain at least 7/8 data points per chromatographic peak. Regarding signal

threshold, the signal threshold should not be too high or too low. Too high results in restricted MS/MS coverage and too low results in low quality MS/MS spectra. Finally, the optimal collision energy depends on the collision cell geometry, the collision gas pressure and type, or the polarity of the ions. Generally, in metabolomics studies, the DDA is not performed for all samples, but only for the so-called "pool" samples, which result from mixing samples from the same group equally. [134]

1.3.1.2. Data Independent Acquisition – SWATH-MS

Multiple DIA methods were developed based on the type of mass spectrometers, usually with high resolution mass analyzers. Commonly used DIA methods include all ion fragmentation (AIF) and sequential window acquisition of all theoretical mass spectra (SWATH-MS). Data independent acquisition methods can be divided in two groups, those that acquire the fragmentation spectra (MS/MS spectra) of the entire mass range simultaneously, and those that scan the *m/z* range in sequential isolated windows, which results in decreased complexity of the fragmentation spectra, which leads to an improvement in the quality of the quantitative data. [124,131]

A characteristic of the SWATH-MS method is the parallel analysis of samples that combines optimized DDA for analyte identification with a DIA method used to extract the quantitative information of the previously identified analytes. Using the DDA mode, information about an identified analyte can be extracted, such as retention time (RT), precursor *m/z* and MS/MS spectra. [124]

In SWATH-MS (**Figure 17**), the MS instrument does not require the initial detection of a full-scan mass spectrum to proceed to MS/MS analysis, because the MS/MS spectra are acquired for all the precursor ions independently of their intensities. Moreover, in SWATH-MS, the instrument works in a cyclic mode covering the entire *m/z* range of interest in sequential isolated Q1 windows of defined size resulting in a high-resolution fragmentation spectrum of the sample. The widths of the Q1 isolation windows are typically of 20-25 Da, but can be adjusted to optimize specificity and cycle time, and even changed during a SWATH-MS analysis, depending on the absolute Q1 *m/z* range, the acquisition speed of the mass spectrometer, and the required method's selectivity. [124,135]

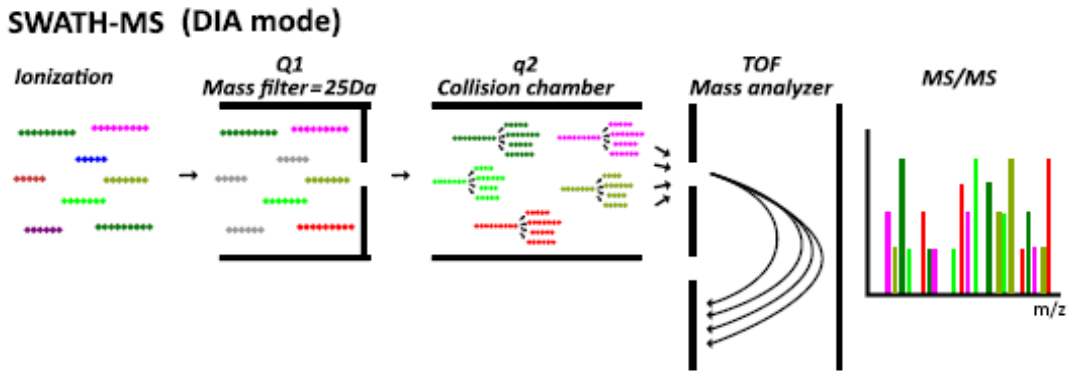

Figure 17. Sequential window acquisition of all theoretical mass spectra (SWATH-MS) method performed in a QTOF system. DIA: data independent acquisition; Q1: first quadrupole; q2: collision cell; TOF: time-of-flight; MS/MS: fragmentation spectrum; *m/z*: mass-to-charge ratio. Adapted from Anjo, Santa, & Manadas, 2017 [124].

An overview of the characteristics, strengths and weaknesses of the DDA mode and the SWATH-MS method is summarized in **Table 2**.

Table 2. Overview of the data dependent acquisition (DDA) and sequential window acquisition of all theoretical mass spectra (SWATH-MS) methods with their characteristics, strengths and weaknesses. QqQ: triple quadrupole; QTOF: quadrupole time-of-flight; Full-scan MS: full-scan mass spectra; N/A: not applicable; Da: Dalton; CID: collision-induced dissociation; LC: liquid chromatography. Adapted from Raetz, Bonner, & Hopfgartner, 2020 [136].

Method	DDA	SWATH-MS
Instruments	QqQ, QTOF, Orbitrap	QTOF, Orbitrap
Precursor selection mode	Real-time based on full-scan MS survey	Pre-defined
Precursor selection rules	Top N (most intense)	N/A
Precursor selection width	1 Da	Wide (e.g. 10-50 Da)
Precursor selection range	Defined by survey full-scan MS	Selected
Product ion mass range	Full mass range	Full mass range
Product ion generation	CID of selected precursor	All precursors in selected window
Precursor-product determination	Known from selected precursor	Match LC profiles
Compound identification	Library search	Library search
Qualitative performance	Very good	Good
Quantification modes	Precursor ion chromatograms, Mass peak ratio to labelled standard	Fragment chromatograms, Precursor chromatograms
Quantification performance	Acceptable	Very good
Strengths	Efficient use of time, 1 Da precursor window (good selectivity), Widely accepted	Reproducible (consistent data acquisition), Permanent record of all fragments, Post-acquisition data analysis
Weaknesses	Stochastic precursor selection, Quantification only from full-scan MS chromatograms or ion ratios	Data is large, complex and requires special processing tools

1.3.2. Metabolomics Data Analysis

1.3.2.1. Pre-processing of LC-MS Data, Targeted and Untargeted Analysis

In LC-MS, the raw data is converted into a peak list that can be easily interpreted and compared across runs. Several pre-processing steps can be performed, such as baseline

correction, peak detection, peak matching and retention time alignment, ion annotation, normalization, transformation, filtering and outlier screening [129].

Baseline correction algorithms estimate the low-frequency baseline, and then subtract this baseline from the raw signal. The baseline is the signal obtained when only the mobile phase (eluent) is passing through the column during the chromatographic separation. [129]

Peak detection has two advantages, namely, part of the noise in the raw data is removed and data dimension is reduced without much information loss. Peak detection is generally performed on extracted ion chromatograms (EIC(s) or XIC(s)), since *m/z* has less variation when compared with retention time. [129]

Peak matching and retention time alignment allow the comparison of LC-MS-based metabolomics data across samples. For studies with multiple samples, the retention time alignment is used to correct the retention time drift of an ion and to ensure the comparison of the same ion across different samples. The addition of reference compounds to the samples is an approach used to correct/align the retention time. [129]

Ion annotation groups ions which are likely to originate from the same compound (metabolite), since these ions have similarly shaped chromatographic peaks (elution profiles), which can be represented by their XIC(s). In LC-MS-based metabolomics, one metabolite can be represented by multiple peaks in LC-MS data with different *m/z* values, but similar retention times, due to the presence of isotopes, adducts and fragments. [129]

Normalization of the peak intensities reduces the systematic variation of LC-MS data. The addition of the same amount of external internal standards into all the samples and the normalization to the total area sum of all detected peaks for each sample are methods to normalize the LC-MS data. [129]

Outlier screening aims to eliminate LC-MS samples that exhibit significative deviation from the majority of their analytical or biological replicates, which are called outliers. Principal component analysis (PCA) is often used to identify sample outliers through the observation of the 2-D (or 3-D) scores plots of the data. [129]

Metabolomics studies can be divided in two complementary approaches, targeted and untargeted [128]. The targeted analysis focuses on identify and quantify defined metabolites or group of metabolites related to a metabolic pathway or a class of compounds. In the targeted analysis, the chemical properties of the analyzed compounds are known and the sample preparation is planned to reduce the matrix effects and interference from other associated

compounds. [129,137] Targeted analysis facilitates metabolite identification and quantification and reduces the risk of false annotation, while the metabolome coverage is limited [138]. On the other hand, untargeted analysis is a global analysis that detects as many metabolites as possible of a biological system, that may be altered in response to disease, environmental or genetic perturbations, in a single or integrated analysis and offers the potential to discover new biomarkers without pre-existing knowledge [129,137,138].

1.3.2.2. Statistical Analysis – Univariate and Multivariate Analysis

As mentioned before, after pre-processing, the raw LC-MS data are summarized in a peak list. The statistical analysis aims to detect the peaks whose intensity levels are significantly altered between distinct biological groups. The statistical analysis methods can be divided in two groups, univariate and multivariate analysis. [129]

The univariate analysis evaluates the statistical significance of each peak individually, which helps to reduce the potential large number of measured analytes to only those that have the strongest response under the investigated conditions. Commonly used univariate analysis methods include Student's *t* test (*t*-test), analysis of variance (ANOVA), Mann-Whitney test, among others. The *t*-test and ANOVA are statistical methods where testing variable (dependent variable) should be continuous and normally distributed. For a continuous variable with a normal distribution, mean is the representative measure, while median is the representative measure for non-normal continuous variable. Statistical methods that are used to compare the means between groups are called parametric methods. The *t*-test is a parametric method used to test whether the mean difference between two groups is statistically significant. The null hypothesis assumes that the difference between both means is not statistically significant, whereas alternative hypothesis assumes that there is a statistically significant difference between the two means. The ANOVA is used to compare the means among three or more groups. The two main types of ANOVA are one-way ANOVA (used for independent groups) and one-way repeated measures ANOVA (used for dependent groups). [139-141] On the other hand, statistical methods that are used to compare the medians between groups are called non-parametric methods. The Mann-Whitney test is the most widely used non-parametric method to compare the medians between two independent groups if the data distribution is non-normal and the sample groups are small [142].

The multivariate analysis considers the combined effect of multiple variables and can be classified as unsupervised and supervised methods. Unsupervised methods allow the structure within the data to be determined and visualized without knowing the group/class labels. In contrast, supervised methods use prior knowledge of the sample groups/classes to determine the variables that distinguish the groups. Supervised methods are widely used in biomarker discovery and prediction. A supervised method deals with data sets that have response variables, which can be discrete (such as, control group versus disease group) or continuous (such as, metabolite concentration). In metabolomics data analysis, two of the most commonly used unsupervised multivariate analysis methods are PCA and clustering analysis, while partial least squares-discriminant analysis (PLS-DA) is a widely used supervised multivariate analysis method. [129,143,144]

Principal component analysis is an unsupervised method that reduces the dimensionality of a data set, while preserving as much variability as possible, that can be translated into new variables, the principal components (PCs). Principal components are linear functions of those in the original data set that are uncorrelated with each other and that are ordered according to the amount of variance that they explain, that is, the first PC explains the largest variance and the second and the following PCs explain the maximum amount of variance remaining, being orthogonal (at a 90˚ angle) to the previous PC. Thus, it is possible to visualize the data in 2D (if two PCs are selected) or 3D (if three PCs are selected) plots, called scores and loadings plots. The scores plot is essentially used to discover the groups, while the loadings plot is mainly used to find the variables that are responsible for the separation of the groups. [129,143,144]

Partial least squares-discriminant analysis is used for classification purposes, identifying the variables that maximize the separation between pre-defined sample groups or predicting the class affiliations of unclassified samples. This supervised method does not imply a specific distribution of the data. [142,143]

Clustering analysis aims to identify groups in the original data set, using different clustering algorithms that group the variables based on their similarity (the variables in the same group or cluster are more similar to each other than to variables in other groups/clusters). Hierarchical clustering is one of the most common clustering methods in metabolomics. It uses a dendrogram to relate the data in a hierarchical structure. To form the

hierarchical tree, the similarity metric between pairs of subjects (distance functions) and pairs of clusters (linkage functions) must be chosen. [144]

Chapter 2
Objectives

2. OBJECTIVES

Hypoxic-ischemic encephalopathy is a devastating episode that causes newborn death, many long-term injuries, and brain injury, and at present, the diagnosis of newborns suffering from HIE is not accurate and objective. Thus, it is critical that HIE diagnosis can be accurate, equally accessible worldwide, and fast enough for application of the therapeutic.

In this way, the present study aims to characterize the metabolomics profile of an HIE *in vitro* model, and identify potential biomarkers that can be used in the diagnosis of HIE. For this purpose, a metabolomics screening of primary cultures of cerebrocortical neurons subjected, separately, to two neuronal death stimuli – an OGD model and a glutamate excitotoxicity model – was performed, using LC-MS/MS. Two approaches were then applied on data analysis: an untargeted metabolomics analysis (for detection of endogenous and exogenous metabolites) and a targeted metabolomics analysis (for identification of endogenous metabolites).

Chapter 3
Materials and Methods

3. MATERIALS and METHODS

3.1. Primary Cerebrocortical Cultures

The procedures regarding the preparation of the primary cell cultures detailed below were performed by members of the research team.

3.1.1. Coating the Culture Dishes with Poly-D-Lysine

To promote cellular adhesion, tissue culture (TC) polystyrene dishes (Corning® Costar®) were coated with a poly-D-lysine (PDL) solution (Sigma-Aldrich) at a final concentration of 0.1 mg/ml (diluted in 166.3 mM boric acid (pH 8.2)), overnight in a humidified incubator (Binder) with 5% of carbon dioxide (CO_2), at 37 ºC. Culture dishes were washed twice with sterile distilled water and left to dry.

3.1.2. Isolation of Primary Cultures of Cerebrocortical Neurons from Rat Embryos

Cell culture procedures regarding the preparation of primary cerebrocortical cultures were performed on a class II laminar air flow cabinet (Herasafe™ KS 12, Thermo Scientific™) under sterile conditions.

The preparation of primary cultures of cerebrocortical neurons from rat embryos was previously described by Salazar *et al.*, in 2017 [145]. Succintly, primary cultures of rat cerebrocortical neurons were prepared from cerebral cortices of E17-18 Wistar rat embryos. After dissection, the cerebral cortices were washed three/four times with cold Hank's balanced salt solution (HBSS: 5.36 mM KCl (AppliChem), 0.44 mM KH_2PO_4 (Merck), 137 mM NaCl (AppliChem), 4.16 mM $NaHCO_3$ (Acros Organics), 0.34 mM $Na_2HPO_4 \cdot 2H_2O$ (Merck), 5 mM glucose (VWR), 1 mM sodium pyruvate (Sigma-Aldrich), 10 mM HEPES (Fisher Scientific) and 0.001% phenol red (Sigma-Aldrich), filtered, pH 7.2). Then, 1.5 ml of a freshly prepared trypsin (Thermo Fisher Scientific, Gibco™) solution at a final concentration of 2 mg/ml was filtered (with a 0.2 µm cellulose acetate membrane (VWR)) and added to 6 ml of HBSS containing the cortices and incubated in a water-bath system (GFL®) for 10 minutes at 37 °C, to promote primary tissue dissociation [146]. Next, the cerebral cortices were washed five/six times with cold HBSS (6-9 ml), followed by their mechanical dissociation, using a sterile glass pipette, by pipetting up and down to the bottom of the

Falcon tube, until a cloudy cell suspension was obtained. This cell suspension was filtered using a sterile cell strainer of 70 µm (Falcon®) to separate the cells in suspension from the aggregates of non-dissociated tissue.

For cell count, cell viability was assessed with trypan blue (compromised cells are permeable to the dye). For that, cell suspension was diluted in 1:3 proportion (equal parts of HBSS, cell suspension and trypan blue solution 0.4% (Sigma-Aldrich)) and added to a hemocytometer. Viable cells present in each of the four quadrants were counted using a phase contrast inverted microscope (Zeiss, model: Axiovert 40 C). Cells were then plated in neuronal plating medium (minimum essential medium Eagle (9.50 g/L, Sigma-Aldrich), glucose (0.6%, VWR), sodium pyruvate (1 mM, Sigma-Aldrich), and $NaHCO_3$ (3.64 g/L, Acros Organics)) at 92.8 × 10^3 cells/cm^2 and left to adhere for 2 hours at 37 °C in a humidified incubator (Binder) with 5% CO_2. Then, plating medium was replaced by neurobasal medium supplemented with 0.5 mM L-glutamine and 0.12 mg/ml gentamycin (all from Thermo Fisher Scientific, Gibco™) and NeuroCult SM1 neuronal supplement (1:50 dilution, STEMCELL Technologies) [145].

3.1.3. Maintenance of Primary Cerebrocortical Cultures

Cells were maintained in a humidified incubator (Binder) with 5% CO_2, at 37 °C for 9 days. Each 3 days, 1/3 of culture medium was replaced by fresh supplemented neurobasal medium, as previously described. At day *in vitro* (DIV) 3, 5-fluoro-2'-deoxyuridine (5-FDU, Sigma-Aldrich), a mitotic inhibitor, was added at a final concentration of 10 µM to the cultures to stop the proliferation of non-neuronal cells.

3.2. OGD Insult

Prior to the insult, approximately 24 hours, oxygen and glucose deprivation medium (25 mM sucrose, 1.8 mM $CaCl_2$, 25 mM $NaHCO_3$, 10 mM HEPES, 116 mM NaCl, 5.4 mM KCl, 0.8 mM $MgSO_4$, 1 mM NaH_2PO_4, 0.001% phenol red, pH 7.3) was placed in the OGD chamber (Invivo$_2$ 400, Baker Ruskinn) with 0% O_2 and 5% CO_2, to remove the oxygen dissolved in the medium.

Oxygen and glucose deprivation insult was performed at DIV 9. Cerebrocortical neurons medium was replaced by the OGD medium and placed in an OGD chamber with 0% O_2 and 5% CO_2, at 37 °C for 2 hours. For control conditions (Sham), cerebrocortical

neurons medium was replaced by a sham medium (similar to OGD medium, but with 25 mM of glucose instead of sucrose), and were kept in a humidified incubator (Binder) with an atmosphere of 5% CO_2, at 37 °C for the same period of time. At the end of the insult, OGD and sham media were replaced by the conditioned neuronal culture medium and left in the incubator for 24 hours.

3.3. Glutamate Stimulus

At DIV 9, cerebrocortical neurons were submitted to a glutamate stimulus. Briefly, these cells were incubated with 125 µM glutamate (Sigma-Aldrich) in supplemented neurobasal medium for 20 minutes, at 37 °C in a humidified incubator (Binder) with 5% CO_2. At the end of the stimulus, cells were placed back in the conditioned neuronal culture medium, and left in the incubator for 6 hours. For control conditions, cerebrocortical neurons were maintained in the supplemented neurobasal medium in the humidified incubator with an atmosphere of 5% CO_2, at 37 ºC.

3.4. Metabolomics Study of Primary Cultures of Cerebrocortical Neurons using LC-MS/MS

3.4.1. Cellular Proteome and Metabolome Extraction and Protein Precipitation

At each timepoint (after 24 hours for OGD insult and after 6 hours for glutamate stimulus), cerebrocortical neurons were lysed to extract their proteome and metabolome. Culture medium was initially removed and cells were washed once with 1× phosphate-buffered saline (PBS) to remove possible contaminants of the culture medium. Next, an 80% methanol (MeOH) solution, at -20 °C, was added to the cells and left at -80 °C, overnight. This approach allows protein to precipitate, while metabolites remain in the soluble fraction. On the following day, cellular extracts were scrapped with cell scrappers (VWR) on ice, then collected into microcentrifuge tubes and were sonicated (Sonicator VibraCell™ 75041, Bioblock Scientific) with a cup horn at 60% of amplitude for 1 minute (3 seconds on and 1 second off cycles) to burst cells that may not have burst and to homogenize the samples. Next, cellular extracts were centrifuged (Centrifuge 5430 R with rotor FA-45-30-11, Eppendorf) at 20 000 × g at 4 °C for 30 minutes, to separate the pellet (containing the proteins and cellular debris) and the supernatant (containing the metabolites). The protein pellet was

resuspended in sample buffer (SB) 1× and stored at -20 °C. The supernatant was evaporated until dryness at 60 °C using a vacuum evaporator (Concentrator plus with rotor F-45-48-11, Eppendorf) to concentrate the metabolites.

3.4.2. Sample Preparation

For SWATH-MS acquisition, the dryed samples were resuspended in 35 µl of internal standard (IS) solution (IS 99: mixed solution of 1 µM of two drugs, penicillin V potassium salt (for ESI source in negative ionization mode) and sulfamethazine-D4 (for ESI source in positive ionization mode) prepared with the mobile phase (2% ACN and 0.1% formic acid (FA) in distilled water)), sonicated (Sonicator VibraCell™ 75041, Bioblock Scientific) with a cup horn at 40% of amplitude for 2 minutes (1 second on and 1 second off cycles) to homogenize, and centrifuged (Microcentrifuge MiniSpin® plus with rotor F-45-12-11, Eppendorf) at 14,100 rpm for 5 minutes.

For IDA acquisition, a representative pool for each of the four groups was prepared. For groups with n equal to three (OGD and Sham), 7 µl were collected from each of the respective samples for SWATH-MS acquisition, and for groups with n equal to four (Glutamate and Control), were collected 5 µl (see **Figure 18**).

Finally, the samples were transferred to vials for LC-MS/MS analysis.

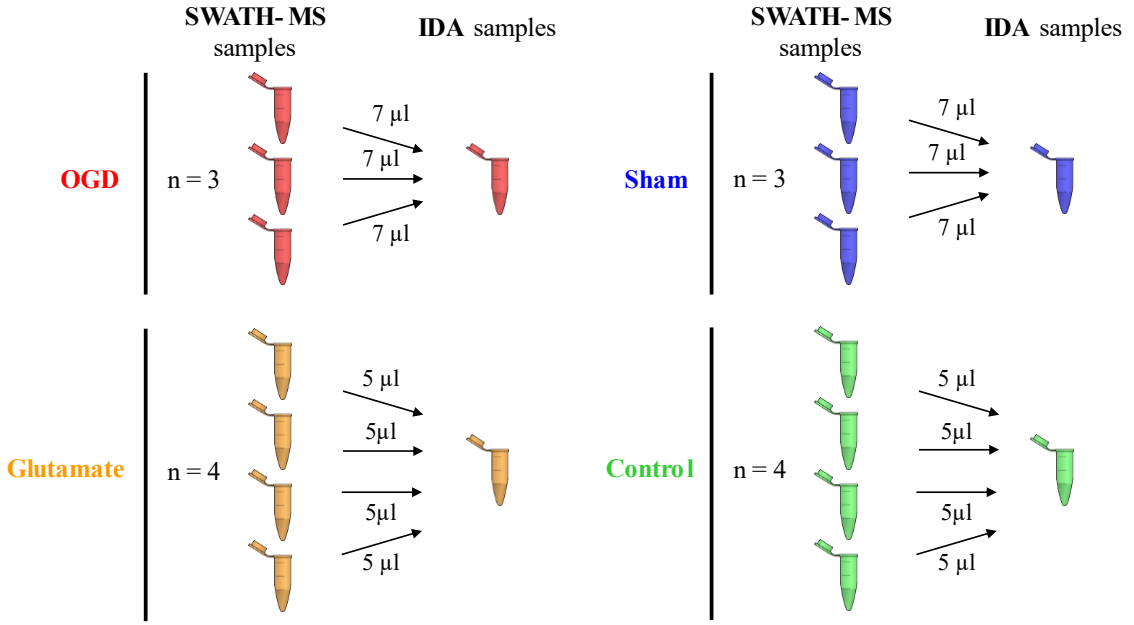

Figure 18. Schematic representation of sample preparation for IDA acquisition. SWATH-MS: sequential window acquisition of all theoretical mass spectra; IDA: information-dependent acquisition; n: biological replicates; OGD: oxygen and glucose deprivation; Sham: OGD control.

3.4.3. LC-MS/MS Analysis of Cellular Metabolites

3.4.3.1. LC-MS/MS Data Acquisition

The samples were analyzed on a NanoLC™ 425 System (Eksigent) coupled to a Triple TOF™ 6600 system mass spectrometer (AB Sciex) with an ionization source ESI DuoSpray™ Source (AB Sciex). Metabolites were separated in a Triart C18 Capillary Column (12 nm, S-3 µm, 150 × 0.3 mm, YMC) and a Triart C_{18} Capillary Guard Column (12 nm, 3 µm, 0.5 × 5 mm, YMC) at 50 °C at 5 µl/min. For the elution gradient, two mobile phases were used (0.1% FA in water and 0.1% FA in ACN, mobile phases A and B, respectively). The following elution gradient was used: 5-60% of B for 50 minutes, 60-95% for 2 minutes, 95% for 2 minutes, 95-5% for 1 minute and 5% for 10 minutes. The ESI DuoSpray™ Source was operated in the positive ionization mode at an ion spray voltage floating of 5500 V, 25 psi for nebulizer gas 1 (GS1), 10 psi for nebulizer gas 2 (GS2), 25 psi for the curtain gas (CUR), 85 eV for declustering potential (DP) and 100 °C for temperature (TEM).

With the above chromatographic conditions, the mass spectrometer was programmed for two types of data acquisition: IDA (also called DDA) and SWATH-MS (a DIA method). The mass spectrometer was controlled by Analyst® TF Software v1.8 (AB Sciex).

For IDA experiments, full-scan MS (*m/z* 50-2250) were acquired for 250 milliseconds, followed by 40 MS/MS scans for 40 ms/spectrum. For each MS/MS scan, was used a collision energy (CE) of 40 eV and a collision energy spread (CES) of 30 eV.

For SWATH-MS experiments, at the beginning, full-scan MS (*m/z* 50-2250) were acquired for 50 milliseconds, followed by 73 product ions covering the precursor mass range of 50-1500 *m/z* by overlapping windows with an isolation width of 21 *m/z*. The SWATH MS/MS spectra were collected from 50-2250 *m/z* for 23.3 milliseconds, resulting in a cycle time of 1.802 seconds. For each window, was used a CE of 40 eV and a CES of 30 eV.

3.4.3.2. LC-MS/MS Data Processing and Analysis

Concerning data analysis, two complementary analyses were performed, an untargeted analysis and a targeted analysis.

For the untargeted analysis, to compare the data acquired by LC-MS/MS from the analyzed samples for each of the study groups, the files obtained by SWATH-MS were imported into the MarkerView™ software v1.3.1 (AB Sciex) for data processing before data analysis. Data processing includes peak detection and alignment, and data normalization. For peak detection, the parameters were selected for "Period 1, Experiment 1" and the following parameters were defined: retention time above 0 minutes, subtraction offset of 10 scans, subtraction multiplication factor of 1.3, noise threshold superior to 100 counts, minimum spectral peak width of 0.01 Da, and minimum retention time peak width of 5 scans. For peak alignment, were defined a retention time tolerance of 1 minute and a mass tolerance of 10 ppm. The peak alignment step was important to decide if two peaks found in two samples or within the same sample represent the same chemical compound or not, that is, if their *m/z* values and retention times were both within the specified tolerances, they were considered to be the same "feature". Then, the data normalization was performed using the "total area sums" tool. After data processing, in order to reduce the large number of features to make data analysis possible, first, only monoisotopic features were selected followed by a filtering step, in which the features (*m/z*; RT) present in all samples of at least one of the study groups of each insult were selected.

For the comparative analysis of the two groups, OGD and Sham groups (OGD insult), and Glutamate and Control groups (glutamate stimulus), based on the intensity values of each selected feature obtained after the data processing performed in MarkerView™ software, two approaches were performed: (1) in the first approach, after the data filtering step, to compare the OGD and Sham groups, a Student's *t*-test was performed in MarkerView™ software v1.3.1 (AB Sciex) and to compare the Glutamate and Control groups, a Mann-Whitney test was performed using IBM SPSS Statistics v23.0 (IBM®). Next, the features with a *p*-value (*p*) smaller than 0.05 were selected, the PLS-DA method was performed and the features with a variable importance in projection (VIP) score greater than 1 were selected for the subsequent analysis; (2) in the second approach, after the data filtering step, the PLS-DA method was performed and the features with a VIP score greater than 1 were selected for the subsequent analysis.

To proceed to the identification of the interesting features, which were selected in each of the previous approaches, a new method was created in Sciex OS™ software v2.1.6 (AB Sciex) using the MQ4 peak area integration algorithm. The data files from the IDA experiments were imported into Sciex OS™ software to search for the precursor and its MS/MS spectrum. The method was built based on the *m/z* values and the retention times of the interesting features previously selected and the IS (sulfamethazine-D4) was imported from the "Internal Standards" library. The obtained identifications that had a mass error smaller than 50 ppm and a library score greater than 70 were selected for quantification. After that, the compounds identified through precursor analysis (IDA) were identified in the SWATH data files and quantified based on the precursor and fragments profiles. For this purpose, another method was created in Sciex OS™ software using the MQ4 peak area integration algorithm and the SWATH data files. The method was built based on importing each identified precursor and each of its three most intense fragments from the corresponding library, the number of SWATH experiment (corresponding to the SWATH window where the precursor was fragmented), and the IS precursor and its three most intense fragments were imported from the "Internal Standards" library. For each precursor and its fragments, the retention time used was that of the feature from which the identification was made. For each identification, the following criteria were used to select which peak (precursor or one of the three most intense fragments) was used for quantification: peak with a good intensity (S/N > 10), a gaussian-shaped chromatogram, a mass error smaller than 50 ppm, and a library

score greater than 70. For both identification and quantification, the library search was performed using the candidate search algorithm and the following libraries: “Metabolite_HR-MS/MS_1.0”; “Antibiotic_HR-MS/MS_1.0”; “Pesticide_HR-MS/MS_1.0”; “Fluorochemical_HR-MS/MS_2.0”; “IROA_CE40CES30_Eksigent”; “Internal Standards”; “Forensic_HR-MS/MS_2.1”; “Mycotoxin_HR-MS/MS_1.0”; “Natural_Products_HR-MS/MS_2.0”.

For both approaches (first approach: features with *p*-value smaller than 0.05 and VIP score greater than 1; second approach: features with VIP score greater than 1), features for which no identification with Sciex OS™ software was obtained were also quantified, but in the second approach, for each insult, only the 10 features with the highest VIP score were quantified, due to the large number of features.

Regarding targeted analysis, for identification, a new method was created in Sciex OS™ software v2.1.6 (AB Sciex) using the AutoPeak peak area integration algorithm and the IDA data files for precursor analysis. The method components were imported from two libraries: “Metabolite_HR-MS/MS_1.0” (AB Sciex library) and “IROA_CE40CES30_Eksigent” (laboratory library, which was built by injecting and analyzing each metabolite into the equipment that was used to analyze the samples of this study). The IS (sulfamethazine-D4) was imported from the "Internal Standards" library. The peak integration parameters were defined as a XIC width of 0.01 Da and low for smoothing. The library search was performed using the confirmation search algorithm and the three libraries previously mentioned. The identifications with a mass error smaller than 50 ppm and a library score greater than 70 were selected for quantification. Next, as for the untargeted analysis, the compounds identified through precursor analysis (IDA) were identified in the SWATH data files and quantified based on the precursor and fragment profiles. For quantification, a method was created in Sciex OS™ software with the MQ4 peak area integration algorithm and the SWATH data files. Regarding method components, for the precursors, the method was built based on the information obtained through the identification, namely, name, chemical formula, adduct, *m/z* value and retention time. The information about the three most intense fragments was imported from the library where the respective precursor is located. The IS precursor and its three most intense fragments were imported from the "Internal Standards" library. The library search was performed using the smart confirmation search algorithm and the three libraries: “Metabolite_HR-MS/MS_1.0”

(AB Sciex library); "IROA_CE40CES30_Eksigent" (laboratory library); "Internal Standards". For each identification, to select which fragment (one of the three most intense fragments) was used for quantification the following criteria were used: peak with a good intensity (S/N > 10), a gaussian-shaped chromatogram, a mass error smaller than 50 ppm, and a library score greater than 70.

In both analyses (untargeted and targeted), the peak integration parameters for the MQ4 peak area integration algorithm were defined as: a XIC width of 0.02 Da, a minimum peak width of 3 points, a minimum peak height of 10, a Gaussian smooth width of 2 points, a noise percentage of 80% and a baseline subtract window of 1 minute.

For the untargeted analysis, in order to try to get more potential biomarkers from the features for which no identification was obtained before and that showed statistically significant differences ($p < 0.05$) for the quantification obtained with the Sciex OS™ software, the online platform XCMS™ v3.7.1 (The Scripps Research Institute, https://xcmsonline.scripps.edu) was used. Since small peptides were obtained, they were searched in the ProteinPilot™ software v5.0.1 (AB Sciex) to see if they belonged to possible proteins that might be present in the samples.

The analysis of metabolic pathways was perfomed in MetaboAnalyst 5.0 (https://www.metaboanalyst.ca) [147]. The functional analysis of untargeted metabolomics data was performed using the Pareto scaling and the Mummichog algorithm in positively ionized *m/z* values with a mass tolerance of 50 ppm and retention time in minutes. In the Mummichog algorithm the features are ranked by *p*-values [148]. *Rattus norvegicus* (rat) library was the pathway library used. The monoisotopic features previously selected for each of the groups pairs (OGD vs Sham and Glutamate vs Control) were the data used to perform the analysis.

The KEGG compound entries obtained from the functional analysis were quantified in Sciex OS™ software v2.1.6 (AB Sciex) by creating a new method similar to the one used for the untargeted analysis. The method was built using the MQ4 peak area integration algorithm, the SWATH data files and the *m/z* values and the retention times of the respective monoisotopic features. The peak integration parameters used for MQ4 algorithm were the following: a XIC width of 0.02 Da, a minimum peak width of 3 points, a minimum peak height of 10, a Gaussian smooth width of 2 points, a noise percentage of 80% and a baseline subtract window of 1 minute. The library search was performed with the candidate search

algorithm and the following libraries: “Metabolite_HR-MS/MS_1.0”; “Antibiotic_HR-MS/MS_1.0”; “Pesticide_HR-MS/MS_1.0”; “Fluorochemical_HR-MS/MS_2.0”; “IROA_CE40CES30_Eksigent”; “Forensic_HR-MS/MS_2.1”; “Mycotoxin_HR-MS/MS_1.0”; “Natural_Products_HR-MS/MS_2.0”.

At the end, for all the analyses (untargeted analysis, targeted analysis and functional analysis), the peak areas obtained from Sciex OS™ software were exported to Excel and the data were normalized to the total area sum of all detected features in MarkerView™ software for each sample, individually. The data were normalized to the total area sum and not to the internal standard, since normalization to the total area sum allows to account for what happens to the samples from proteome and metabolome extraction to LC-MS/MS analysis, whereas normalization to the internal standard only allows to account for what happens from its addition to the samples. Then, with the area ratios obtained, a new comparative analysis was performed between the two groups of each insult, between the OGD and Glutamate groups, and between the Sham and Control groups on GraphPad Prism v8.0.1 (GraphPad Software Inc). To compare the OGD and Sham groups, a Student's *t*-test (unpaired samples) was performed and to compare the Glutamate and Control groups, the OGD and Glutamate groups, and the Sham and Control groups, a Mann-Whitney test (unpaired samples) was performed. The fold change (FC) of the mean of each condition comparing to its control was calculated. Data is represented in box and whiskers graphs, where the whiskers represent the minimum and maximum values. The *p*-values are represented as: * $p < 0.05$ and ** $p < 0.01$.

In relation to the statistical analysis, the volcano plots, the PCA, the hierarchical clustering heatmaps, and the PLS-DA were performed in MetaboAnalyst 5.0 (https://www.metaboanalyst.ca) [147]. No data transformation was performed for any of the analyses, while auto scaling was done for all the analyses mentioned before. The data scaling allows comparison at the same level of variables with very different responses [149]. In PCA and PLS-DA, the ellipses present in the scores plots represent the 95% confidence regions.

Chapter 4
Results

4. RESULTS

Metabolomics Study of Primary Cultures of Cerebrocortical Neurons using LC-MS/MS – Data Analysis

In this study, the metabolome of primary cultures of cerebrocortical neurons subjected to two neuronal death stimuli was analyzed using LC-MS/MS. For data analysis, two approaches were carried out, an untargeted analysis and a targeted analysis.

4.1. Untargeted Analysis

For the untargeted analysis, with the filtered features processed in MarkerView™ Volcano plots were built (**Figure 19**) in order to demonstrate the features that were considered statistically different and with a FC smaller than 0.5 or greater than 2. For OGD and Sham groups (**Figure 19.A**), 73 of the 367 filtered features showed statistically significant differences ($-\log_{10}(p) > 1.30$, $p < 0.05$), 15 (in blue) are decreased in the OGD group compared to the Sham group ($\log_2(FC) < -1$, $FC < 0.5$) and 58 (in red) are increased in the OGD group compared to the Sham group ($\log_2(FC) > 1$, $FC > 2$). For Glutamate and Control groups (**Figure 19.B**), 11 of the 119 filtered features showed statistically significant differences ($-\log_{10}(p) > 1.30$, $p < 0.05$), 7 (in blue) are decreased in the Glutamate group compared to the Control group ($\log_2(FC) < -1$, $FC < 0.5$) and 4 (in red) are increased in the Glutamate group compared to the Control group ($\log_2(FC) > 1$, $FC > 2$). The data for both Volcano plots are detailed in Supplementary Table 1.

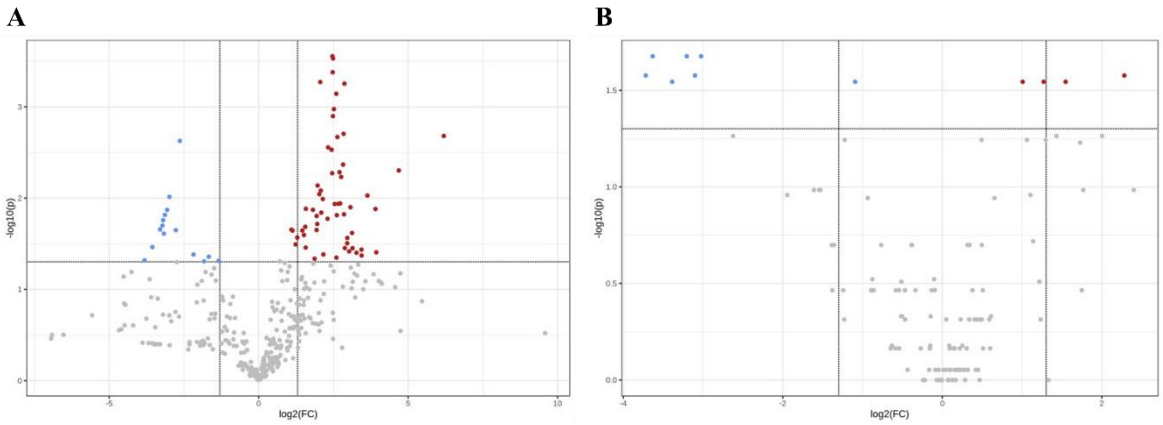

Figure 19. Volcano plots obtained in the comparison of data acquired by LC-MS/MS and processed in MarkerView™ software for the filtered metabolomics features of OGD and Sham groups (n = 3) (A), and of Glutamate and Control groups (n = 4) (B). Blue points represent features with statistically significant differences ($-\log_{10}(p) > 1.30$, $p < 0.05$) downregulated ($\log_2(FC) < -1$, $FC < 0.5$). Red points represent features with statistically significant differences ($-\log_{10}(p) > 1.30$, $p < 0.05$) upregulated ($\log_2(FC) > 1$, $FC > 2$). Grey points represent non-statistically significant features ($-\log_{10}(p) < 1.30$, $p > 0.05$). Volcano plots were performed in MetaboAnalyst 5.0 with auto scaling, fold change (FC) threshold of 2, direction of comparison of OGD/Sham (A) and Glutamate/Control (B), and *p*-value (*p*) threshold of 0.05.

After the filtering step, two approaches were carried out to compare the groups of each insult (**Figure 20**). In the first approach, univariate analysis was performed followed by multivariate analysis, while in the second approach, only multivariate analysis was performed. Univariate analysis was performed to select only the features with statistically significant differences ($p < 0.05$) between the two groups of each insult, in order to reduce the data matrix, while multivariate analysis was performed to select the most important features (features with VIP score > 1).

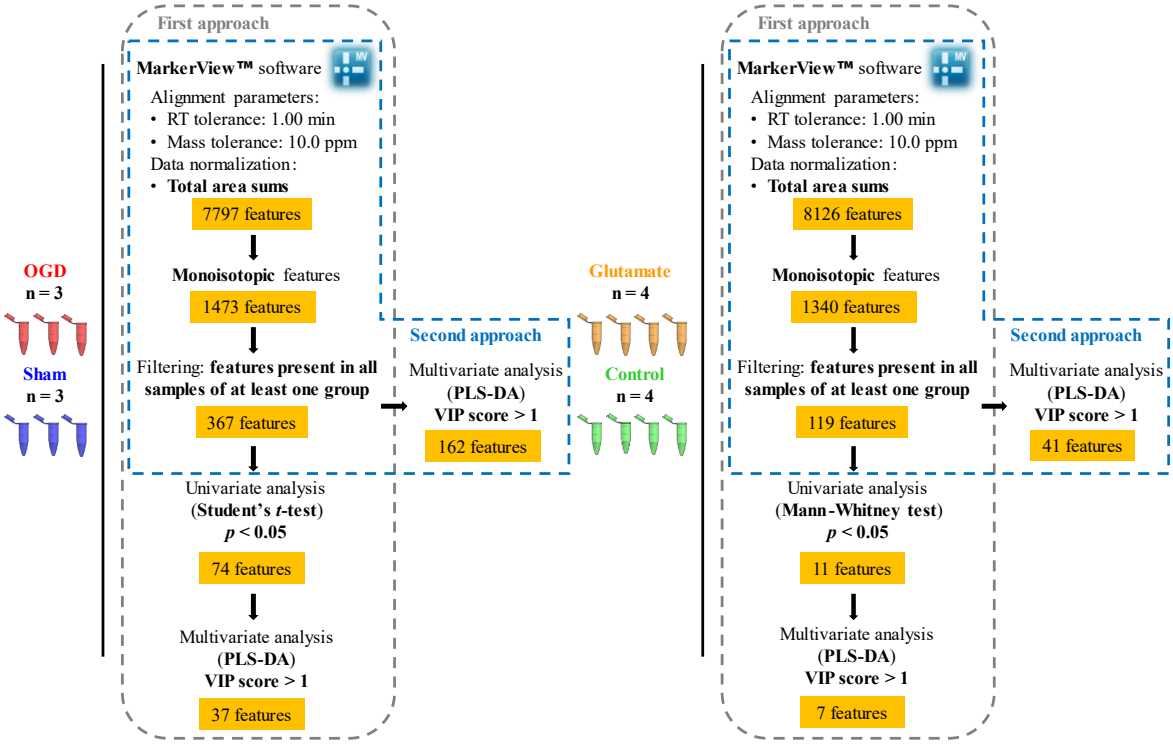

Figure 20. Approaches performed in the comparison of the groups of each insult (OGD insult: OGD (in red) and Sham (in blue) groups; glutamate stimulus: Glutamate (in yellow) and Control (in green) groups). First approach is represented by the grey dashed line and second approach is represented by the blue dashed line. After data processing in MarkerView™ software, selection of the monoisotopic features and of the features present in all samples of at least one group, in the first approach, univariate analysis (OGD vs Sham (n = 3): Student's *t*-test; Glutamate vs Control (n = 4): Mann-Whitney test) was performed followed by multivariate analysis (partial least squares-discriminant analysis (PLS-DA)), and in the second approach, only multivariate analysis (PLS-DA) was performed. RT: retention time; *p*: *p*-value; VIP: variable importance in projection.

Regarding first approach, to compare the OGD and Sham groups a Student's *t*-test was applied, and to compare the Glutamate and Control groups a Mann-Whitney test was applied. The most correct would have been to perform a non-parametric test to compare OGD and Sham groups, since the number of biological replicates performed for each group is small (n = 3), but a parametric test was performed, since it was not possible to apply a non-parametric test with a good response for n equal to 3 with the statistical analysis tools available.

The scores plots obtained from the multivariate analysis (PLS-DA) performed in each of the two approaches to select the features with VIP score greater than 1 are represented in Supplementary Figures 1.A and C (for the first approach) and in Supplementary Figures 2.A and C (for the second approach). The scores plots show the evident formation and separation

of the two respective groups (Supplementary Figures 1.A and 2.A: OGD group in red and Sham group in blue; Supplementary Figures 1.C and 2.C: Glutamate group in yellow and Control group in green). In Supplementary Figure 1.B and in Supplementary Figures 2.B and D are represented the VIP scores for the top 10 features for the respective groups. Supplementary Figure 1.D shows the VIP scores for all the 11 features with statistically significant differences ($p < 0.05$) of Glutamate and Control groups and 7 features have VIP score greater than 1.

In order to characterize, separately, the groups under analysis for each of the applied insults and to find the features responsible for the formation and separation of those groups, principal component analysis, an unsupervised method, was performed before and after the two approaches. Before performing the two approaches, PCA was performed using the LC-MS/MS data processed in MarkerView™ of the filtered features (OGD and Sham groups: 367 features; Glutamate and Control groups: 119 features) (**Figure 21**). After performing the two approaches, PCA was performed using the LC-MS/MS data of the features obtained in each of the approaches (first approach (**Figure 22**): 37 features (OGD and Sham groups) and 7 features (Glutamate and Control groups) with statistically significant differences ($p < 0.05$) and VIP score greater than 1; second approach (Supplementary Figure 3): 162 features (OGD and Sham groups) and 41 features (Glutamate and Control groups) with VIP score greater than 1).

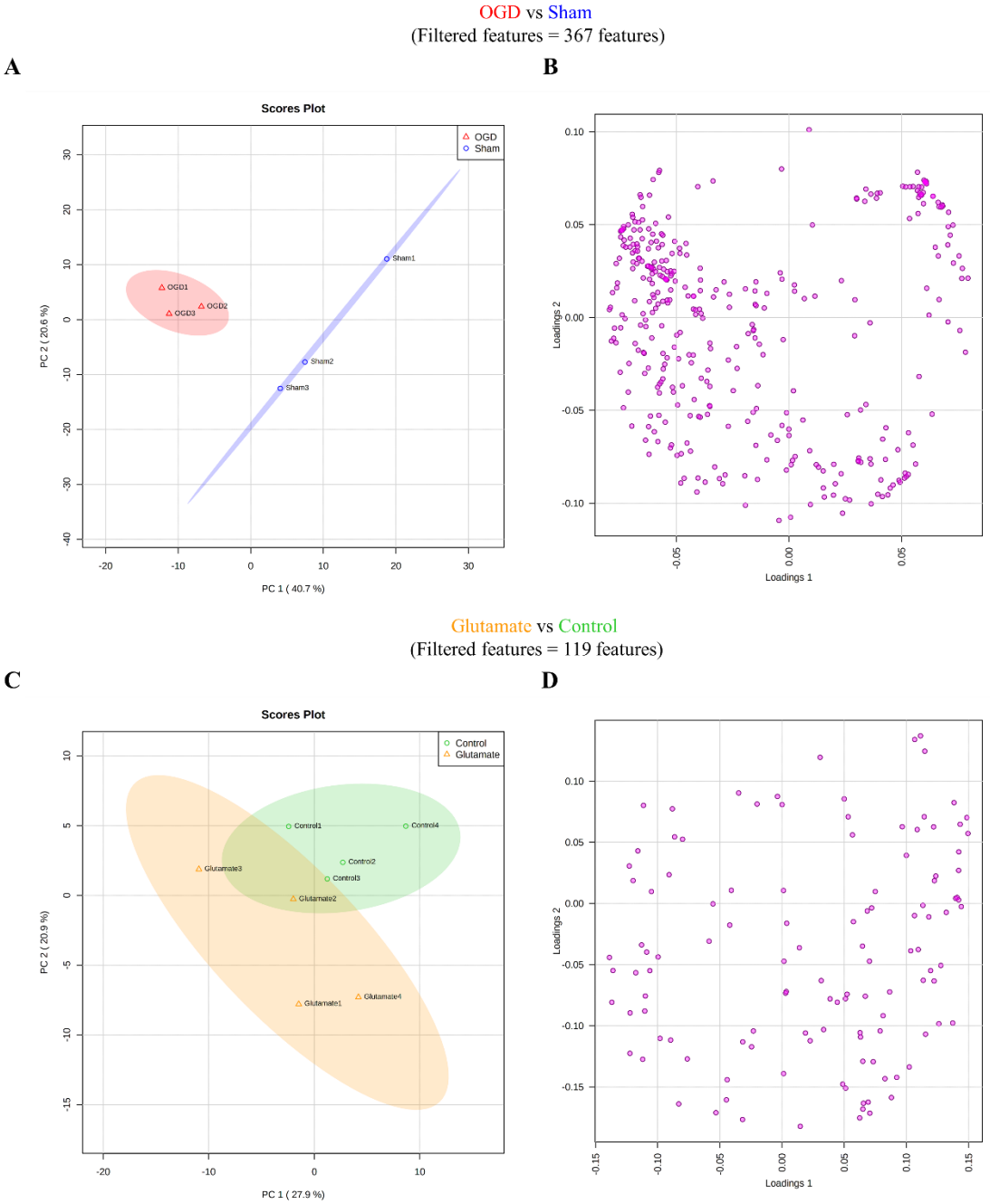

Figure 21. Principal component analysis (PCA) of data acquired by LC-MS/MS and processed in MarkerView™ software for OGD and Sham groups (n = 3) (A and B) and for Glutamate and Control groups (n = 4) (C and D). Scores plot (A) and loadings plot (B) obtained using the data of the 367 filtered features of OGD and Sham groups. Scores plot (C) and loadings plot (D) obtained using the data of the 119 filtered features of Glutamate and Control groups. The scores plot (A) shows the formation and separation of the respective two groups along the PC1: OGD group in red and Sham group in blue. The scores plot (C) shows an overlap of the two respective groups: Glutamate group in yellow and Control group in green. The ellipses represent the 95% confidence regions. PCA was performed in MetaboAnalyst 5.0 with auto scaling.

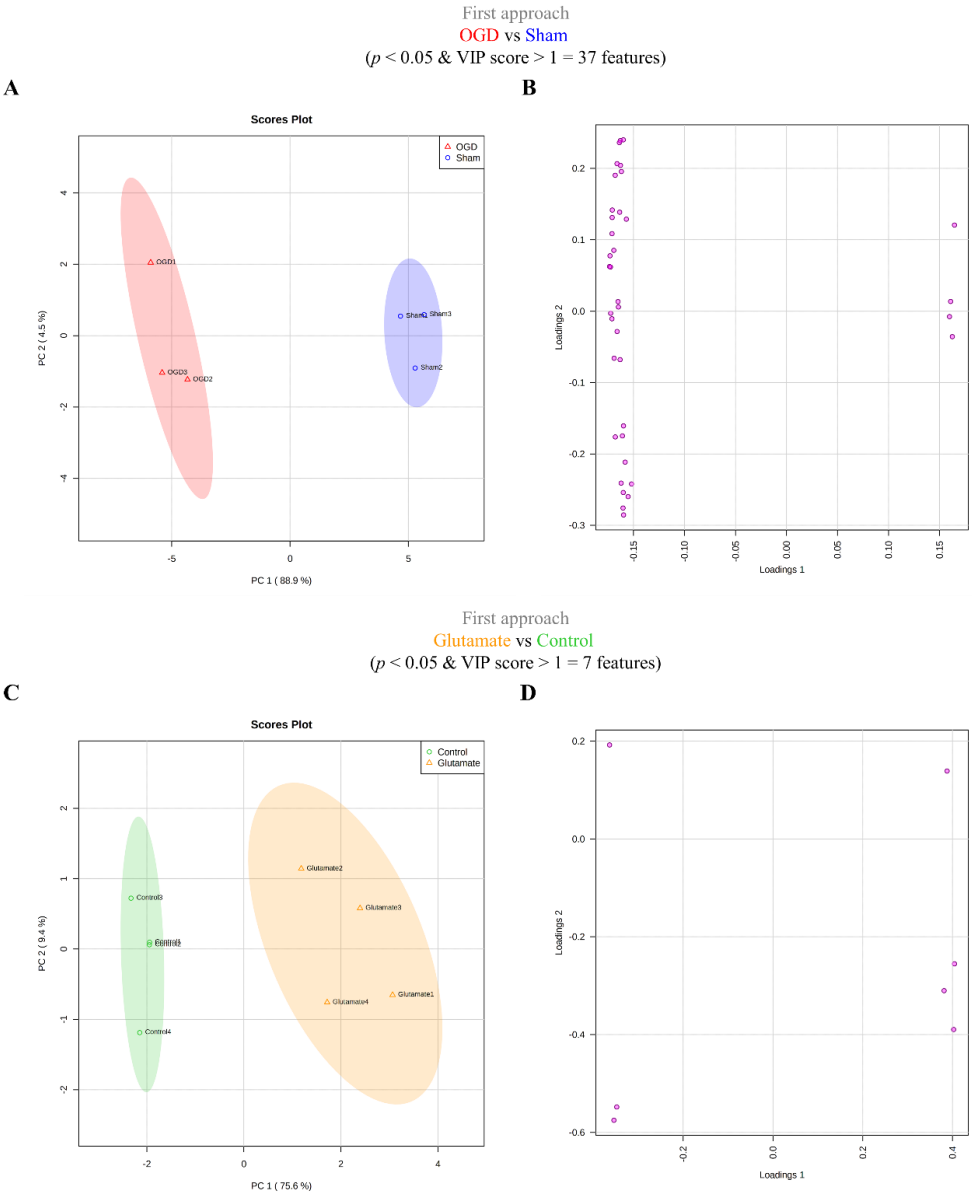

Figure 22. Principal component analysis (PCA) of data acquired by LC-MS/MS and processed in MarkerView™ software for OGD and Sham groups (n = 3) (A and B) and for Glutamate and Control groups (n = 4) (C and D). Scores plot (A) and loadings plot (B) obtained using the data of the 37 features with statistically significant differences (*p*-value (*p*) < 0.05) from Student's *t*-test and variable importance in projection (VIP) score greater than 1 from PLS-DA (first approach) of OGD and Sham groups. Scores plot (C) and loadings plot (D) obtained using the data of the 7 features with statistically significant differences ($p < 0.05$) from Mann-Whitney test and VIP score greater than 1 from PLS-DA (first approach) of Glutamate and Control groups. The scores plots (A and C) show the formation and separation of the respective two groups along the PC1 (OGD group in red and Sham group in blue (A); Glutamate group in yellow and Control group in green (C)), which are explained by the features with the largest contribution along the loadings 1 on the respective loadings plots (B and D). The ellipses represent the 95% confidence regions. PCA was performed in MetaboAnalyst 5.0 with auto scaling.

All the scores plots (**Figures 21.A** and **C**, **Figures 22.A** and **C**, and Supplementary Figures 3.A and C) show the scores values for the corresponding samples represented in the first two principal components (PC1 and PC2) using auto scaling and explain 61.3%, 48.8%, 93.4%, 85%, 78,6%, and 68% of the sample variance, respectively. The sample variance is better explained by the scores plots obtained using the data from the features selected in the first approach (**Figures 22.A** and **C**), since this approach is more selective and differential.

The scores plot (**Figure 21.A**) shows the formation and separation of the two groups (OGD group in red and Sham group in blue) along the first principal component (PC1), while the scores plot (**Figure 21.C**) shows an overlap of the two groups (Glutamate group in yellow and Control group in green). In **Figure 22** and Supplementary Figure 3, the scores plots show the formation and separation of the two respective groups (**Figure 22.A** and Supplementary Figure 3.A: OGD group in red and Sham group in blue; **Figure 22.C** and Supplementary Figure 3.C: Glutamate group in yellow and Control group in green) along the PC1, which are explained by the features with the largest contribution along the loadings 1 (features with the highest and lowest loadings 1 values) on the respective loadings plot (**Figure 22.B**, Supplementary Figure 3.B, **Figure 22.D** and Supplementary Figure 3.D).

After PCA, hierarchical clustering heatmaps were performed to identify samples and/or features that are unusually high or low between samples, using the LC-MS/MS data processed in MarkerView™ of the features obtained in each of the approaches for the groups of each insult (Supplementary Figure 4 and Supplementary Figure 5). In the hierarchical clustering heatmaps, the hierarchical clustering analysis (on top) shows the separation of the two groups, OGD group in red and Sham group in blue (Supplementary Figure 4), and Glutamate group in yellow and Control group in green (Supplementary Figure 5). Through the heatmaps it is possible to verify the formation of two clusters (1 and 2). In Supplementary Figure 4, cluster 1 contains the features increased in the Sham group and cluster 2 contains the features increased in the OGD group, which correspond to the features with positive and negative loading values across the loadings 1, respectively, in **Figure 22.B** and Supplementary Figure 3.B. In Supplementary Figure 5, cluster 1 contains the features increased in the Glutamate group and cluster 2 contains the features increased in the Control group, which correspond to the features with positive and negative loading values across the loadings 1, respectively, in **Figure 22.D** and Supplementary Figure 3.D. Through the heatmaps it is also possible to verify that there is no homogeneity among the samples

(columns) of each group, since there are features (rows) that are more increased or more decreased in only one or two samples of the same group.

Hierarchical clustering heatmaps were also performed using the data obtained through the quantification performed in Sciex OS™ software for the features obtained in the first approach for the groups of each insult. For OGD and Sham groups (Supplementary Figure 6.B), similar to what was observed in the hierarchical clustering heatmap obtained with the data derived from the quantification performed in MarkerView™ (Supplementary Figure 6.A), the hierarchical clustering analysis (on top) shows the separation of the two groups with different features than those obtained for the quantification performed in MarkerView™. On the other hand, for Glutamate and Control groups (Supplementary Figure 7.B), the separation of the two groups is not visible with the hierarchical clustering analysis, as observed in the hierarchical clustering heatmap obtained with the data derived from the quantification performed in MarkerView™ (Supplementary Figure 7.A). For the quantification done in Sciex OS™, no clustering is visible on the heatmaps.

Metabolite Identification performed in Sciex OS™ Software

Following the analyses performed on MetaboAnalyst 5.0 platform, regarding untargeted analysis, metabolite identification was performed in Sciex OS™ software using the IDA data files and looking specifically at the *m/z* values and retention times of the interesting features selected in each of the two approaches performed to compare the two groups of each insult (**Figure 20**) (first approach: 37 features (OGD and Sham groups) and 7 features (Glutamate and Control groups) with statistically significant differences ($p < 0.05$) and VIP score greater than 1; second approach: 162 features (OGD and Sham groups) and 41 features (Glutamate and Control groups) with VIP score greater than 1), and all the available libraries to perform the search, in order to be able to identify endogenous (coming from the cells) and exogenous metabolites. With the LC-MS/MS data of the features of OGD and Sham groups, 2 metabolites were identified for the first approach and with the second approach 7 more metabolites were identified, obtaining a total of 9 metabolites. The criteria used to consider as an identification were a mass error smaller than 50 ppm and a library score greater than 70.

Next, 7 of the 9 metabolites identified were quantified in Sciex OS™ software using the SWATH data files, namely: tyrosine, tryptophan, diaveridine, methylthioadenosine,

sphinganine, maltose/sucrose, and helvolic acid. The criteria used to select which peak (precursor or one of the three most intense fragments) was used for quantification were: peak with a good intensity (S/N > 10), a gaussian-shaped chromatogram, a mass error smaller than 50 ppm, and a library score greater than 70.

In the untargeted analysis, the peak area integration algorithm used in metabolite identification was MQ4, since the method was created using the peaks (features) previously detected by MarkerView™ software. On the other hand, in the targeted analysis, the AutoPeak was the peak area integration algorithm used in metabolite identification, since in this analysis, the detection of the peaks was necessary and this algorithm makes a better distinction of signal versus noise. Regarding quantification, in both analyses, the MQ4 algorithm was used, since this algorithm performs a better integration of the peaks and, consequently, a more correct quantification.

The limit of quantification (LOQ) and the limit of detection (LOD) are characteristics evaluated in the determination of the validation of an analytical procedure. The LOQ corresponds to the lowest amount of an analyte that can be quantitatively determined with appropriate accuracy and precision in a sample, whereas the LOD corresponds to the lowest amount of an analyte that can be detected but not necessarily quantified as an exact value in a sample. Both can be determined based on signal-to-noise ratio (S/N), which in turn is determined by comparing signals from samples with known low concentrations of analyte and signals from blank samples. For LOQ, the S/N is 10 and for LOD is 3, which corresponds to the minimum concentration at which the analyte can be quantified and detected with confidence, respectively. [150,151] Thus, in this work, one of the criteria used to select which peak to use to perform the quantification was a S/N greater than 10.

For each identified metabolite, the precursor *m/z* and the retention time used for metabolite identification are represented in Supplementary Table 2 and the precursor or fragment *m/z* and the retention time used for metabolite quantification are represented in **Table 3**. The results of the quantification performed in Sciex OS™ for the 7 metabolites identified and quantified are graphically represented in **Figure 23** for the two groups of each insult. The data represented correspond to the area ratio for each sample of each group, that is, the peak area obtained from Sciex OS™ software normalized to the total area sum of all detected features in MarkerView™ software for each sample. In **Table 4** are represented the

data obtained after quantification (mean values of each group, *p*-value resulting from the statistical test, and base-2 logarithm (log) of the FC) for the aforementioned metabolites.

Table 3. Metabolites identified in Sciex OS™ software using the LC-MS/MS data of the interesting features selected in each of the two approaches for OGD and Sham groups for the untargeted metabolomics analysis of the primary cultures of cerebrocortical neurons submitted to an OGD insult and a glutamate stimulus, with the respective precursor or fragment mass-to-charge ratio (*m/z*) and retention time (RT) used for quantification. M+Na: sodium adduct.

Untargeted analysis			
Metabolite	**Precursor *m/z***	**Fragment *m/z***	**RT (min)**
Tyrosine	182.08117	136.0754	4.56
Tryptophan	205.09715	188.0706	7.66
Diaveridine	261.13460	-	2.09
Methylthioadenosine	298.09684	136.0667	7.89
Sphinganine	302.30536	284.2949	26.03
Maltose/Sucrose, M+Na	365.10543	203.0533	2.88
Helvolic acid	569.31089	-	25.17

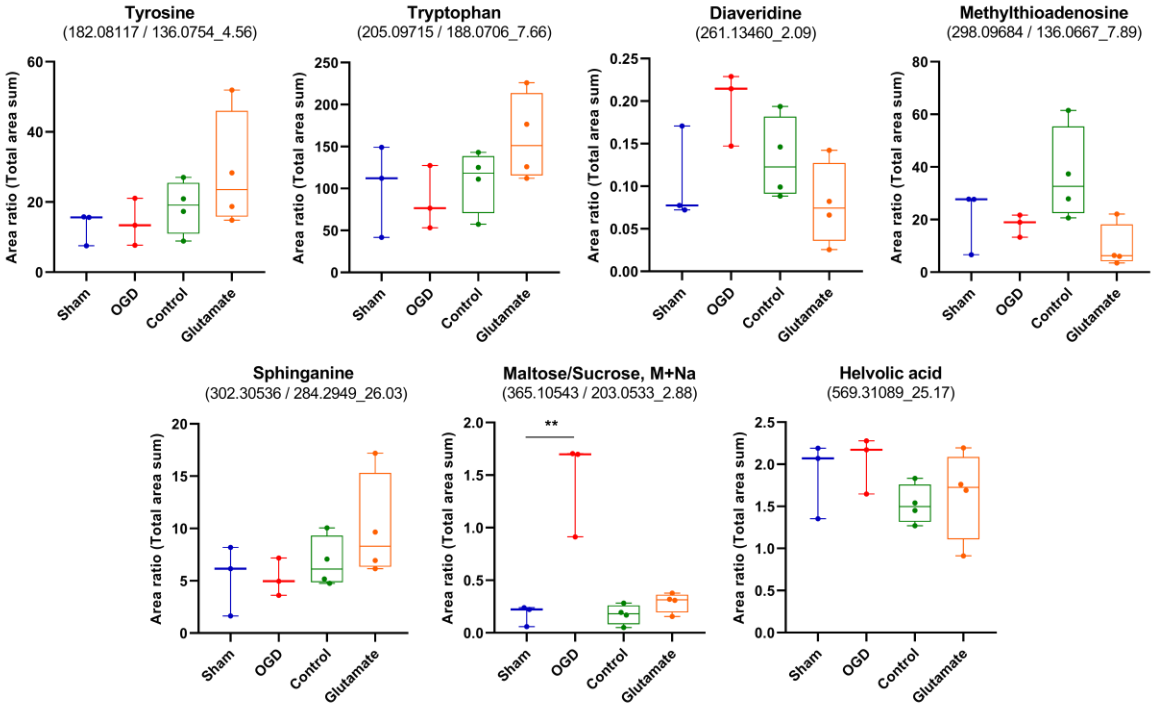

Figure 23. Quantification of the metabolite identifications obtained in Sciex OS™ software using the LC-MS/MS data of the interesting features selected in each of the approaches performed (first approach: features with statistically significant differences ($p < 0.05$) and VIP score greater than 1; second approach: features with VIP score greater than 1) for OGD and Sham groups (n = 3). In brackets are represented the precursor *m/z* value followed by the fragment *m/z* value and the retention time used to perform the quantification. The metabolite identifications with only one *m/z* value were quantified using the precursor *m/z* value. The data represent the area ratio for each sample of each group (Sham, OGD, Control and Glutamate). Area ratio corresponds to the peak area obtained from Sciex OS™ software normalized to the total area sum of all detected features in MarkerView™ software for each sample. The whiskers represent the minimum and maximum area ratio values. Significance (Sham vs OGD: Student's *t*-test): ** $p < 0.01$. M+Na: sodium adduct.

As presented in **Figure 23**, after quantification, of the 7 metabolites identified and quantified only maltose/sucrose showed statistically significant differences ($p = 0.0093$; see **Table 4**) between the Sham and OGD groups.

Table 4. Metabolites identified in Sciex OS™ software using the LC-MS/MS data of the interesting features selected in each of the two approaches for OGD and Sham groups for the untargeted metabolomics analysis. The data represented were obtained from two models of induced neuronal death based on oxygen and glucose deprivation (OGD) and glutamate excitotoxicity, with the respective controls for each model, performed on primary cultures of cerebrocortical neurons. For each model (OGD vs Sham and Glutamate vs Control), the data obtained after quantification in Sciex OS™ software (mean values of each group, *p*-value, and base-2 logarithm (log) of fold change (FC)) are represented. To compare the OGD and Sham groups was performed a Student's *t*-test and to compare the Glutamate and Control groups was performed a Mann-Whitney test. The FC is the ratio between the two group means. SEM: standard error of the mean; M+Na: sodium adduct.

Untargeted analysis								
	OGD vs Sham				**Glutamate vs Control**			
Metabolite	**Sham mean ± SEM**	**OGD mean ± SEM**	***p*-value**	**log_2(FC) (OGD/Sham)**	**Control mean ± SEM**	**Glutamate mean ± SEM**	***p*-value**	**log_2(FC) (Glutamate/Control)**
Tyrosine	12.975 ± 2.713	14.037 ± 3.891	0.8339	0.113	18.543 ± 3.791	28.455 ± 8.319	0.4857	0.618
Tryptophan	101.038 ± 31.468	85.719 ± 21.878	0.7098	-0.237	109.158 ± 18.467	160.116 ± 25.940	0.2000	0.553
Diaveridine	0.107 ± 0.032	0.197 ± 0.025	0.0917	0.882	0.132 ± 0.024	0.079 ± 0.024	0.1143	-0.738
Methylthioadenosine	20.686 ± 7.037	18.014 ± 2.473	0.7383	-0.200	36.833 ± 8.897	9.509 ± 4.240	0.0571	-1.954
Sphinganine	5.330 ± 1.934	5.246 ± 1.042	0.9711	-0.023	6.769 ± 1.210	9.989 ± 2.518	0.4857	0.561
Maltose/Sucrose, M+Na	0.173 ± 0.058	1.438 ± 0.263	0.0093	3.053	0.174 ± 0.048	0.290 ± 0.047	0.2000	0.737
Helvolic acid	1.871 ± 0.262	2.033 ± 0.195	0.6463	0.120	1.523 ± 0.117	1.640 ± 0.267	0.6857	0.106

Metabolite Annotation performed in XCMS™ Platform

After metabolite identification and quantification in Sciex OS™ software, the interesting features, selected in each of the two approaches performed for the comparison of the groups of each insult, for which no metabolite identification was obtained in Sciex OS™ were also quantified. For the second approach, due to the large number of features, only the 10 features with the highest VIP score were quantified. After quantification, 21 features showed statistically significant differences ($p < 0.05$), 19 features for OGD and Sham groups, and 2 features for Glutamate and Control groups. Then, in order to find for more potential biomarkers with the data of these features, an analysis was performed in the online platform XCMS™. Through this analysis, 4 metabolite annotations were obtained for 4 of the 19 features that showed statistically significant differences between the OGD and Sham groups (feature 431.1643_7.79: tamsulosin; feature 621.4069_25.05: hericenone D/hericenone G; features 437.1894_24.98 and 506.3134_32.93: small peptides with 3/4 amino acids, such as ACFP, MTW, and CKKK). For the 2 features that showed statistically significant differences between the Glutamate and Control groups were obtained 2 metabolite annotations (features 506.3188_27.42 and 599.3116_25.30: small peptides with 4 amino acids, such as KKCK and HRTW). As annotations corresponding to small peptides were obtained, an analysis was performed in the ProteinPilot™ software to verify if these small peptides matched to sequences of eventual proteins that might be present in the samples, but no match was obtained.

The results of the quantification of the metabolite annotations are graphically represented in **Figure 24** for the two groups of each insult, and the data obtained after quantification (mean values of each group, *p*-value resulting from the statistical test, and base-2 logarithm of the FC) for each metabolite annotation are shown in **Table 5**. In Supplementary Table 3 are represented the interesting features of OGD and Sham groups (first thirty-one) and of Glutamate and Control groups (last eight) for which no metabolite identification was obtained in Sciex OS™ and no metabolite annotation was obtained in XCMS™, with the respective data obtained after quantification.

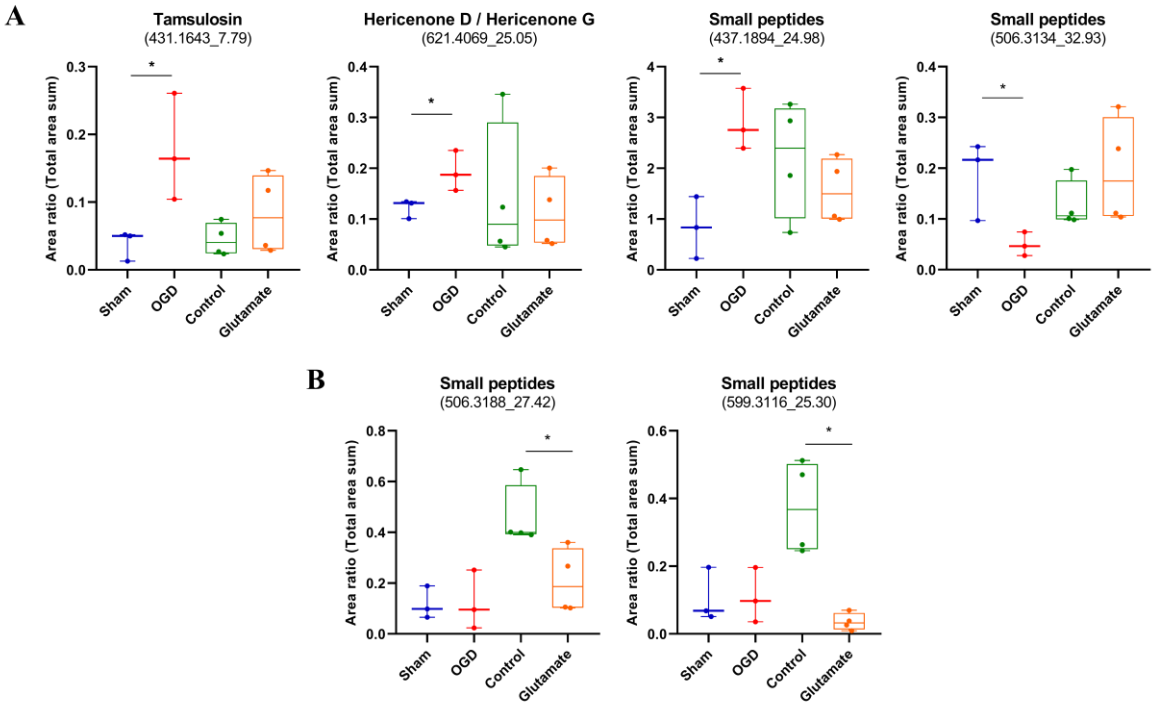

Figure 24. Quantification of the metabolite annotations obtained in XCMS™ platform for the features that showed statistically significant differences after quantification in Sciex OS™ software, which derived from the features selected in each of the approaches performed (first approach: features with statistically significant differences ($p < 0.05$) and VIP score greater than 1; second approach: features with VIP score greater than 1) for which no identification was obtained in Sciex OS™ software for OGD and Sham groups (n = 3) (A) and for Glutamate and Control groups (n = 4) (B). For each metabolite annotation, the respective *m/z* value and retention time used to perform the quantification are represented in brackets. The data represent the area ratio for each sample of each group (Sham, OGD, Control and Glutamate). Area ratio corresponds to the peak area obtained from Sciex OS™ software normalized to the total area sum of all detected features in MarkerView™ software for each sample. The whiskers represent the minimum and maximum area ratio values. Significance (Sham vs OGD: Student's *t*-test; Control vs Glutamate: Mann-Whitney test): * $p < 0.05$.

Table 5. Metabolite annotations obtained in XCMS™ platform and respective statistically different features, which derived from the interesting features selected in each of the two approaches for which no identification was obtained in Sciex OS™ software for OGD and Sham groups (first four) and for Glutamate and Control groups (last two). The data represented were obtained from two models of induced neuronal death based on oxygen and glucose deprivation (OGD) and glutamate excitotoxicity, with the respective controls for each model, performed on primary cultures of cerebrocortical neurons. For each model (OGD vs Sham and Glutamate vs Control), the data obtained after quantification in Sciex OS™ software (mean values of each group, *p*-value, and base-2 logarithm (log) of fold change (FC)) are represented. To compare the OGD and Sham groups was performed a Student's *t*-test and to compare the Glutamate and Control groups was performed a Mann-Whitney test. The FC is the ratio between the two group means. *m/*z: mass-to-charge ratio; RT: retention time; SEM: standard error of the mean.

Untargeted analysis								
	OGD vs Sham				**Glutamate vs Control**			
Metabolite annotation (**Feature** (*m/*z_RT))	**Sham mean ± SEM**	**OGD mean ± SEM**	***p*-value**	**log_2(FC) (OGD/Sham)**	**Control mean ± SEM**	**Glutamate mean ± SEM**	***p*-value**	**log_2(FC) (Glutamate/Control)**
Tamsulosin (431.1643_7.79)	0.038 ± 0.013	0.176 ± 0.046	0.0432	2.205	0.045 ± 0.012	0.082 ± 0.029	0.3429	0.879
Hericenone D/G (621.4069_25.05)	0.122 ± 0.011	0.193 ± 0.023	0.0485	0.660	0.143 ± 0.070	0.112 ± 0.035	0.8857	-0.347
Small peptides (437.1894_24.98)	0.834 ± 0.352	2.908 ± 0.350	0.0139	1.803	2.197 ± 0.572	1.565 ± 0.319	0.6857	-0.490
Small peptides (506.3134_32.93)	0.185 ± 0.045	0.050 ± 0.014	0.0444	-1.899	0.127 ± 0.024	0.194 ± 0.053	0.2000	0.608
Small peptides (506.3188_27.42)	0.118 ± 0.037	0.124 ± 0.067	0.9435	0.069	0.459 ± 0.063	0.209 ± 0.063	0.0286	-1.136
Small peptides (599.3116_25.30)	0.105 ± 0.046	0.110 ± 0.047	0.9495	0.059	0.373 ± 0.069	0.036 ± 0.013	0.0286	-3.380

Metabolic Pathways Analysis performed in MetaboAnalyst

Finally, regarding untargeted analysis, metabolic pathways analysis (functional analysis) was performed to verify which metabolic pathways are altered after performing each of the two insults (OGD insult and glutamate stimulus). The analysis was performed in Metaboanalyst 5.0 using possible metabolite matches/annotations obtained from the LC-MS/MS data (*m/*z values and retention times) of the monoisotopic features of OGD and Sham groups (**Figure 25.A**) and of Glutamate and Control groups (**Figure 25.B**), the Mummichog algorithm, and *Rattus norvegicus* (rat) library. The Mummichog algorithm has the ability to predict the biological activity directly from the mass spectrometry data without previous identification of the metabolites, but considering putative annotations [148].

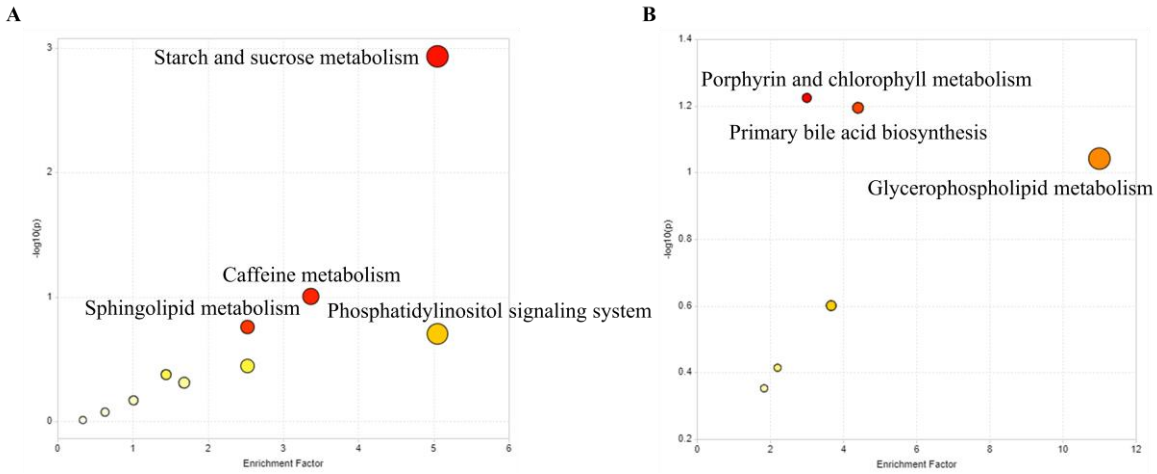

Figure 25. Metabolic pathways analysis (functional analysis) using the annotations obtained from the LC-MS/MS data processed in MarkerView™ software of the monoisotopic features of OGD and Sham groups (A) and of Glutamate and Control groups (B). The enrichment factor (*x*-axis) is the ratio between the number of significant pathway hits from the uploaded data and the expected number of hits within that pathway, while the *p*-value in -$\log_{10}(p)$ (y-axis) corresponds to how significant a pathway is given the input data. The analysis was performed in MetaboAnalyst 5.0 using Pareto scaling, the Mummichog algorithm and *Rattus norvegicus* (rat) library.

For OGD insult, the metabolic pathways found to be significantly altered were the following: starch and sucrose metabolism; phosphatidylinositol signaling system; caffeine metabolism; and sphingolipid metabolism (**Figure 25.A**). For glutamate stimulus, the metabolic pathways found to be significantly altered were: porphyrin and chlorophyll

metabolism; primary bile acid biosynthesis; and glycerophospholipid metabolism (**Figure 25.B**).

In **Table 6** are summarized the KEGG compound entries resulting from the metabolic pathways analysis performed for the two groups of each insult (OGD vs Sham and Glutamate vs Control), with the corresponding metabolites, metabolic pathways, and *m/z* values and retention times used to perform the quantification in Sciex OS™ software. The results of the quantification of the KEGG compound entries are graphically represented in Supplementary Figure 8 (for OGD and Sham groups) and in Supplementary Figure 9 (for Glutamate and Control groups). In Supplementary Table 4, are depicted the data obtained after quantification (mean values of each group, *p*-value resulting from the statistical test, and base-2 logarithm of the FC) for each KEGG compound entry.

Through this analysis, it was possible to annotate the metabolites maltose/sucrose and sphinganine, which had been previously identified and quantified in the Sciex OS™ software (**Figure 23**) by matching their fragmentation spectra with a metabolite library.

Table 6. KEGG compound entries obtained through the metabolic pathways analysis (functional analysis) obtained from LC-MS/MS data of the monoisotopic features of OGD and Sham groups (OGD vs Sham) and of Glutamate and Control groups (Glutamate vs Control) using the Mummichog algorithm and *Rattus norvegicus* (rat) library, with the respective metabolites, metabolic pathways, mass-to-charge ratio (*m/z*) and retention time (RT) used for quantification. Entries with an asterisk (*) indicate significant hits and entries with a number sign (#) indicate non-significant hits. CDP-choline: cytidine 5-diphosphocholine.

					Feature (*m/z*_RT)	
	KEGG compound entries	*** / #**	**Metabolites**	**Metabolic pathways**	***m/z***	**RT (min)**
OGD vs Sham	C00095/C00031/ C00137/ C13747/C07480	*	Fructose/Glucose/ *myo*-Inositol/ Paraxanthine/Theobromine	Starch and sucrose metabolism/ Phosphatidylinositol signaling system/ Caffeine metabolism	203.0478	2.12
	C16361	*	1,3,7-Trimethyluric acid	Caffeine metabolism	211.0872	14.50
	C00319/C02934	*	Sphingosine/ 3-Dehydrosphinganine	Sphingolipid metabolism	300.2813	25.08
	C12144	#	Phytosphingosine		318.2940	24.57
	C00721	*	Dextrin	Starch and sucrose metabolism	527.1562	21.72
	C00208/C00089/C00252/ C01083/C00185	*	Maltose/Sucrose/Isomaltose/ α-Trealose/Cellobiose		203.0533	2.88
	C00836	*	Sphinganine	Sphingolipid metabolism	284.2949	26.03
Glutamate vs Control	C00695	#	Cholate	Primary bile acid biosynthesis	431.2681	23.56
	C01921	*	Glycocholate		466.3109	21.12
	C00307	*	CDP-choline	Glycerophospholipid metabolism	471.1257	21.41
	C05465	*	Taurochenodeoxycholate	Primary bile acid biosynthesis	482.3139	32.81
	C05122	#	Taurocholate		516.2925	25.93
	C01079	#	Protoporphyrinogen IX	Porphyrin and chlorophyll metabolism	569.3056	12.76
	C05791	*	D-Urobilinogen		573.2958	25.27
	C00486	*	Bilirubin		585.2828	12.79
	C00500	#	Biliverdin		641.2362	12.38
	C05770	*	Coproporphyrin III		655.2990	26.31
	C03263/C05768	#	Coproporphyrinogen III/ Coproporphyrinogen I		661.3385	25.24

	C01051/C05766	#	Uroporphyrinogen III/ Uroporphyrinogen I		859.3006	25.11

4.2. Targeted Analysis

After performing the untargeted metabolomics analysis, in which the identification of all possible metabolites was performed from features previously detected in the MarkerView™ software, a targeted metabolomics analysis was performed, in which the metabolite identification was performed from prior information of precursor *m/z* values and retention times of a set of metabolites imported from libraries, which allowed the identification of other compounds.

Regarding targeted analysis, performed in Sciex OS™ software, metabolite identification and quantification were also performed. Metabolite identification was performed using the IDA data files and only two libraries, the AB Sciex library and the laboratory (in-house) library, to perform the search, in order to identify only endogenous metabolites. Thus, for targeted analysis, 44 metabolites were identified. The criteria used to consider as an identification were the following: a mass error smaller than 50 ppm and a library score greater than 70.

Then, 27 of the 44 metabolites identified were quantified using the SWATH data files and the criteria used to select which fragment (one of the three most intense fragments) was used for quantification were: peak with a good intensity (S/N > 10), a gaussian-shaped chromatogram, a mass error smaller than 50 ppm, and a library score greater than 70.

For each of the 27 metabolites, in Supplementary Table 5, are represented the precursor *m/z* used for metabolite identification, the fragment *m/z* used for metabolite quantification, and the retention time used for both. The results of the quantification performed in Sciex OS™ for the 3 metabolites that showed statistically significant differences between the Control and Glutamate groups (*O*-acetylcarnitine, β-nicotinamide adenine dinucleotide, and flavin adenine dinucleotide (FAD)), and for the metabolite that showed statistically significant differences between the Sham and OGD groups (maltose/sucrose), after quantification, are graphically represented in **Figure 26**. As before, the data represented correspond to the area ratio for each sample of each group, that is, the peak area obtained from Sciex OS™ software normalized to the total area sum of all detected features in MarkerView™ software for each sample. In **Table 7**, are represented the data obtained after quantification (mean values of each group, *p*-value resulting from the statistical test, and base-2 logarithm of the FC) for the metabolites mentioned above. The results of the quantification for the metabolites that showed no statistically significant

differences are not shown, but in Supplementary Table 6, are depicted the data obtained after quantification for these metabolites and it can be seen that the metabolites methylthioadenosine and *S*-adenosylhomocysteine have a *p*-value close to 0.05 (the threshold for considering it a statistically significant difference) for Glutamate and Control groups.

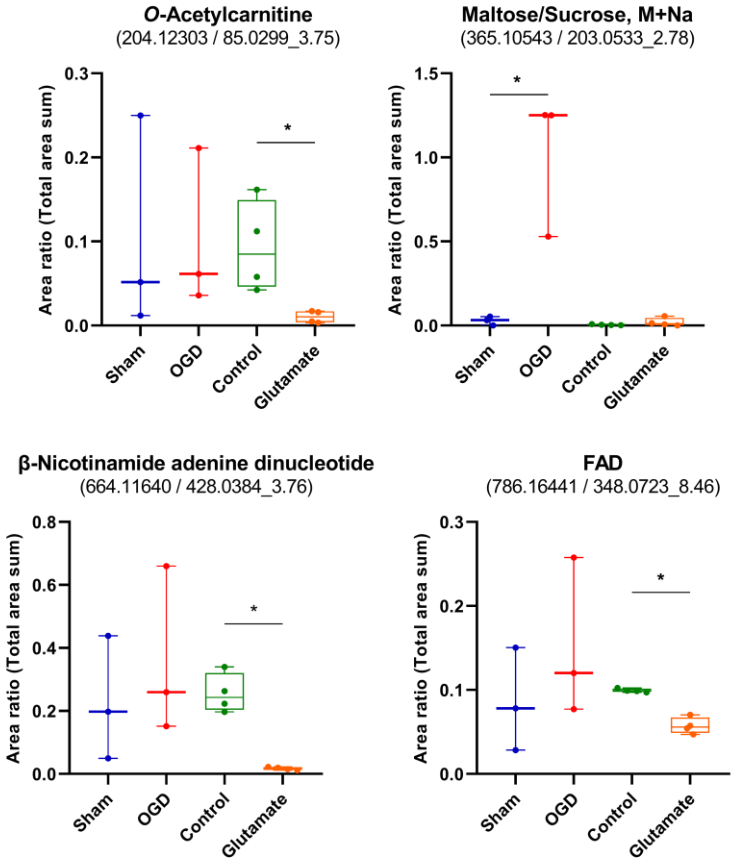

Figure 26. Quantification of the metabolites with statistically significant differences obtained for the targeted analysis performed in Sciex OS™ software. In brackets are represented the precursor *m/z* value followed by the fragment *m/z* value and the retention time used to perform the quantification. The data represent the area ratio for each sample of each group (Sham, OGD, Control and Glutamate). Area ratio corresponds to the peak area obtained from Sciex OS™ software normalized to the total area sum of all detected features in MarkerView™ software for each sample. The whiskers represent the minimum and maximum area ratio values. Significance (Control vs Glutamate: Mann-Whitney test; Sham vs OGD: Student's *t*-test): * $p < 0.05$. M+Na: sodium adduct; FAD: flavin adenine dinucleotide.

Table 7. Metabolites identified and quantified in Sciex OS™ software for the targeted metabolomics analysis that showed statistically significant differences (*p*-value smaller than 0.05) after quantification. The data represented were obtained from two models of induced neuronal death based on oxygen and glucose deprivation (OGD) and glutamate excitotoxicity, with the respective controls for each model, performed on primary cultures of cerebrocortical neurons. For each model (OGD vs Sham and Glutamate vs Control), the data obtained after quantification in Sciex OS™ software (mean values of each group, *p*-value, and base-2 logarithm (log) of fold change (FC)) are represented. To compare the OGD and Sham groups was performed a Student's *t*-test and to compare the Glutamate and Control groups was performed a Mann-Whitney test. The FC is the ratio between the two group means. SEM: standard error of the mean; M+Na: sodium adduct; FAD: flavin adenine dinucleotide.

Targeted analysis								
	OGD vs Sham				**Glutamate vs Control**			
Metabolite	**Sham mean ± SEM**	**OGD mean ± SEM**	***p*-value**	**log_2(FC) (OGD/Sham)**	**Control mean ± SEM**	**Glutamate mean ± SEM**	***p*-value**	**log_2(FC) (Glutamate/Control)**
O-Acetylcarnitine	0.105 ± 0.074	0.103 ± 0.055	0.9865	-0.023	0.093 ± 0.027	0.010 ± 0.004	0.0286	-3.176
Maltose/Sucrose, M+Na	0.029 ± 0.015	1.011 ± 0.241	0.0152	5.147	0.005 ± 0.001	0.019 ± 0.013	0.4857	2.055
β-Nicotinamide adenine dinucleotide	0.229 ± 0.113	0.357 ± 0.154	0.5395	0.643	0.256 ± 0.031	0.017 ± 0.002	0.0286	-3.894
FAD	0.086 ± 0.035	0.152 ± 0.054	0.3673	0.824	0.099 ± 0.001	0.057 ± 0.005	0.0286	-0.794

Chapter 5
Discussion

5. DISCUSSION

Hypoxic-ischemic encephalopathy is a disease that results from an event of hypoxia-ischemia following perinatal asphyxia, that in turn can lead to newborn brain injury. Currently, the absence of accuracy, accessibility, and speed in the diagnosis of HIE, and the incapability to differentiate and identify the newborns who are at risk of evolving to moderate or severe HIE lead to the urgent need for investigation of HIE biomarkers. [152]

In this project, in order to find potential biomarkers that could be applied in the clinical diagnosis of HIE, a metabolomics screening of primary cultures of neurons isolated from the rat cerebral cortex and subjected to two neuronal death induction models, an OGD model and a glutamate-based model, was performed. The OGD model mimics what happens in a HIE situation, from primary brain energy failure, due to decreased oxygen and glucose levels caused by an inadequate blood supply to the brain, to neuronal death. In the case of the glutamate-based model, specifically, induces neuronal death due to high concentrations of this neurotransmitter, triggering excessive depolarization of the neuron membranes, over-stimulation of the glutamate receptors, and therefore neuronal death. [10,17,25]

The glutamate model acted as the positive control of the OGD model performed in this study. Through glutamate stimulus it is possible to infer about the functionality of the glutamate receptors present on the surface of the neuron membranes, which is directly associated to excitotoxicity-induced neuronal death. If the receptors are not functional, adding glutamate to the neurons does not cause their death by excitotoxicity. Thus, if neuronal death occured, it is possible to infer that excitotoxicity pathways were activated and glutamate receptors were functional. If excitotoxicity-induced neuronal death had not occurred in the glutamate model there could possibly be cell death in the OGD model not by excitotoxicity, but by other mechanisms associated with changes in metabolism due to the absence of oxygen and glucose, such as, imbalance of cellular homeostasis due to the failure of ATP-dependent pumps. [25-27]

After performing both models, OGD model and glutamate-based model, and before extracting both the proteome and the metabolome from the cells, it was observed by phase-contrast microscopy that the neuronal network was more destroyed in the primary cultures that were submitted to the glutamate stimulus than in the primary cultures that were

submitted to the OGD insult, indicating a different extent of neuronal death between the two insults/stimuli. These data were previously validated by other team members by immunocytochemistry and Western blot by tagging the microtubule associated protein 2 (MAP2). [153] In order to make the extent of neuronal death of the two insults comparable, it is necessary to increase the insult time for the OGD model in order to try to be more severe, which is being optimized by the research team. Nevertheless, this does not imply that the glutamate model is not a good positive control of the OGD model, since the glutamate model was used as a positive control to deduce about the functionality of the glutamate receptors.

For both analyses (untargeted and targeted), after quantification of the metabolites identified (**Figure 23** and **Figure 26**, respectively), it is possible to observe that the control groups of both insults do not show significant differences between them. This allows to infer that the change to Sham medium when studying the OGD insult control group had no interference in the results.

Regarding the untargeted metabolomics analysis, after acquisition by LC-MS/MS, the first analysis performed was the Volcano plots, which combine FC and *p*-value analyses in a single graph, which allows the selection of features (characterized by a *m/z* and a retention time) with biologically and/or statistically significant differences [147]. Through this analysis it was found that for the glutamate stimulus (Glutamate and Control groups) a lower number of features with significant biological and statistical differences was obtained compared to the OGD insult (OGD and Sham groups) (**Figure 19**). A possible justification for this observation lies in the fact that the data used to perform this analysis correspond to the data obtained after the filtering step, in which, for each insult, only the features present in all the samples of at least one of the groups were selected. The number of samples for OGD and Sham groups was equal to three and for Glutamate and Control groups was equal to four, which makes the filtering performed for Glutamate and Control groups more restricted and selective. Another justification could be that the metabolites might have been released into the extracellular space, and therefore be present in the secretome of the glutamate-stimulated samples, since the cellular membranes of primary cultures submitted to the glutamate stimulus were visibly more destroyed than in the OGD insult. However, the total signal intensity was similar between Glutamate and Control groups, as well as between Glutamate

and OGD groups. Nevertheless, in order to evaluate this possibility, metabolomics analysis of the secretomes could be performed in future studies.

Regarding the analysis performed in Sciex OS™ software, for the untargeted metabolomics analysis, 7 metabolites were identified and quantified, namely, tryptophan, tyrosine, diaveridine, helvolic acid, methylthioadenosine, sphinganine, and maltose/sucrose (**Figure 23**). For the targeted metabolomics analysis, of the 27 metabolites identified and quantified, only 4 showed statistically significant differences, namely, *O*-acetylcarnitine, β-nicotinamide adenine dinucleotide (β-NAD), FAD, and maltose/sucrose (**Figure 26**).

Regarding the tryptophan and tyrosine metabolites, there are studies conducted with newborns who presented clinical or biochemical signs of perinatal asphyxia and evolved to HIE, in which tryptophan [154] and tyrosine [155] were also identified. Regarding tryptophan levels, they were found to be decreased in infants with mild and moderate HIE and increased in infants with severe HIE. Tyrosine levels were found to be increased in infants with HIE. These results are in agreement with the tendency of increase seen for these two metabolites in the Glutamate group (**Figure 23**). Another study, demonstrated that tryptophan metabolism is one of the metabolic pathways found to be significantly altered in HIE [156]. Through the kynurenine pathway, tryptophan is degraded to produce alanine, which originates pyruvate. In situations of reduced energy, there is conversion of the pyruvate into acetyl coenzyme A (acetyl-CoA), which will be used in the Krebs cycle to produce reduced electron carriers (NADH and $FADH_2$) that integrate the electron transport chain and, subsequent ATP production through mitochondrial oxidative phosphorylation. This mechanism may be an alternative to obtain pyruvate, since in situations of hypoxia-ischemia, glycolysis is compromised due to the reduced delivery of oxygen and glucose.

Regarding the metabolites β-NAD and FAD, obtained as identifications for the targeted analysis, it was verified a decrease in the Glutamate group compared to the Control group after quantification (**Figure 26**). This result can potentially be justified by the fact that during the excitotoxicity process, induced by glutamate, the neurons require greater amounts of energy, namely, in order to try to support the normal functioning of the ATP-dependent pumps and to maintain ion homeostasis and electrochemical membrane potential [157]. Adenosine triphosphate consumption requires its production, which can be performed through mitochondrial oxidative phosphorylation when the mitochondria is functional, but

also through glycolysis when mitochondrial function is compromised, which is the case during the excitotoxicity process. The oxidative stress characteristic of excitotoxicity can lead to the activation of uncoupling proteins (UCPs) located in the inner mitochondrial membrane, such as UCP4 (a brain-specific mitochondrial protein), which promotes a change in energy metabolism consisting of increased glucose uptake and, consequently, increased glycolysis, in order to compensate for the reduced ATP production by oxidative phosphorylation [158]. Thus, ATP production occurs significantly through glycolysis, in which the reduction of NAD^+ to NADH occurs. After glycolysis, in the conversion of pyruvate (the end product of glycolysis) to acetyl-CoA there is also reduction of NAD^+ to NADH and, in turn, the acetyl-CoA obtained integrates the Krebs cycle, in which there is also reduction of NAD^+ to NADH and reduction of FAD to $FADH_2$, thus decreasing the levels of the coenzymes NAD and FAD. The decreased NAD levels may also be related to the fact that under conditions of oxidative and metabolic stress, activation of the enzymes poly (ADP-ribose) polymerase 1 (PARP1), an essential enzyme involved in DNA repair, and sirtuin 1 (SIRT1) occurs, which promotes depletion of intracellular NAD^+ levels [157].

For maltose/sucrose identification, the significant increase observed in the OGD group compared to the Sham group (**Figure 23** and **Figure 26**) is likely due to the experimental protocol, that is, it is not biologically significant, since at the time of performing the OGD insult, for the OGD samples, the medium added to the cells (cerebrocortical neurons) contained sucrose, unlike the medium added to the control (Sham) samples that contained glucose.

The metabolites diaveridine and helvolic acid correspond to exogenous metabolites, since they have no biological significance for this study. Diaveridine and helvolic acid, a mycotoxin, show antibacterial activity against most Gram-negative and Gram-positive bacteria [159]. Regarding methylthioadenosine, a sulfur-containing adenine nucleoside, there are no studies related to HIE, but it has been shown that methylthioadenosine administration can be a beneficial and effective therapy for the treatment of multiple sclerosis and other autoimmune diseases [160].

The analysis performed on the XCMS™ platform allowed the annotation of 2 metabolites, tamsulosin and hericenone D or G, and of small peptides composed of 3/4 amino acids (**Figure 24**). One step in sample preparation was protein precipitation with

methanol in order to allow their separation from metabolites after centrifugation, as methanol (an organic solvent) promotes the decrease of the dielectric constant of the sample and the decrease of the solvation power of water in the hydrophilic regions of the protein surface, which in turn leads to the increase of the electrostatic forces between the protein molecules (higher protein-protein interaction) with consequent decrease of their solubility and aggregation followed by precipitation [161]. However, this process is not fully effective, since small peptides may not precipitate, remaining in the supernatant together with the metabolites.

Tamsulosin is an alpha-1 adrenoceptor antagonist, belonging to a group of medicines called alpha-blockers, that is used in the treatment of benign prostatic hypertrophy and, occasionally, in the treatment of kidney stones [162]. For the model under study, the OGD cellular model of HIE, the annotation of this compound has no biological significance.

Hericenones are aromatic compounds isolated from the mushroom *Hericium erinaceum*. They promote nerve growth factor (NGF) biosynthesis *in vitro*, namely hericenones C, D and E. [163,164] For this study, a possible justification for obtaining hericenone D or G as an annotation lies in the fact that it is an exogenous metabolite possibly coming from the diet of the mothers from which the Wistar rat embryos used to perform the study were obtained, but for this it was supposed that there were no statistically significant differences between the different study groups (OGD, Sham, Glutamate, and Control) (**Figure 24**), as for each biological replicate, the cells that were submitted to the two stimuli were from the same mother and the isolation was the same for all. Thus, this annotation most likely corresponds to an annotation error, since at the annotation level, the metabolites obtained correspond only to preliminary/provisory identifications, which means that annotation errors can occur.

Through the metabolic pathways analysis (**Figure 25**), one of the pathways found to be altered was the starch and sucrose metabolism, which can be justified because sucrose (previously identified in Sciex OS™ for untargeted and targeted analyses) and glucose were obtained as significant hits (**Table 6**). These two metabolites may have been obtained as they are components of the media used to perform the OGD insult (the OGD medium contained sucrose and the Sham medium contained glucose).

Caffeine metabolism was another pathway found to be altered, which has no biological significance for this study. The analysis of the results obtained showed that 2 of the 3 metabolites obtained as hits for this pathway, namely paraxanthine and theobromine, had the same *m/z* value as glucose and fructose, which were obtained as significant hits for starch and sucrose metabolism (**Table 6**). This observation may justify the fact that the caffeine metabolism was altered, since the metabolic pathways analysis was performed using the Mummichog algorithm, which assigns a possible metabolite match to an *m/z* value based on the precursor ion present in the data introduced to perform the analysis [148], thus, for a single *m/z* value, several metabolites can correspond. Being at the annotation level, the most likely is that the annotation of paraxanthine and theobromine is an algorithm annotation error, since when metabolite identification was performed in the Sciex OS™ software these two metabolites were not identified by comparing the fragmentation spectra. To be able to distinguish between metabolites belonging to different pathways, more metabolites would have to have been annotated at higher confidence levels. Given that theobromine can be found in cocoa and in seeds, it would be interesting to see if this metabolite can originate from the mothers' diet.

Sphingolipid metabolism was also detected to be altered through the metabolic pathways analysis. For this pathway, 3-dehydrosphinganine, sphinganine (previously identified in Sciex OS™ for untargeted analysis), and sphingosine were the metabolites obtained as significant hits (**Table 6**). Since sphinganine was previously identified as a metabolite identification (level 2) it is possible to prove that this annotation is correct, which allows for more confidence for this pathway. The metabolites 3-dehydrosphinganine and sphinganine belong to the sphingosine biosynthesis pathway. As mentioned before, mitochondria dysfunction is one of the pathophysiological features of HIE, which is a disease characterized by brain injury. A study from 2014 [165], demonstrated that traumatic brain injury (TBI) leads to the disruption of the sphingolipid metabolism, more precisely, of the sphingosine metabolism in the brain. Traumatic brain injury promotes activation of the enzyme neutral ceramidase (NCDase), which allows sphingosine to be obtained from ceramide, and decreases the activity of the enzyme sphingosine kinase 2 (SphK2), which converts sphingosine into sphingosine 1-phosphate (S1P) in the mitochondria. In turn, activation of NCDase and reduced activity of SphK2 lead to the accumulation of sphingosine in mitochondria. The increase in sphingosine levels in mitochondria is also related to the fact

that TBI prevents the association of SphK2 with NCDase, which interferes with the flow of sphingosine from NCDase to SphK2. Finally, after TBI, the elevated sphingosine levels within the mitochondria result in decreased cytochrome *c* oxidase activity and, consequently, in reduced electron transport chain activity. For this study, an increase trend was seen in the Glutamate group compared to the Control group for sphinganine (**Figure 23**).

In the last few years, the advances in technology have led to the development of the field of systems biology [128]. In this work, as mentioned before, metabolomics was the "*omics*" approach used. Metabolomics is a global approach that encompasses the comprehensive qualitative and quantitative metabolomics screening of a biological system (cell, tissue, fluid, or organism) [127,128]. It has been fundamental for the characterization of the biological systems in diseases and in medicine since metabolites play an important and active role in the biological processes of these systems as a whole [166,167].

Recently, there has been a constant evolution in the area of metabolomics due to developments in technology and analytical methodologies, including developments in analytical techniques, instruments, statistical analysis, computer processing capacity, and software used for data acquisition, analysis, and interpretation [168]. Nuclear magnetic resonance spectroscopy and LC-MS or LC-MS/MS are examples of the most commonly used analytical techniques in metabolomics studies. Both techniques have advantages and disadvantages/limitations. Nuclear magnetic resonance spectroscopy has many advantages compared to MS, including high reproducibility, involves minimal sample preparation and no sample destruction, and can be used for direct analysis of tissue samples and for *in vivo* research. On the other hand, MS has higher sensitivity allowing the detection of metabolites with low concentrations (at the nanomolar level), higher selectivity conferred by the high resolution of the technique, being able to distinguish co-eluting compounds by their precursor and fragment ions, the amount of sample required for the analysis is small and it usually needs a previous separation step, using different chromatographic separation techniques, such as liquid or gas chromatography, which allows the detection of different classes of metabolites, and reduces sample complexity and the ionization suppression effects. Regarding disadvantages, MS is a destructive technique not allowing sample recovery. [130,168-170] In this work, LC-MS/MS was the analytical technique used to perform the metabolomics study of the primary cultures of cerebrocortical neurons, since it is a

sensitive technique, that allows the analysis of small sample amounts, as well as a selective technique, because it uses a high-resolution technique allowing the analysis of thousands of metabolites simultaneously.

Currently, metabolite identification in LC-MS/MS based-metabolomics remains a challenge. In proteomics, peptides, the constituents of proteins, can be sequenced while metabolites have a big physical and chemical diversity and wide concentration ranges making their identification more difficult, because they are small molecules that can share *m/z* values at the precursor or even fragment level, which for proteins it hardly happens [137,171]. Regarding fragmentation data, in proteomics, fragmentation patterns are predictable due to prior knowledge of protein sequences and enzyme cleavage patterns, and, in metabolomics, it is possible to predict the fragmentation pattern of each metabolite, but these may differ given the equipment and parameters used to perform the analysis [172,173].

The identification of metabolites in LC-MS/MS is classified according to five different confidence levels. At level 5, the lowest confidence level, the acquisition of an accurate mass for a unique feature allows database searching, but a high number of compounds/metabolites can correspond to this unique feature. Successive application of higher mass accuracy reduces the number of possible molecular formulas until only a unique molecular formula is obtained (level 4), to which a large number of isomers and thus, a large number of structures correspond. In addition to mass accuracy, the isotope abundance distribution, charge state and adduct ion determination are important for the determination of the tentative structures (level 3) through the database search. The tentative structures match precursor *m/z* to a metabolite database (correspondence at the precursor ion level (full-scan mass spectrum)). At this stage, in theory, level 3 corresponds to metabolite annotation, but in practice, everything at or below level 3 is considered an annotation. Next, at level 2, the putative identifications require matching the fragmentation data (MS/MS spectrum) with the fragmentation data from metabolite libraries (correspondence at the fragment ion level). This level corresponds to metabolite identification in screening studies. Finally, at level 1, the level of highest confidence, to obtain a validated identification it is necessary additional data evidence that correspond to data from a pure reference standard acquired under similar analytical conditions. This level represents the ideal metabolite identification. [171,174]

In this metabolomics study, metabolite identifications (level 2) were obtained through the Sciex OS™ software, metabolite annotations through the XCMS™ online platform, and possible metabolite matches/annotations through the metabolic pathways analysis performed on MetaboAnalyst 5.0. All of them were quantified in Sciex OS™. The metabolites tryptophan, tyrosine, diaveridine, helvolic acid, methylthioadenosine, sphinganine, *O*-acetylcarnitine, β-NAD, FAD, and maltose/sucrose were obtained as identifications (level 2), while the metabolites tamsulosin and hericenone D or G were obtained as annotations, as were the metabolites obtained for each of the metabolic pathways (level 3 or lower). Of these metabolites, for this study, tryptophan, β-NAD, FAD, and sphinganine were selected as potential biomarkers as they demonstrated biological significance. Sphingolipid metabolism was found to be a possibly altered metabolic pathway. These results require future validation, namely, in the animal model of HIE and later on in humans.

Chapter 6
Conclusion

6. CONCLUSION

The main objective of this study was to perform a metabolomics profiling of primary cultures of cerebrocortical neurons of two models of neuronal death: an OGD model and a glutamate-based model, in order to identify potential biomarkers for HIE diagnosis. Nowadays, the diagnostic tools remain inaccurate, since there is no objective measurement and is based on neuroimaging, which is not accessible in several hospital units. While the OGD model mimic the *in vivo* insult, the glutamate-based model functioned as the positive control of the OGD model.

Due to its high resolution and high sensitivity, LC-MS/MS was the analytical technique used in this study, which allowed the acquisition of two types of data: IDA and SWATH. Information dependent acquisition supported the identification of metabolites and SWATH was used for their quantification.

The multivariate analysis allowed the separation of the OGD and Glutamate groups from their respective control groups, demonstrating the metabolomics changes upon stimuli. Thus, since differences were seen between the OGD and Sham groups for this study, it can be stated that metabolomics can be used for the investigation and discovery of potential biomarkers for HIE. Using different approaches, the present metabolomics study allowed the identification and annotation of potential biomarkers for the diagnosis of HIE and the analysis of potentially altered metabolic pathways in a HIE situation. The metabolites tryptophan, β-NAD, FAD, and sphinganine were identified as potential biomarkers. Regarding pathways, sphingolipid metabolism, which includes sphinganine, was found as a possible altered metabolic pathway. These results may contribute to translational biomarker profiling for HIE. In the future, since the metabolomics study was performed in *in vitro* models, the results obtained require further validation in the animal model of HIE, the modified Vannucci rat model, followed by validation in humans. In addiction, the metabolomics analysis of the secretomes could be a good approach to infer about circulating biomarkers.

Chapter 7
References

7. REFERENCES

1 Adstamongkonkul, D. & Hess, D. C. Ischemic Conditioning and neonatal hypoxic ischemic encephalopathy: a literature review. *Conditioning medicine* **1**, 9-16 (2017).

2 Liu, J., Li, J. & Gu, M. The correlation between myocardial function and cerebral hemodynamics in term infants with hypoxic-ischemic encephalopathy. *Journal of tropical pediatrics* **53**, 44-48, doi:10.1093/tropej/fml053 (2007).

3 Busl, K. M. & Greer, D. M. Hypoxic-ischemic brain injury: pathophysiology, neuropathology and mechanisms. *NeuroRehabilitation* **26**, 5-13, doi:10.3233/nre-2010-0531 (2010).

4 Liu, L., Oza, S., Hogan, D., Perin, J., Rudan, I., Lawn, J. E., Cousens, S., Mathers, C. & Black, R. E. Global, regional, and national causes of child mortality in 2000-13, with projections to inform post-2015 priorities: an updated systematic analysis. *Lancet (London, England)* **385**, 430-440, doi:10.1016/s0140-6736(14)61698-6 (2015).

5 Kurinczuk, J. J., White-Koning, M. & Badawi, N. Epidemiology of neonatal encephalopathy and hypoxic-ischaemic encephalopathy. *Early human development* **86**, 329-338, doi:10.1016/j.earlhumdev.2010.05.010 (2010).

6 Yıldız, E. P., Ekici, B. & Tatlı, B. Neonatal hypoxic ischemic encephalopathy: an update on disease pathogenesis and treatment. *Expert Rev Neurother* **17**, 449-459, doi:10.1080/14737175.2017.1259567 (2017).

7 Vannucci, R. C. & Vannucci, S. J. A model of perinatal hypoxic-ischemic brain damage. *Annals of the New York Academy of Sciences* **835**, 234-249, doi:10.1111/j.1749-6632.1997.tb48634.x (1997).

8 Al-Macki, N., Miller, S. P., Hall, N. & Shevell, M. The spectrum of abnormal neurologic outcomes subsequent to term intrapartum asphyxia. *Pediatric neurology* **41**, 399-405, doi:10.1016/j.pediatrneurol.2009.06.001 (2009).

9 Lai, M. C. & Yang, S. N. Perinatal hypoxic-ischemic encephalopathy. *J Biomed Biotechnol* **2011**, 609813, doi:10.1155/2011/609813 (2011).

10 Riljak, V., Kraf, J., Daryanani, A., Jiruska, P. & Otahal, J. Pathophysiology of perinatal hypoxic-ischemic encephalopathy - biomarkers, animal models and treatment perspectives. *Physiol Res* **65**, S533-S545, doi:10.33549/physiolres.933541 (2016).

11 Back, S. A., Riddle, A. & McClure, M. M. Maturation-dependent vulnerability of perinatal white matter in premature birth. *Stroke* **38**, 724-730, doi:10.1161/01.str.0000254729.27386.05 (2007).

12 Gonzalez, F. F. & Ferriero, D. M. Therapeutics for neonatal brain injury. *Pharmacology & therapeutics* **120**, 43-53, doi:10.1016/j.pharmthera.2008.07.003 (2008).

13 Miller, S. P., Ramaswamy, V., Michelson, D., Barkovich, A. J., Holshouser, B., Wycliffe, N., Glidden, D. V., Deming, D., Partridge, J. C., Wu, Y. W., Ashwal, S. & Ferriero, D. M. Patterns of brain injury in term neonatal encephalopathy. *The Journal of pediatrics* **146**, 453-460, doi:10.1016/j.jpeds.2004.12.026 (2005).

14 Harteman, J. C., Nikkels, P. G., Benders, M. J., Kwee, A., Groenendaal, F. & de Vries, L. S. Placental pathology in full-term infants with hypoxic-ischemic neonatal encephalopathy and association with magnetic resonance imaging pattern of brain injury. *The Journal of pediatrics* **163**, 968-995.e962, doi:10.1016/j.jpeds.2013.06.010 (2013).

15 Puyal, J., Ginet, V. & Clarke, P. G. Multiple interacting cell death mechanisms in the mediation of excitotoxicity and ischemic brain damage: a challenge for neuroprotection. *Progress in neurobiology* **105**, 24-48, doi:10.1016/j.pneurobio.2013.03.002 (2013).

16 Perlman, J. M. Summary proceedings from the neurology group on hypoxic-ischemic encephalopathy. *Pediatrics* **117**, S28-33, doi:10.1542/peds.2005-0620E (2006).

17 Douglas-Escobar, M. & Weiss, M. D. Hypoxic-ischemic encephalopathy: a review for the clinician. *JAMA Pediatr* **169**, 397-403, doi:10.1001/jamapediatrics.2014.3269 (2015).

18 Wassink, G., Gunn, E. R., Drury, P. P., Bennet, L. & Gunn, A. J. The mechanisms and treatment of asphyxial encephalopathy. *Frontiers in neuroscience* **8**, 40, doi:10.3389/fnins.2014.00040 (2014).

19 Tan, W. K., Williams, C. E., During, M. J., Mallard, C. E., Gunning, M. I., Gunn, A. J. & Gluckman, P. D. Accumulation of cytotoxins during the development of seizures and edema after hypoxic-ischemic injury in late gestation fetal sheep. *Pediatric research* **39**, 791-797, doi:10.1203/00006450-199605000-00008 (1996).

20 Bennet, L., Roelfsema, V., Dean, J. M., Wassink, G., Power, G. G., Jensen, E. C. & Gunn, A. J. Regulation of cytochrome oxidase redox state during umbilical cord occlusion in preterm fetal sheep. *American journal of physiology. Regulatory, integrative and comparative physiology* **292**, R1569-1576, doi:10.1152/ajpregu.00743.2006 (2007).

21 Bennet, L., Roelfsema, V., Pathipati, P., Quaedackers, J. S. & Gunn, A. J. Relationship between evolving epileptiform activity and delayed loss of mitochondrial activity after asphyxia measured by near-infrared spectroscopy in preterm fetal sheep. *The Journal of physiology* **572**, 141-154, doi:10.1113/jphysiol.2006.105197 (2006).

22 Vannucci, S. J. & Hagberg, H. Hypoxia-ischemia in the immature brain. *The Journal of experimental biology* **207**, 3149-3154, doi:10.1242/jeb.01064 (2004).

23 Hagberg, H., Mallard, C., Rousset, C. I. & Thornton, C. Mitochondria: hub of injury responses in the developing brain. *The Lancet. Neurology* **13**, 217-232, doi:10.1016/s1474-4422(13)70261-8 (2014).

24 Bennet, L., Tan, S., Van den Heuij, L., Derrick, M., Groenendaal, F., van Bel, F., Juul, S., Back, S. A., Northington, F., Robertson, N. J., Mallard, C. & Gunn, A. J. Cell therapy for neonatal hypoxia-ischemia and cerebral palsy. *Annals of neurology* **71**, 589-600, doi:10.1002/ana.22670 (2012).

25 Edwards, A. B., Anderton, R. S., Knuckey, N. W. & Meloni, B. P. Perinatal Hypoxic-Ischemic Encephalopathy and Neuroprotective Peptide Therapies: A Case for Cationic Arginine-Rich Peptides (CARPs). *Brain sciences* **8**, doi:10.3390/brainsci8080147 (2018).

26 Johnston, M. V., Trescher, W. H., Ishida, A. & Nakajima, W. Neurobiology of hypoxic-ischemic injury in the developing brain. *Pediatric research* **49**, 735-741, doi:10.1203/00006450-200106000-00003 (2001).

27 Barks, J. D. & Silverstein, F. S. Excitatory amino acids contribute to the pathogenesis of perinatal hypoxic-ischemic brain injury. *Brain pathology (Zurich, Switzerland)* **2**, 235-243, doi:10.1111/j.1750-3639.1992.tb00697.x (1992).

28 Lu, Y., Tucker, D., Dong, Y., Zhao, N., Zhuo, X. & Zhang, Q. Role of Mitochondria in Neonatal Hypoxic-Ischemic Brain Injury. *Journal of neuroscience and rehabilitation* **2**, 1-14 (2015).

29 Ankarcrona, M., Dypbukt, J. M., Bonfoco, E., Zhivotovsky, B., Orrenius, S., Lipton, S. A. & Nicotera, P. Glutamate-induced neuronal death: a succession of necrosis or apoptosis depending on mitochondrial function. *Neuron* **15**, 961-973, doi:10.1016/0896-6273(95)90186-8 (1995).

30 Ferriero, D. M., Holtzman, D. M., Black, S. M. & Sheldon, R. A. Neonatal mice lacking neuronal nitric oxide synthase are less vulnerable to hypoxic-ischemic injury. *Neurobiology of disease* **3**, 64-71, doi:10.1006/nbdi.1996.0006 (1996).

31 Gilland, E., Puka-Sundvall, M., Hillered, L. & Hagberg, H. Mitochondrial function and energy metabolism after hypoxia-ischemia in the immature rat brain: involvement of NMDA-receptors. *Journal of cerebral blood flow and metabolism : official journal of the International Society of Cerebral Blood Flow and Metabolism* **18**, 297-304, doi:10.1097/00004647-199803000-00008 (1998).

32 Zubrow, A. B., Delivoria-Papadopoulos, M., Ashraf, Q. M., Fritz, K. I. & Mishra, O. P. Nitric oxide-mediated Ca2+/calmodulin-dependent protein kinase IV activity during hypoxia in neuronal nuclei from newborn piglets. *Neuroscience letters* **335**, 5-8, doi:10.1016/s0304-3940(02)01138-2 (2002).

33 Groenendaal, F., Vles, J., Lammers, H., De Vente, J., Smit, D. & Nikkels, P. G. Nitrotyrosine in human neonatal spinal cord after perinatal asphyxia. *Neonatology* **93**, 1-6, doi:10.1159/000106432 (2008).

34 Cao, W., Carney, J. M., Duchon, A., Floyd, R. A. & Chevion, M. Oxygen free radical involvement in ischemia and reperfusion injury to brain. *Neuroscience letters* **88**, 233-238, doi:10.1016/0304-3940(88)90132-2 (1988).

35 McDonald, J. W. & Johnston, M. V. Physiological and pathophysiological roles of excitatory amino acids during central nervous system development. *Brain research. Brain research reviews* **15**, 41-70, doi:10.1016/0165-0173(90)90011-c (1990).

36 Hagberg, H., Mallard, C., Rousset, C. I. & Xiaoyang, W. Apoptotic mechanisms in the immature brain: involvement of mitochondria. *Journal of child neurology* **24**, 1141-1146, doi:10.1177/0883073809338212 (2009).

37 Lee, Y., Lee, S. R., Choi, S. S., Yeo, H. G., Chang, K. T. & Lee, H. J. Therapeutically targeting neuroinflammation and microglia after acute ischemic stroke. *BioMed research international* **2014**, 297241, doi:10.1155/2014/297241 (2014).

38 Swanson, R. A., Ying, W. & Kauppinen, T. M. Astrocyte influences on ischemic neuronal death. *Current molecular medicine* **4**, 193-205, doi:10.2174/1566524043479185 (2004).

39 Anderson, C. M. & Swanson, R. A. Astrocyte glutamate transport: review of properties, regulation, and physiological functions. *Glia* **32**, 1-14 (2000).

40 Liu, F. & McCullough, L. D. Inflammatory responses in hypoxic ischemic encephalopathy. *Acta pharmacologica Sinica* **34**, 1121-1130, doi:10.1038/aps.2013.89 (2013).

41 Volpe, J. J. Neonatal encephalopathy: an inadequate term for hypoxic-ischemic encephalopathy. *Annals of neurology* **72**, 156-166, doi:10.1002/ana.23647 (2012).

42 D'Alton, M. E., Hankins, G. D.V., Berkowitz, R. L., Bienstock, J., Ghidini, A., Goldsmith, J., Higgins, R., Moore, T. R., Natale, R., Nelson, K. B., Papile, L., Peebles, D., Romero, R. J., Schendel, D., Spong, C. Y., Waldman, R. N., Wu, Y., Joseph Jr, G. F., Hawks, D., Politzer, A., Emig, C. & Thomas, K. Neonatal

Encephalopathy and Neurologic Outcome, Second Edition *Pediatrics* **133**, e1482-e1488, doi:10.1542/peds.2014-0724 (2014).

43 Apgar, V. A proposal for a new method of evaluation of the newborn infant. *Current researches in anesthesia & analgesia* **32**, 260-267 (1953).

44 AMERICAN ACADEMY OF PEDIATRICS COMMITTEE ON FETUS AND NEWBORN & AMERICAN COLLEGE OF OBSTETRICIANS AND GYNECOLOGISTS COMMITTEE ON OBSTETRIC PRACTICE. The Apgar Score. *Pediatrics* **136**, 819-822, doi:10.1542/peds.2015-2651 (2015).

45 NIBIB. *Magnetic Resonance Imaging (MRI)*, <https://www.nibib.nih.gov/science-education/science-topics/magnetic-resonance-imaging-mri> (2021) Access date: 07/12/2021.

46 Buonocore, M. H. & Maddock, R. J. Magnetic resonance spectroscopy of the brain: a review of physical principles and technical methods. *Rev Neurosci* **26**, 609-632, doi:10.1515/revneuro-2015-0010 (2015).

47 Krishnan, P. & Shroff, M. Neuroimaging in Neonatal Hypoxic Ischemic Encephalopathy. *Indian J Pediatr* **83**, 995-1002, doi:10.1007/s12098-016-2042-1 (2016).

48 Glass, H. C. Hypoxic-Ischemic Encephalopathy and Other Neonatal Encephalopathies. *Continuum (Minneap Minn)* **24**, 57-71, doi:10.1212/con.0000000000000557 (2018).

49 Murray, D. M. Biomarkers in neonatal hypoxic-ischemic encephalopathy-Review of the literature to date and future directions for research. *Handb Clin Neurol* **162**, 281-293, doi:10.1016/B978-0-444-64029-1.00013-8 (2019).

50 Sarnat, H. B. & Sarnat, M. S. Neonatal encephalopathy following fetal distress. A clinical and electroencephalographic study. *Arch Neurol* **33**, 696-705, doi:10.1001/archneur.1976.00500100030012 (1976).

51 Papile, L. A., Baley, J. E., Benitz, W., Cummings, J., Carlo, W. A., Eichenwald, E., Kumar, P., Polin, R. A., Tan, R. C. & Wang, K. S. Hypothermia and neonatal encephalopathy. *Pediatrics* **133**, 1146-1150, doi:10.1542/peds.2014-0899 (2014).

52 Lemyre, B. & Chau, V. Hypothermia for newborns with hypoxic-ischemic encephalopathy. *Paediatr Child Health* **23**, 285-291, doi:10.1093/pch/pxy028 (2018).

53 Roka, A., Kelen, D., Halasz, J., Beko, G., Azzopardi, D. & Szabo, M. Serum S100B and neuron-specific enolase levels in normothermic and hypothermic infants after perinatal asphyxia. *Acta Paediatr* **101**, 319-323, doi:10.1111/j.1651-2227.2011.02480.x (2012).

54 Ennen, C. S., Huisman, T. A., Savage, W. J., Northington, F. J., Jennings, J. M., Everett, A. D. & Graham, E. M. Glial fibrillary acidic protein as a biomarker for neonatal hypoxic-ischemic encephalopathy treated with whole-body cooling. *Am J Obstet Gynecol* **205**, 251.e251-257, doi:10.1016/j.ajog.2011.06.025 (2011).

55 Chalak, L. F., Sanchez, P. J., Adams-Huet, B., Laptook, A. R., Heyne, R. J. & Rosenfeld, C. R. Biomarkers for severity of neonatal hypoxic-ischemic encephalopathy and outcomes in newborns receiving hypothermia therapy. *The Journal of pediatrics* **164**, 468-474 e461, doi:10.1016/j.jpeds.2013.10.067 (2014).

56 Looney, A. M., Walsh, B. H., Moloney, G., Grenham, S., Fagan, A., O'Keeffe, G. W., Clarke, G., Cryan, J. F., Dinan, T. G., Boylan, G. B. & Murray, D. M. Downregulation of Umbilical Cord Blood Levels of miR-374a in Neonatal Hypoxic

Ischemic Encephalopathy. *The Journal of pediatrics* **167**, 269-273.e262, doi:10.1016/j.jpeds.2015.04.060 (2015).

57 Mehta, A., Chawla, D., Kaur, J., Mahajan, V. & Guglani, V. Salivary lactate dehydrogenase levels can provide early diagnosis of hypoxic-ischaemic encephalopathy in neonates with birth asphyxia. *Acta Paediatr* **104**, e236-240, doi:10.1111/apa.12964 (2015).

58 Silveira, R. C. & Procianoy, R. S. Hypothermia therapy for newborns with hypoxic ischemic encephalopathy. *J Pediatr (Rio J)* **91**, S78-83, doi:10.1016/j.jped.2015.07.004 (2015).

59 Drury, P. P., Gunn, E. R., Bennet, L. & Gunn, A. J. Mechanisms of hypothermic neuroprotection. *Clinics in perinatology* **41**, 161-175, doi:10.1016/j.clp.2013.10.005 (2014).

60 Akula, V. P., Joe, P., Thusu, K., Davis, A. S., Tamaresis, J. S., Kim, S., Shimotake, T. K., Butler, S., Honold, J., Kuzniewicz, M., DeSandre, G., Bennett, M., Gould, J., Wallenstein, M. B. & Van Meurs, K. A randomized clinical trial of therapeutic hypothermia mode during transport for neonatal encephalopathy. *The Journal of pediatrics* **166**, 856-861.e851-852, doi:10.1016/j.jpeds.2014.12.061 (2015).

61 Jacobs, S. E., Berg, M., Hunt, R., Tarnow-Mordi, W. O., Inder, T. E. & Davis, P. G. Cooling for newborns with hypoxic ischaemic encephalopathy. *The Cochrane database of systematic reviews* **2013**, Cd003311, doi:10.1002/14651858.CD003311.pub3 (2013).

62 Shankaran, S., Laptook, A. R., Pappas, A., McDonald, S. A., Das, A., Tyson, J. E., Poindexter, B. B., Schibler, K., Bell, E. F., Heyne, R. J., Pedroza, C., Bara, R., Van Meurs, K. P., Grisby, C., Huitema, C. M., Garg, M., Ehrenkranz, R. A., Shepherd, E. G., Chalak, L. F., Hamrick, S. E., Khan, A. M., Reynolds, A. M.., Laughon, M. M., Truog, W. E., Dysart, K. C., Carlo, W. A., Walsh, M. C., Watterberg, K. L. & Higgins, R. D. Effect of depth and duration of cooling on deaths in the NICU among neonates with hypoxic ischemic encephalopathy: a randomized clinical trial. *Jama* **312**, 2629-2639, doi:10.1001/jama.2014.16058 (2014).

63 Northington, F. J., Graham, E. M. & Martin, L. J. Apoptosis in perinatal hypoxic-ischemic brain injury: how important is it and should it be inhibited? *Brain research. Brain research reviews* **50**, 244-257, doi:10.1016/j.brainresrev.2005.07.003 (2005).

64 Drury, P. P., Bennet, L. & Gunn, A. J. Mechanisms of hypothermic neuroprotection. *Seminars in fetal & neonatal medicine* **15**, 287-292, doi:10.1016/j.siny.2010.05.005 (2010).

65 Tagin, M. A., Woolcott, C. G., Vincer, M. J., Whyte, R. K. & Stinson, D. A. Hypothermia for neonatal hypoxic ischemic encephalopathy: an updated systematic review and meta-analysis. *Archives of pediatrics & adolescent medicine* **166**, 558-566, doi:10.1001/archpediatrics.2011.1772 (2012).

66 Gluckman, P. D., Wyatt, J. S., Azzopardi, D., Ballard, R., Edwards, A. D., Ferriero, D. M., Polin, R. A., Robertson, C. M., Thoresen, M., Whitelaw, A. & Gunn, A. J. Selective head cooling with mild systemic hypothermia after neonatal encephalopathy: multicentre randomised trial. *Lancet (London, England)* **365**, 663-670, doi:10.1016/s0140-6736(05)17946-x (2005).

67 Shankaran, S., Laptook, A. R., Ehrenkranz, R. A., Tyson, J. E., McDonald, S. A., Donovan, E. F., Fanaroff, A. A., Poole, W. K., Wright, L. L., Higgins, R. D., Finer, N. N., Carlo, W. A., Duara, S., Oh, W., Cotten, C. M., Stevenson, D. K., Stoll, B. J., Lemons, J. A., Guillet, R. & Jobe, A. H. Whole-body hypothermia for neonates with

hypoxic-ischemic encephalopathy. *The New England journal of medicine* **353**, 1574-1584, doi:10.1056/NEJMcps050929 (2005).

68 Zhou, W. H., Cheng, G. Q., Shao, X. M., Liu, X. Z., Shan, R. B., Zhuang, D. Y., Zhou, C. L., Du, L. Z., Cao, Y., Yang, Q. & Wang, L. S. Selective head cooling with mild systemic hypothermia after neonatal hypoxic-ischemic encephalopathy: a multicenter randomized controlled trial in China. *The Journal of pediatrics* **157**, 367-372, 372.e361-363, doi:10.1016/j.jpeds.2010.03.030 (2010).

69 Jacobs, S. E., Morley, C. J., Inder, T. E., Stewart, M. J., Smith, K. R., McNamara, P. J., Wright, I. M., Kirpalani, H. M., Darlow, B. A. & Doyle, L. W. Whole-body hypothermia for term and near-term newborns with hypoxic-ischemic encephalopathy: a randomized controlled trial. *Archives of pediatrics & adolescent medicine* **165**, 692-700, doi:10.1001/archpediatrics.2011.43 (2011).

70 Wu, Y. W., Mathur, A. M., Chang, T., McKinstry, R. C., Mulkey, S. B., Mayock, D. E., Van Meurs, K. P., Rogers, E. E., Gonzalez, F. F., Comstock, B. A., Juul, S. E., Msall, M. E., Bonifacio, S. L., Glass, H. C., Massaro, A. N., Dong, L., Tan, K. W., Heagerty, P. J. & Ballard, R. A. High-Dose Erythropoietin and Hypothermia for Hypoxic-Ischemic Encephalopathy: A Phase II Trial. *Pediatrics* **137**, doi:10.1542/peds.2016-0191 (2016).

71 Zhu, C., Kang, W., Xu, F., Cheng, X., Zhang, Z., Jia, L., Ji, L., Guo, X., Xiong, H., Simbruner, G., Blomgren, K. & Wang, X. Erythropoietin improved neurologic outcomes in newborns with hypoxic-ischemic encephalopathy. *Pediatrics* **124**, e218-226, doi:10.1542/peds.2008-3553 (2009).

72 Aly, H., Elmahdy, H., El-Dib, M., Rowisha, M., Awny, M., El-Gohary, T., Elbatch, M., Hamisa, M. & El-Mashad, A. R. Melatonin use for neuroprotection in perinatal asphyxia: a randomized controlled pilot study. *J Perinatol* **35**, 186-191, doi:10.1038/jp.2014.186 (2015).

73 Gunes, T., Ozturk, M. A., Koklu, E., Kose, K. & Gunes, I. Effect of allopurinol supplementation on nitric oxide levels in asphyxiated newborns. *Pediatric neurology* **36**, 17-24, doi:10.1016/j.pediatrneurol.2006.08.005 (2007).

74 Torrance, H. L., Benders, M. J., Derks, J. B., Rademaker, C. M., Bos, A. F., Van Den Berg, P., Longini, M., Buonocore, G., Venegas, M., Baquero, H., Visser, G. H. & Van Bel, F. Maternal allopurinol during fetal hypoxia lowers cord blood levels of the brain injury marker S-100B. *Pediatrics* **124**, 350-357, doi:10.1542/peds.2008-2228 (2009).

75 Nie, X., Lowe, D. W., Rollins, L. G., Bentzley, J., Fraser, J. L., Martin, R., Singh, I. & Jenkins, D. Sex-specific effects of N-acetylcysteine in neonatal rats treated with hypothermia after severe hypoxia-ischemia. *Neurosci Res* **108**, 24-33, doi:10.1016/j.neures.2016.01.008 (2016).

76 Rouse, D. J., Hirtz, D. G., Thom, E., Varner, M. W., Spong, C. Y., Mercer, B. M., Iams, J. D., Wapner, R. J., Sorokin, Y., Alexander, J. M., Harper, M., Thorp, J. M., Jr., Ramin, S. M., Malone, F. D., Carpenter, M., Miodovnik, M., Moawad, A., O'Sullivan, M. J., Peaceman, A. M., Hankins, G. D., Langer, O., Caritis, S. N. & Roberts, J. M. A randomized, controlled trial of magnesium sulfate for the prevention of cerebral palsy. *The New England journal of medicine* **359**, 895-905, doi:10.1056/NEJMoa0801187 (2008).

77 Sirén, A. L., Fratelli, M., Brines, M., Goemans, C., Casagrande, S., Lewczuk, P., Keenan, S., Gleiter, C., Pasquali, C., Capobianco, A., Mennini, T., Heumann, R., Cerami, A., Ehrenreich, H. & Ghezzi, P. Erythropoietin prevents neuronal apoptosis

after cerebral ischemia and metabolic stress. *Proceedings of the National Academy of Sciences of the United States of America* **98**, 4044-4049, doi:10.1073/pnas.051606598 (2001).

78 Gorio, A., Gokmen, N., Erbayraktar, S., Yilmaz, O., Madaschi, L., Cichetti, C., Di Giulio, A. M., Vardar, E., Cerami, A. & Brines, M. Recombinant human erythropoietin counteracts secondary injury and markedly enhances neurological recovery from experimental spinal cord trauma. *Proceedings of the National Academy of Sciences of the United States of America* **99**, 9450-9455, doi:10.1073/pnas.142287899 (2002).

79 Campana, W. M. & Myers, R. R. Erythropoietin and erythropoietin receptors in the peripheral nervous system: changes after nerve injury. *FASEB journal : official publication of the Federation of American Societies for Experimental Biology* **15**, 1804-1806, doi:10.1096/fj.00-0857fje (2001).

80 Ozturk, E., Demirbilek, S., Kadir But, A., Saricicek, V., Gulec, M., Akyol, O. & Ozcan Ersoy, M. Antioxidant properties of propofol and erythropoietin after closed head injury in rats. *Progress in neuro-psychopharmacology & biological psychiatry* **29**, 922-927, doi:10.1016/j.pnpbp.2005.04.028 (2005).

81 Wang, L., Zhang, Z., Wang, Y., Zhang, R. & Chopp, M. Treatment of stroke with erythropoietin enhances neurogenesis and angiogenesis and improves neurological function in rats. *Stroke* **35**, 1732-1737, doi:10.1161/01.STR.0000132196.49028.a4 (2004).

82 Jantzie, L. L., Miller, R. H. & Robinson, S. Erythropoietin signaling promotes oligodendrocyte development following prenatal systemic hypoxic-ischemic brain injury. *Pediatric research* **74**, 658-667, doi:10.1038/pr.2013.155 (2013).

83 Juul, S. E. & Pet, G. C. Erythropoietin and Neonatal Neuroprotection. *Clinics in perinatology* **42**, 469-481, doi:10.1016/j.clp.2015.04.004 (2015).

84 Reiter, R. J., Tan, D. X., Osuna, C. & Gitto, E. Actions of melatonin in the reduction of oxidative stress. A review. *Journal of biomedical science* **7**, 444-458, doi:10.1007/bf02253360 (2000).

85 Acuña-Castroviejo, D., Martín, M., Macías, M., Escames, G., León, J., Khaldy, H. & Reiter, R. J. Melatonin, mitochondria, and cellular bioenergetics. *Journal of pineal research* **30**, 65-74, doi:10.1034/j.1600-079x.2001.300201.x (2001).

86 Peeters-Scholte, C., Braun, K., Koster, J., Kops, N., Blomgren, K., Buonocore, G., van Buul-Offers, S., Hagberg, H., Nicolay, K., van Bel, F. & Groenendaal, F. Effects of allopurinol and deferoxamine on reperfusion injury of the brain in newborn piglets after neonatal hypoxia-ischemia. *Pediatric research* **54**, 516-522, doi:10.1203/01.pdr.0000081297.53793.c6 (2003).

87 Khan, M., Sekhon, B., Jatana, M., Giri, S., Gilg, A. G., Sekhon, C., Singh, I. & Singh, A. K. Administration of N-acetylcysteine after focal cerebral ischemia protects brain and reduces inflammation in a rat model of experimental stroke. *Journal of neuroscience research* **76**, 519-527, doi:10.1002/jnr.20087 (2004).

88 Marret, S., Doyle, L. W., Crowther, C. A. & Middleton, P. Antenatal magnesium sulphate neuroprotection in the preterm infant. *Seminars in fetal & neonatal medicine* **12**, 311-317, doi:10.1016/j.siny.2007.04.001 (2007).

89 Costantine, M. M. & Weiner, S. J. Effects of antenatal exposure to magnesium sulfate on neuroprotection and mortality in preterm infants: a meta-analysis. *Obstetrics and gynecology* **114**, 354-364, doi:10.1097/AOG.0b013e3181ae98c2 (2009).

90 Qin, X., Cheng, J., Zhong, Y., Mahgoub, O. K., Akter, F., Fan, Y., Aldughaim, M., Xie, Q., Qin, L., Gu, L., Jian, Z., Xiong, X. & Liu, R. Mechanism and Treatment Related to Oxidative Stress in Neonatal Hypoxic-Ischemic Encephalopathy. *Front Mol Neurosci* **12**, 88, doi:10.3389/fnmol.2019.00088 (2019).

91 Shen, Q., Goderie, S. K., Jin, L., Karanth, N., Sun, Y., Abramova, N., Vincent, P., Pumiglia, K. & Temple, S. Endothelial cells stimulate self-renewal and expand neurogenesis of neural stem cells. *Science (New York, N.Y.)* **304**, 1338-1340, doi:10.1126/science.1095505 (2004).

92 Ahn, S. Y., Chang, Y. S., Sung, D. K., Sung, S. I., Yoo, H. S., Lee, J. H., Oh, W. I. & Park, W. S. Mesenchymal stem cells prevent hydrocephalus after severe intraventricular hemorrhage. *Stroke* **44**, 497-504, doi:10.1161/strokeaha.112.679092 (2013).

93 MacFarlane, R. J., Graham, S. M., Davies, P. S., Korres, N., Tsouchnica, H., Heliotis, M., Mantalaris, A. & Tsiridis, E. Anti-inflammatory role and immunomodulation of mesenchymal stem cells in systemic joint diseases: potential for treatment. *Expert opinion on therapeutic targets* **17**, 243-254, doi:10.1517/14728222.2013.746954 (2013).

94 Li, J., Yawno, T., Sutherland, A., Loose, J., Nitsos, I., Bischof, R., Castillo-Melendez, M., McDonald, C. A., Wong, F. Y., Jenkin, G. & Miller, S. L. Preterm white matter brain injury is prevented by early administration of umbilical cord blood cells. *Experimental neurology* **283**, 179-187, doi:10.1016/j.expneurol.2016.06.017 (2016).

95 Paton, M. C. B., McDonald, C. A., Allison, B. J., Fahey, M. C., Jenkin, G. & Miller, S. L. Perinatal Brain Injury As a Consequence of Preterm Birth and Intrauterine Inflammation: Designing Targeted Stem Cell Therapies. *Frontiers in neuroscience* **11**, 200, doi:10.3389/fnins.2017.00200 (2017).

96 Parekkadan, B. & Milwid, J. M. Mesenchymal stem cells as therapeutics. *Annu Rev Biomed Eng* **12**, 87-117, doi:10.1146/annurev-bioeng-070909-105309 (2010).

97 Hofer, H. R. & Tuan, R. S. Secreted trophic factors of mesenchymal stem cells support neurovascular and musculoskeletal therapies. *Stem Cell Res Ther* **7**, 131, doi:10.1186/s13287-016-0394-0 (2016).

98 Caplan, A. I. & Dennis, J. E. Mesenchymal stem cells as trophic mediators. *Journal of cellular biochemistry* **98**, 1076-1084, doi:10.1002/jcb.20886 (2006).

99 Majumdar, M. K., Thiede, M. A., Haynesworth, S. E., Bruder, S. P. & Gerson, S. L. Human marrow-derived mesenchymal stem cells (MSCs) express hematopoietic cytokines and support long-term hematopoiesis when differentiated toward stromal and osteogenic lineages. *Journal of hematotherapy & stem cell research* **9**, 841-848, doi:10.1089/152581600750062264 (2000).

100 Greenbaum, A., Hsu, Y. M., Day, R. B., Schuettpelz, L. G., Christopher, M. J., Borgerding, J. N., Nagasawa, T. & Link, D. C. CXCL12 in early mesenchymal progenitors is required for haematopoietic stem-cell maintenance. *Nature* **495**, 227-230, doi:10.1038/nature11926 (2013).

101 Li, F., Zhang, K., Liu, H., Yang, T., Xiao, D. J. & Wang, Y. S. The neuroprotective effect of mesenchymal stem cells is mediated through inhibition of apoptosis in hypoxic ischemic injury. *World journal of pediatrics : WJP* **16**, 193-200, doi:10.1007/s12519-019-00310-x (2020).

102 Cotten, C. M., Fisher, K., Kurtzberg, J. & Simmons, R. Phase I Trial of Allogeneic Umbilical Cord Tissue-Derived Mesenchymal Stromal Cells in Neonates with

Hypoxic-Ischemic Encephalopathy. *Cytotherapy* **22**, doi:10.1016/j.jcyt.2020.04.052 (2020).

103 Kabataş, S., Civelek, E., Kaplan, N., Savrunlu, E. C., Sezen, G. B., Chasan, M., Can, H., Genç, A., Akyuva, Y., Boyalı, O., Diren, F. & Karaöz, E. Phase I study on the safety and preliminary efficacy of allogeneic mesenchymal stem cells in hypoxic-ischemic encephalopathy. *World journal of experimental medicine* **11**, 17-29, doi:10.5493/wjem.v11.i2.17 (2021).

104 Kabatas, S., Civelek, E., Savrunlu, E. C., Kaplan, N., Boyalı, O., Diren, F., Can, H., Genç, A., Akkoç, T. & Karaöz, E. Feasibility of allogeneic mesenchymal stem cells in pediatric hypoxic-ischemic encephalopathy: Phase I study. *World journal of stem cells* **13**, 470-484, doi:10.4252/wjsc.v13.i5.470 (2021).

105 Garnier, Y., Middelanis, J., Jensen, A. & Berger, R. Neuroprotective effects of magnesium on metabolic disturbances in fetal hippocampal slices after oxygen-glucose deprivation: mediation by nitric oxide system. *Journal of the Society for Gynecologic Investigation* **9**, 86-92, doi:10.1016/s1071-5576(01)00161-7 (2002).

106 Cristòfol, R. M., Rodríguez-Farré, E. & Sanfeliu, C. Effects of glucose and oxygen deprivation on phosphoinositide hydrolysis in cerebral cortex slices from neonatal rats. *Life sciences* **59**, 587-597, doi:10.1016/0024-3205(96)00340-2 (1996).

107 Fernández-López, D., Martínez-Orgado, J., Casanova, I., Bonet, B., Leza, J. C., Lorenzo, P., Moro, M. A. & Lizasoain, I. Immature rat brain slices exposed to oxygen-glucose deprivation as an in vitro model of neonatal hypoxic-ischemic encephalopathy. *Journal of neuroscience methods* **145**, 205-212, doi:10.1016/j.jneumeth.2005.01.005 (2005).

108 Caldeira, M. V., Curcio, M., Leal, G., Salazar, I. L., Mele, M., Santos, A. R., Melo, C. V., Pereira, P., Canzoniero, L. M. & Duarte, C. B. Excitotoxic stimulation downregulates the ubiquitin-proteasome system through activation of NMDA receptors in cultured hippocampal neurons. *Biochimica et biophysica acta* **1832**, 263-274, doi:10.1016/j.bbadis.2012.10.009 (2013).

109 Curcio, M., Salazar, I. L., Inácio, A. R., Duarte, E. P., Canzoniero, L. M. & Duarte, C. B. Brain ischemia downregulates the neuroprotective GDNF-Ret signaling by a calpain-dependent mechanism in cultured hippocampal neurons. *Cell death & disease* **6**, e1645, doi:10.1038/cddis.2014.578 (2015).

110 Mele, M., Aspromonte, M. C. & Duarte, C. B. Downregulation of GABA(A) Receptor Recycling Mediated by HAP1 Contributes to Neuronal Death in In Vitro Brain Ischemia. *Molecular neurobiology* **54**, 45-57, doi:10.1007/s12035-015-9661-9 (2017).

111 Levine, S. Anoxic-ischemic encephalopathy in rats. *The American journal of pathology* **36**, 1-17 (1960).

112 Rice, J. E., 3rd, Vannucci, R. C. & Brierley, J. B. The influence of immaturity on hypoxic-ischemic brain damage in the rat. *Annals of neurology* **9**, 131-141, doi:10.1002/ana.410090206 (1981).

113 Vannucci, R. C., Connor, J. R., Mauger, D. T., Palmer, C., Smith, M. B., Towfighi, J. & Vannucci, S. J. Rat model of perinatal hypoxic-ischemic brain damage. *Journal of neuroscience research* **55**, 158-163, doi:10.1002/(sici)1097-4547(19990115)55:2<158::aid-jnr3>3.0.co;2-1 (1999).

114 Shrader, S. *Introductory Mass Spectrometry*. Second edn, (2014).

115 Greaves, J. & Roboz, J. *Mass Spectrometry for the Novice.* First edn, (2014).

116 Reusch, W. *Mass Spectrometry* <https://chem.libretexts.org/Bookshelves/Organic_Chemistry/Supplemental_Modules_(Organic_Chemistry)/Spectroscopy/Mass_Spectrometry > (2020) Access date: 03/03/2021.

117 Sciex, A. *TripleTOF 6600 System - System User Guide*. (2018).

118 Andrews, G. L., Simons, B. L., Young, J. B., Hawkridge, A. M. & Muddiman, D. C. Performance characteristics of a new hybrid quadrupole time-of-flight tandem mass spectrometer (TripleTOF 5600). *Analytical chemistry* **83**, 5442-5446, doi:10.1021/ac200812d (2011).

119 Rhoades, Z. & Ghobarah, H. Broader Coverage and Automatic Mass Calibration Using the TripleTOF™ 5600 System with DuoSpray™ Ion Source. (2011).

120 Hoffmann, E. d. & Stroobant, V. *Mass Spectrometry - Principles and Applications.* Third edn, (2007).

121 Blum, F. High performance liquid chromatography. *Br J Hosp Med (Lond)* **75**, C18-21, doi:10.12968/hmed.2014.75.Sup2.C18 (2014).

122 Betancourt, J. & Gottlieb, S. *Liquid Chromatography*, <https://chem.libretexts.org/Bookshelves/Analytical_Chemistry/Supplemental_Modules_(Analytical_Chemistry)/Instrumental_Analysis/Chromatography/Liquid_Chromatography> (2020) Access date: 24/03/2021.

123 Clarke, W. in *Mass Spectrometry for the Clinical Laboratory* Ch. 1, 304 (Academic Press 2017).

124 Anjo, S. I., Santa, C. & Manadas, B. SWATH-MS as a tool for biomarker discovery: From basic research to clinical applications. *Proteomics* **17**, doi:10.1002/pmic.201600278 (2017).

125 Chernushevich, I. V., Loboda, A. V. & Thomson, B. A. An introduction to quadrupole-time-of-flight mass spectrometry. *Journal of mass spectrometry : JMS* **36**, 849-865, doi:10.1002/jms.207 (2001).

126 Guo, J. & Huan, T. Evaluation of significant features discovered from different data acquisition modes in mass spectrometry-based untargeted metabolomics. *Analytica chimica acta* **1137**, 37-46, doi:10.1016/j.aca.2020.08.065 (2020).

127 Kim, Y. M. & Heyman, H. M. in *Fungal Genomics: Methods and Protocols* Vol. 1775 (eds Ronald P. de Vries, Adrian Tsang, & Igor V. Grigoriev) Ch. 10, 107-118 (2018).

128 Dettmer, K., Aronov, P. A. & Hammock, B. D. Mass spectrometry-based metabolomics. *Mass spectrometry reviews* **26**, 51-78, doi:10.1002/mas.20108 (2007).

129 Zhou, B., Xiao, J. F., Tuli, L. & Ressom, H. W. LC-MS-based metabolomics. *Molecular bioSystems* **8**, 470-481, doi:10.1039/c1mb05350g (2012).

130 Klassen, A., Faccio, A. T., Canuto, G. A., da Cruz, P. L., Ribeiro, H. C., Tavares, M. F. & Sussulini, A. Metabolomics: Definitions and Significance in Systems Biology. *Advances in experimental medicine and biology* **965**, 3-17, doi:10.1007/978-3-319-47656-8_1 (2017).

131 Guo, J. & Huan, T. Comparison of Full-Scan, Data-Dependent, and Data-Independent Acquisition Modes in Liquid Chromatography-Mass Spectrometry Based Untargeted Metabolomics. *Analytical chemistry* **92**, 8072-8080, doi:10.1021/acs.analchem.9b05135 (2020).

132 Benton, H. P., Ivanisevic, J., Mahieu, N. G., Kurczy, M. E., Johnson, C. H., Franco, L., Rinehart, D., Valentine, E., Gowda, H., Ubhi, B. K., Tautenhahn, R., Gieschen,

A., Fields, M. W., Patti, G. J. & Siuzdak, G. Autonomous metabolomics for rapid metabolite identification in global profiling. *Analytical chemistry* **87**, 884-891, doi:10.1021/ac5025649 (2015).

133 Hu, A., Noble, W. S. & Wolf-Yadlin, A. Technical advances in proteomics: new developments in data-independent acquisition. *F1000Research* **5**, doi:10.12688/f1000research.7042.1 (2016).

134 Defossez, E., Bourquin, J., von Reuss, S., Rasmann, S. & Glauser, G. Eight key rules for successful data-dependent acquisition in mass spectrometry-based metabolomics. *Mass spectrometry reviews*, doi:10.1002/mas.21715 (2021).

135 Zhang, Y., Bilbao, A., Bruderer, T., Luban, J., Strambio-De-Castillia, C., Lisacek, F., Hopfgartner, G. & Varesio, E. The Use of Variable Q1 Isolation Windows Improves Selectivity in LC-SWATH-MS Acquisition. *Journal of proteome research* **14**, 4359-4371, doi:10.1021/acs.jproteome.5b00543 (2015).

136 Raetz, M., Bonner, R. & Hopfgartner, G. SWATH-MS for metabolomics and lipidomics: critical aspects of qualitative and quantitative analysis. *Metabolomics : Official journal of the Metabolomic Society* **16**, 71, doi:10.1007/s11306-020-01692-0 (2020).

137 Xiao, J. F., Zhou, B. & Ressom, H. W. Metabolite identification and quantitation in LC-MS/MS-based metabolomics. *Trends in analytical chemistry : TRAC* **32**, 1-14, doi:10.1016/j.trac.2011.08.009 (2012).

138 Ribbenstedt, A., Ziarrusta, H. & Benskin, J. P. Development, characterization and comparisons of targeted and non-targeted metabolomics methods. *PloS one* **13**, e0207082, doi:10.1371/journal.pone.0207082 (2018).

139 Mishra, P., Singh, U., Pandey, C. M., Mishra, P. & Pandey, G. Application of student's t-test, analysis of variance, and covariance. *Annals of cardiac anaesthesia* **22**, 407-411, doi:10.4103/aca.ACA_94_19 (2019).

140 Mishra, P., Pandey, C. M., Singh, U., Gupta, A., Sahu, C. & Keshri, A. Descriptive statistics and normality tests for statistical data. *Annals of cardiac anaesthesia* **22**, 67-72, doi:10.4103/aca.ACA_157_18 (2019).

141 Mishra, P., Pandey, C. M., Singh, U., Keshri, A. & Sabaretnam, M. Selection of appropriate statistical methods for data analysis. *Annals of cardiac anaesthesia* **22**, 297-301, doi:10.4103/aca.ACA_248_18 (2019).

142 Lee, L. C., Liong, C. Y. & Jemain, A. A. Partial least squares-discriminant analysis (PLS-DA) for classification of high-dimensional (HD) data: a review of contemporary practice strategies and knowledge gaps. *The Analyst* **143**, 3526-3539, doi:10.1039/c8an00599k (2018).

143 Bartel, J., Krumsiek, J. & Theis, F. J. Statistical methods for the analysis of high-throughput metabolomics data. *Computational and structural biotechnology journal* **4**, e201301009, doi:10.5936/csbj.201301009 (2013).

144 Ren, S., Hinzman, A. A., Kang, E. L., Szczesniak, R. D. & Lu, L. J. Computational and statistical analysis of metabolomics data. *Metabolomics : Official journal of the Metabolomic Society* **11**, 1492-1513, doi:10.1007/s11306-015-0823-6 (2015).

145 Salazar, I. L., Mele, M., Caldeira, M. V., Costa, R. O., Correia, B., Frisari, S. & Duarte, C. B. Preparation of Primary Cultures of Embryonic Rat Hippocampal and Cerebrocortical Neurons. *Bio-protocol* **7**, e2551, doi:10.21769/BioProtoc.2551 (2017).

146 Scientific, T. F. *Trypsin (1:250), powder*, <https://www.thermofisher.com/order/catalog/product/27250018> Access date: 03/01/2022.

147 Pang, Z., Chong, J., Zhou, G., de Lima Morais, D. A.,Chang, L., Barrette, M., Gauthier, C., Jacques, PÉ., Li, S. & Xia, J. MetaboAnalyst 5.0: narrowing the gap between raw spectra and functional insights. *Nucleic acids research* **49**, W388-w396, doi:10.1093/nar/gkab382 (2021).

148 Li, S., Park, Y., Duraisingham, S., Strobel, F. H., Khan, N., Soltow, Q. A., Jones, D. P. & Pulendran, B. Predicting network activity from high throughput metabolomics. *PLoS computational biology* **9**, e1003123, doi:10.1371/journal.pcbi.1003123 (2013).

149 Jackson, J. E. *A User's Guide to Principal Components*. (1991).

150 International Conference on Harmonization (ICH). Validation of analytical procedures: text and methodology Q2(R1). (2005).

151 Peters, F. T., Drummer, O. H. & Musshoff, F. Validation of new methods. *Forensic science international* **165**, 216-224, doi:10.1016/j.forsciint.2006.05.021 (2007).

152 Efstathiou, N., Theodoridis, G. & Sarafidis, K. Understanding neonatal hypoxic-ischemic encephalopathy with metabolomics. *Hippokratia* **21**, 115-123 (2017).

153 Johnson, G. V. & Jope, R. S. The role of microtubule-associated protein 2 (MAP-2) in neuronal growth, plasticity, and degeneration. *Journal of neuroscience research* **33**, 505-512, doi:10.1002/jnr.490330402 (1992).

154 Denihan, N. M., Kirwan, J. A., Walsh, B. H., Dunn, W. B., Broadhurst, D. I., Boylan, G. B. & Murray, D. M. Untargeted metabolomic analysis and pathway discovery in perinatal asphyxia and hypoxic-ischaemic encephalopathy. *Journal of cerebral blood flow and metabolism : official journal of the International Society of Cerebral Blood Flow and Metabolism* **39**, 147-162, doi:10.1177/0271678x17726502 (2019).

155 Walsh, B. H., Broadhurst, D. I., Mandal, R., Wishart, D. S., Boylan, G. B., Kenny, L. C. & Murray, D. M. The metabolomic profile of umbilical cord blood in neonatal hypoxic ischaemic encephalopathy. *PloS one* **7**, e50520, doi:10.1371/journal.pone.0050520 (2012).

156 O'Boyle, D. S., Dunn, W. B., O'Neill, D., Kirwan, J. A., Broadhurst, D. I., Hallberg, B., Boylan, G. B. & Murray, D. M. Improvement in the Prediction of Neonatal Hypoxic-Ischemic Encephalopathy with the Integration of Umbilical Cord Metabolites and Current Clinical Makers. *The Journal of pediatrics* **229**, 175-181.e171, doi:10.1016/j.jpeds.2020.09.065 (2021).

157 Liu, D., Gharavi, R., Pitta, M., Gleichmann, M. & Mattson, M. P. Nicotinamide prevents NAD+ depletion and protects neurons against excitotoxicity and cerebral ischemia: NAD+ consumption by SIRT1 may endanger energetically compromised neurons. *Neuromolecular medicine* **11**, 28-42, doi:10.1007/s12017-009-8058-1 (2009).

158 Liu, D., Chan, S. L., de Souza-Pinto, N. C., Slevin, J. R., Wersto, R. P., Zhan, M., Mustafa, K., de Cabo, R. & Mattson, M. P. Mitochondrial UCP4 mediates an adaptive shift in energy metabolism and increases the resistance of neurons to metabolic and oxidative stress. *Neuromolecular medicine* **8**, 389-414, doi:10.1385/nmm:8:3:389 (2006).

159 Wang, H., Yuan, B., Zeng, Z., He, L., Ding, H., Guo, C., Kong, X., Wang, W. & Huang, X. Identification and elucidation of the structure of in vivo metabolites of diaveridine in chicken. *Journal of chromatography. B, Analytical technologies in the biomedical and life sciences* **965**, 91-99, doi:10.1016/j.jchromb.2014.06.010 (2014).

160 Moreno, B., Hevia, H., Santamaria, M., Sepulcre, J., Muñoz, J., García-Trevijano, E. R., Berasain, C., Corrales, F. J., Avila, M. A. & Villoslada, P. Methylthioadenosine reverses brain autoimmune disease. *Annals of neurology* **60**, 323-334, doi:10.1002/ana.20895 (2006).

161 Yoshikawa, H., Hirano, A., Arakawa, T. & Shiraki, K. Mechanistic insights into protein precipitation by alcohol. *International journal of biological macromolecules* **50**, 865-871, doi:10.1016/j.ijbiomac.2011.11.005 (2012).

162 Lyseng-Williamson, K. A., Jarvis, B. & Wagstaff, A. J. Tamsulosin: an update of its role in the management of lower urinary tract symptoms. *Drugs* **62**, 135-167, doi:10.2165/00003495-200262010-00006 (2002).

163 Kawagishi, H., Ando, M., Sakamoto, H., Yoshida, S., Ojima, F., Ishiguro, Y., Ukai, N. & Furukawa, S. Hericenones C, D and E, stimulators of nerve growth factor (NGF)-synthesis, from the mushroom *Hericium erinaceum*. *Tetrahedron Letters* **32**, 4561-4564, doi:10.1016/0040-4039(91)80039-9 (1991).

164 Ma, Bing-Ji, Shen, Jin-Wen, Yu, Hai-You, Ruan, Yuan, Wu, Ting-Ting & Zhao, X. Hericenones and erinacines: stimulators of nerve growth factor (NGF) biosynthesis in *Hericium erinaceus*. *Mycology* **1**, 92-98, doi:10.1080/21501201003735556 (2010).

165 Novgorodov, S. A., Riley, C. L., Yu, J., Borg, K. T., Hannun, Y. A., Proia, R. L., Kindy, M. S. & Gudz, T. I. Essential roles of neutral ceramidase and sphingosine in mitochondrial dysfunction due to traumatic brain injury. *The Journal of biological chemistry* **289**, 13142-13154, doi:10.1074/jbc.M113.530311 (2014).

166 Cui, L., Lu, H. & Lee, Y. H. Challenges and emergent solutions for LC-MS/MS based untargeted metabolomics in diseases. *Mass spectrometry reviews* **37**, 772-792, doi:10.1002/mas.21562 (2018).

167 Nielsen, J. Systems Biology of Metabolism: A Driver for Developing Personalized and Precision Medicine. *Cell metabolism* **25**, 572-579, doi:10.1016/j.cmet.2017.02.002 (2017).

168 Emwas, A. H., Roy, R., McKay, R. T., Tenori, L., Saccenti, E., Gowda, G. A. N., Raftery, D., Alahmari, F., Jaremko, L., Jaremko, M. & Wishart, D. S. NMR Spectroscopy for Metabolomics Research. *Metabolites* **9**, doi:10.3390/metabo9070123 (2019).

169 Emwas, A. H. The strengths and weaknesses of NMR spectroscopy and mass spectrometry with particular focus on metabolomics research. *Methods in molecular biology (Clifton, N.J.)* **1277**, 161-193, doi:10.1007/978-1-4939-2377-9_13 (2015).

170 Emwas, A. M., Salek, R. M., Griffin, J. L. & Merzaban, J. NMR-based metabolomics in human disease diagnosis: applications, limitations, and recommendations *Metabolomics : Official journal of the Metabolomic Society* **9**, 1048-1072, doi:10.1007/s11306-013-0524-y (2013).

171 Schrimpe-Rutledge, A. C., Codreanu, S. G., Sherrod, S. D. & McLean, J. A. Untargeted Metabolomics Strategies-Challenges and Emerging Directions. *Journal of the American Society for Mass Spectrometry* **27**, 1897-1905, doi:10.1007/s13361-016-1469-y (2016).

172 Fuhrer, T. & Zamboni, N. High-throughput discovery metabolomics. *Current opinion in biotechnology* **31**, 73-78, doi:10.1016/j.copbio.2014.08.006 (2015).

173 Goodacre, R., Vaidyanathan, S., Dunn, W. B., Harrigan, G. G. & Kell, D. B. Metabolomics by numbers: acquiring and understanding global metabolite data. *Trends in biotechnology* **22**, 245-252, doi:10.1016/j.tibtech.2004.03.007 (2004).

174 Godzien, J., Gil de la Fuente, A., Otero, A. & Barbas, C. in *Comprehensive Analytical Chemistry* Vol. Data Analysis for Omic Sciences: Methods and Applications Volume 82 Ch. 15, 415-445 (2018).

Chapter 8
Supplementary Data

8. SUPPLEMENTARY DATA

Metabolomics Study of Primary Cultures of Cerebrocortical Neurons using LC-MS/MS – Data Analysis

8.1. Untargeted Analysis

Supplementary Table 1. Features with statistically significant differences ($-\log_{10}(p) > 1.30$) downregulated ($\log_2(FC) < -1$) and upregulated ($\log_2(FC) > 1$) obtained for the Volcano plots acquired with the LC-MS/MS data of the filtered metabolomics features of OGD and Sham groups, and of Glutamate and Control groups. Up arrow: features upregulated. Down arrow: features downregulated. OGD: oxygen and glucose deprivation; *m/z*: mass-to-charge ratio; RT: retention time; FC: fold change; *p*: *p*-value.

Volcano plot – OGD vs Sham			
Feature (*m/z*_RT)	↑ / ↓	$\log_2(FC)$	$-\log_{10}(p)$
274.2709_23.91	↑	2.464	3.554
1143.3370_21.72	↑	2.487	3.530
1226.8103_25.05	↑	2.475	3.379
520.3333_26.25	↑	2.058	3.272
302.3012_26.03	↑	2.868	3.254
774.5983_32.87	↑	2.594	3.143
737.5020_26.31	↑	2.515	2.975
350.2850_17.32	↑	2.482	2.898
864.4235_2.03	↑	2.840	2.704
290.2648_24.70	↑	6.192	2.681
930.2606_21.63	↑	2.631	2.669
621.4069_25.05	↓	-2.640	2.627
346.3270_25.93	↑	2.321	2.556
390.3528_25.93	↑	2.438	2.530
1228.8285_24.98	↑	2.823	2.367
437.1894_24.98	↑	4.686	2.303
431.1643_7.79	↑	2.703	2.284
867.3696_24.45	↑	2.459	2.273
957.2223_21.63	↑	2.758	2.232
393.2032_10.48	↑	1.970	2.138
306.2597_16.94	↑	2.077	2.083
225.1061_19.54	↑	2.027	2.043
1389.3965_21.63	↑	3.636	2.028
768.5407_32.87	↓	-2.987	2.014
919.2678_21.63	↑	2.145	1.990
330.3319_27.01	↑	2.726	1.942
496.3348_32.87	↑	2.665	1.938
941.2497_21.63	↑	2.543	1.936
599.2575_24.64	↑	3.069	1.900
699.3737_16.31	↑	1.577	1.883

1411.3786_21.63	↑	3.905	1.881
262.2342_16.40	↑	1.814	1.872
506.3134_32.93	↓	-3.064	1.871
683.5352_29.01	↑	2.093	1.841
745.4181_14.50	↑	2.853	1.823
652.3665_32.90	↓	-3.140	1.816
1367.4182_21.63	↑	2.614	1.813
233.0738_16.21	↑	1.938	1.804
533.3616_26.88	↑	2.303	1.774
638.3540_32.87	↓	-3.199	1.758
374.3573_26.92	↑	1.958	1.717
666.3640_32.93	↓	-3.221	1.700
935.2376_21.72	↑	1.558	1.686
776.5647_32.93	↓	-3.300	1.656
493.1055_21.63	↑	1.095	1.654
580.3559_32.84	↑	1.938	1.651
745.4105_14.57	↓	-2.774	1.649
459.2738_11.62	↑	1.458	1.645
549.1382_21.66	↑	1.133	1.644
697.2978_24.70	↑	3.122	1.619
686.0902_3.71	↓	-3.172	1.610
334.2886_21.82	↑	1.512	1.596
571.1194_21.75	↑	1.289	1.567
1345.4310_21.69	↑	2.963	1.564
652.3772_32.84	↑	2.959	1.505
419.0840_15.36	↑	1.234	1.493
290.2625_26.19	↓	-3.557	1.463
277.1359_22.93	↑	1.571	1.458
991.6704_27.26	↑	2.881	1.453
493.2207_24.98	↑	3.140	1.452
881.4868_25.27	↑	3.439	1.435
569.3028_25.17	↑	3.027	1.417
182.0777_4.56	↑	3.932	1.406
731.6020_32.87	↑	3.270	1.401
272.2540_24.79	↑	2.163	1.383
480.2987_33.09	↓	-2.182	1.382
365.1004_2.88	↑	3.441	1.371
529.0306_15.30	↓	-1.672	1.358
624.3426_32.84	↑	2.600	1.348
1148.7653_25.05	↑	1.868	1.336
774.5821_32.87	↓	-3.821	1.318
465.0982_22.89	↓	-1.341	1.314
486.9908_13.21	↓	-1.829	1.308
Volcano plot – Glutamate vs Control			
732.5138_2.15	↑	1.546	1.544
666.3780_32.81	↓	-3.632	1.676

688.5511_2.03	↑	1.271	1.544
530.3176_26.82	↓	-1.093	1.544
599.3116_25.30	↓	-3.719	1.576
628.5959_2.00	↑	1.008	1.544
488.2917_21.15	↑	2.282	1.576
686.0902_3.74	↓	-3.025	1.676
581.2982_25.55	↓	-3.204	1.676
704.5453_32.84	↓	-3.102	1.576
526.2484_20.33	↓	-3.388	1.544

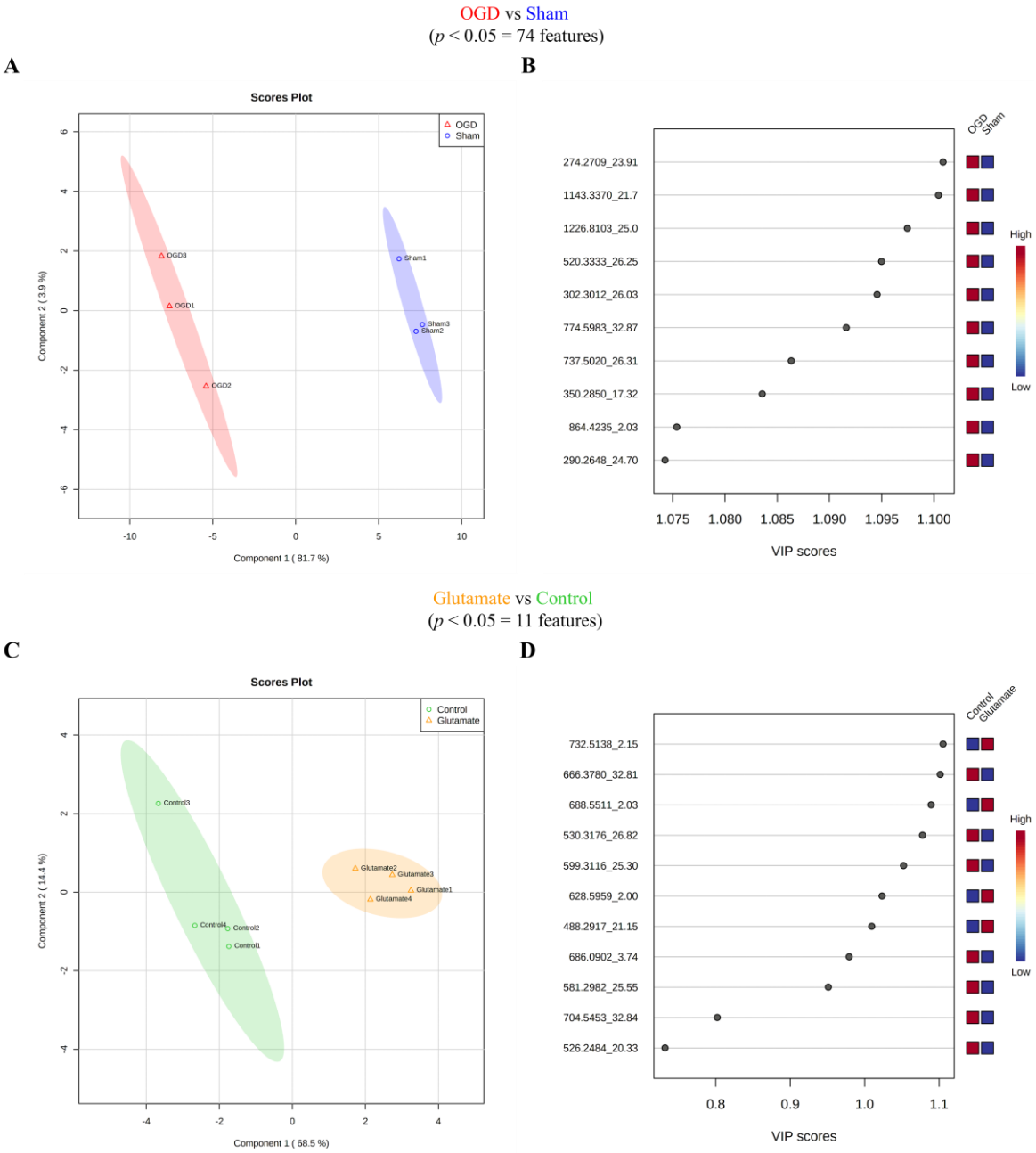

Supplementary Figure 1. Partial least squares-discriminant analysis (PLS-DA) of data acquired by LC-MS/MS and processed in MarkerView™ software for OGD and Sham groups (n = 3) (A and B) and for Glutamate and Control groups (n = 4) (C and D) performed in the first approach. Scores plot (A) and representation of the 10 features with the highest variable importance in projection (VIP) score (B) obtained using the data of the 74 features with statistically significant differences ($p < 0.05$) from Student's *t*-test of OGD and Sham groups. Scores plot (C) and representation of the VIP scores for each feature (D) obtained using the data of the 11 features with statistically significant differences ($p < 0.05$) from Mann-Whitney test of Glutamate and Control groups. The scores plots (A and C) show the clear formation and separation of the respective two groups along the component 1: OGD group in red and Sham group in blue (A); Glutamate group in yellow and Control group in green (C). B) All 10 features are elevated in the OGD group. D) All

the 11 features with statistically significant differences are represented, 4 are elevated in the Glutamate group and 7 have VIP score greater than 1. The ellipses represent the 95% confidence regions. PLS-DA was performed in MetaboAnalyst 5.0 with auto scaling. A) and B) Validation parameters of the model (cross validation method: LOOCV; number of components: 1; R^2: 0.98285; Q^2: 0.9599; p = 0.101). C) and D) Validation parameters of the model (cross validation method: LOOCV; number of components: 4; R^2: 0.99671; Q^2: 0.89058; p = 0.939).

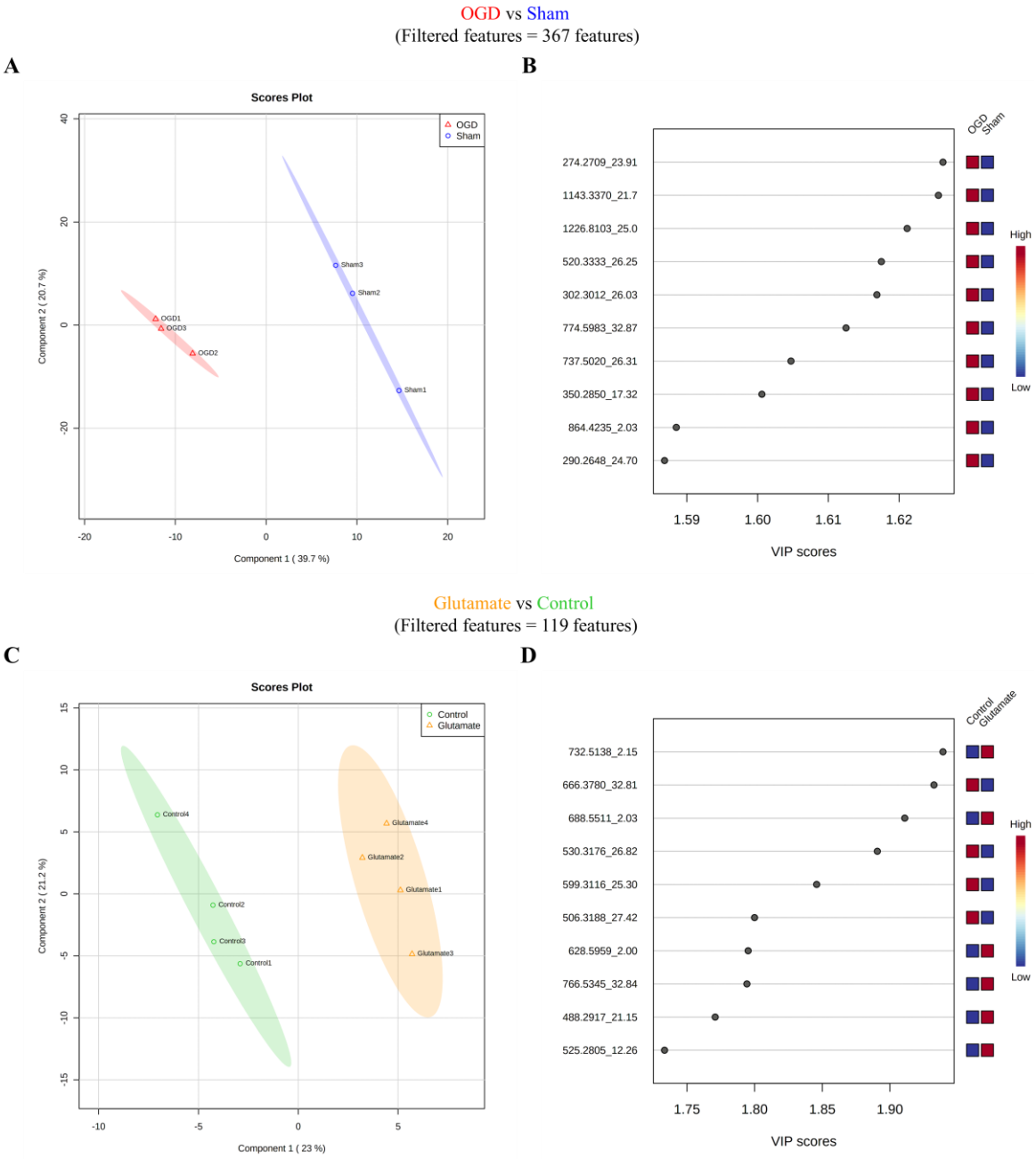

Supplementary Figure 2. Partial least squares-discriminant analysis (PLS-DA) of data acquired by LC-MS/MS and processed in MarkerView™ software for OGD and Sham groups (n = 3) (A and B) and for Glutamate and Control groups (n = 4) (C and D) performed in the second approach. Scores plot (A) and representation of the 10 features with the highest variable importance in projection (VIP) score (B) obtained using the data of the 367 filtered features of OGD and Sham groups. Scores plot (C) and representation of the 10 features with the highest VIP score (D) obtained using the data of the 119 filtered features of Glutamate and Control groups. The scores plots (A and C) show the clear formation and separation of the respective two groups along the component 1: OGD group in red and Sham group in blue (A); Glutamate group in yellow and Control group in green (C). B) All the 10 features are elevated in the OGD group. D) Of the 10 features, 6 are elevated in the Glutamate group. The ellipses represent the 95% confidence regions.

PLS-DA was performed in MetaboAnalyst 5.0 with auto scaling. A) and B) Validation parameters of the model (cross validation method: LOOCV; number of components: 3; R^2: 0.99987; Q^2: 0.69025; p = 1). C) and D) Validation parameters of the model (cross validation method: LOOCV; number of components: 4; R^2: 0.99963; Q^2: 0.50526; p = 1).

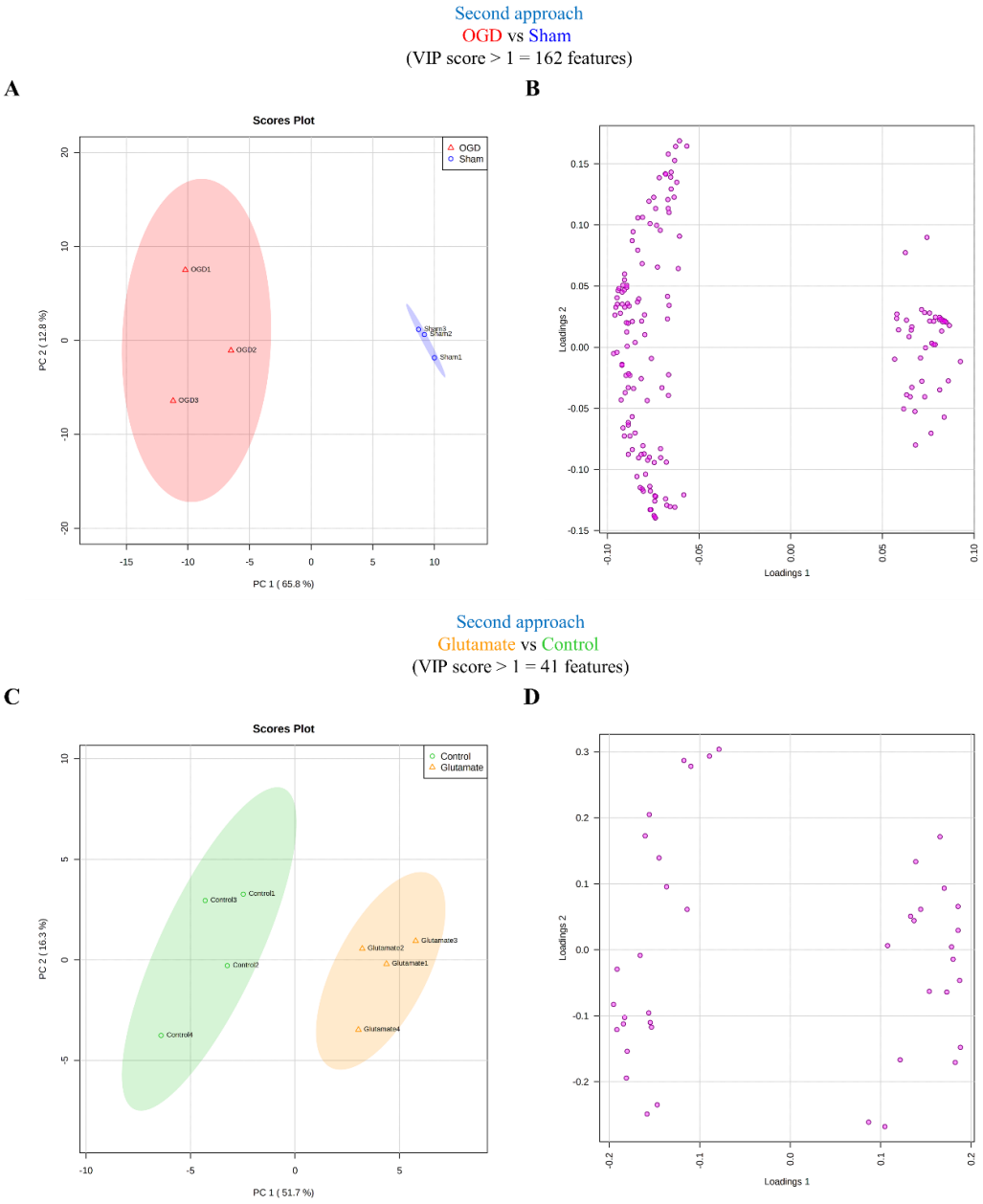

Supplementary Figure 3. Principal component analysis (PCA) of data acquired by LC-MS/MS and processed in MarkerView™ software for OGD and Sham groups (n = 3) (A and B) and for Glutamate and Control groups (n = 4) (C and D). Scores plot (A) and loadings plot (B) obtained using the data of the 162 features with variable importance in projection (VIP) score greater than 1 from PLS-DA (second approach) of OGD and Sham groups. Scores plot (C) and loadings plot (D) obtained using the data of the 41 features with VIP score greater than 1 from PLS-DA (second approach) of Glutamate and Control groups. The scores plots (A and C) show the formation and separation of the respective two groups along the PC1 (OGD group in red and Sham group in blue (A); Glutamate group in yellow and Control group in green (C)), which are explained by the features with the largest contribution along the loadings 1 on the respective loadings plots (B and D). The ellipses represent the 95% confidence regions. PCA was performed in MetaboAnalyst 5.0 with auto scaling.

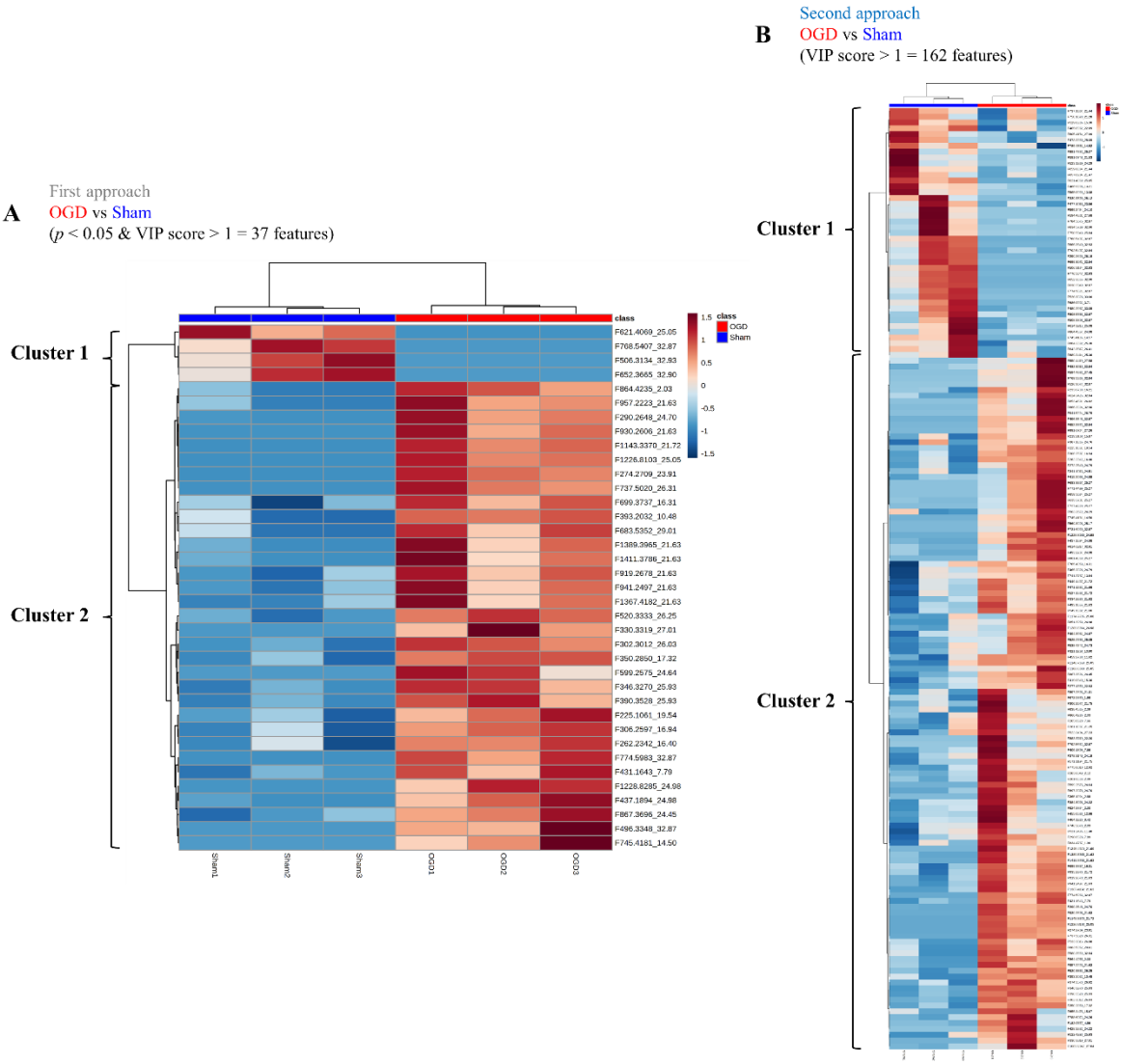

Supplementary Figure 4. Hierarchical clustering heatmaps obtained in the comparison of data acquired by LC-MS/MS and processed in MarkerView™ software for OGD and Sham groups (n = 3). A) Hierarchical clustering heatmap obtained using the data of the 37 features with statistically significant differences (*p*-value (*p*) < 0.05) from Student's *t*-test and variable importance in projection (VIP) score greater than 1 from PLS-DA (first approach). B) Hierarchical clustering heatmap obtained using the data of the 162 features with VIP score greater than 1 from PLS-DA (second approach). Increased features are in red and decreased features are in blue. The hierarchical clustering analysis (on top) shows the separation into two groups (OGD group in red and Sham group in blue). The heatmaps show the formation of two clusters (1 and 2). Cluster 1: features increased in the Sham group. Cluster 2: features increased in the OGD group. Hierarchical clustering heatmaps were performed in MetaboAnalyst 5.0 using auto scaling and the distance measure Euclidean.

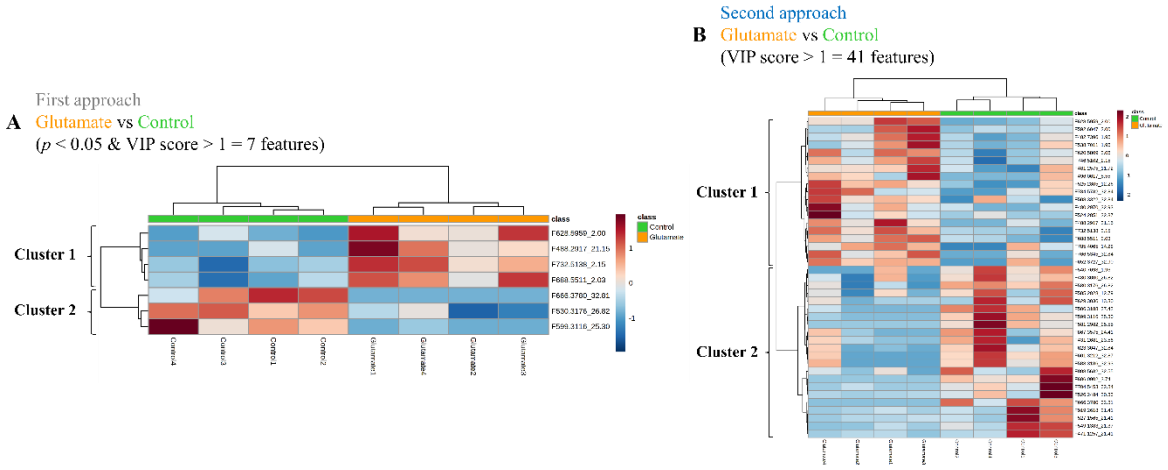

Supplementary Figure 5. Hierarchical clustering heatmaps obtained in the comparison of data acquired by LC-MS/MS and processed in MarkerView™ software for Glutamate and Control groups (n = 4). A) Hierarchical clustering heatmap obtained using the data of the 7 features with statistically significant differences (*p*-value (*p*) < 0.05) from Mann-Whitney test and variable importance in projection (VIP) score greater than 1 from PLS-DA (first approach). B) Hierarchical clustering heatmap obtained using the data of the 41 features with VIP score greater than 1 from PLS-DA (second approach). Increased features are in red and decreased features are in blue. The hierarchical clustering analysis (on top) shows the separation into two groups (Glutamate group in yellow and Control group in green). The heatmaps show the formation of two clusters (1 and 2). Cluster 1: features increased in the Glutamate group. Cluster 2: features increased in the Control group. Hierarchical clustering heatmaps were performed in MetaboAnalyst 5.0 using auto scaling and the distance measure Euclidean.

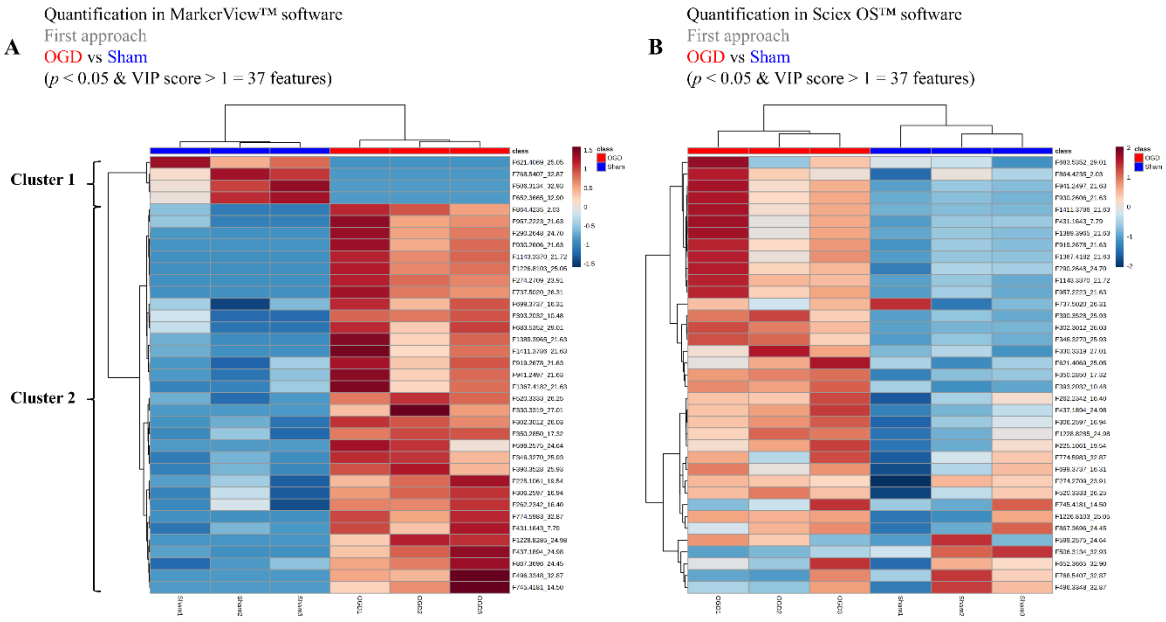

Supplementary Figure 6. Hierarchical clustering heatmaps obtained in the comparison of data acquired by LC-MS/MS for OGD and Sham groups (n = 3). The data used corresponds to the data of the 37 features with statistically significant differences (*p*-value (*p*) < 0.05) from Student's *t*-test and variable importance in projection (VIP) score greater than 1 from PLS-DA (first approach) obtained through the quantification performed in MarkerView™ software (A) and through the quantification performed in Sciex OS™ software (B). Increased features are in red and decreased features are in blue. A) and B) The hierarchical clustering analysis (on top) shows the separation into two groups (OGD group in red and Sham group in blue). A) The heatmap shows the formation of two clusters (1 and 2). Cluster 1: features increased in the Sham group. Cluster 2: features increased in the OGD group. Hierarchical clustering heatmaps were performed in MetaboAnalyst 5.0 using auto scaling and the distance measure Euclidean.

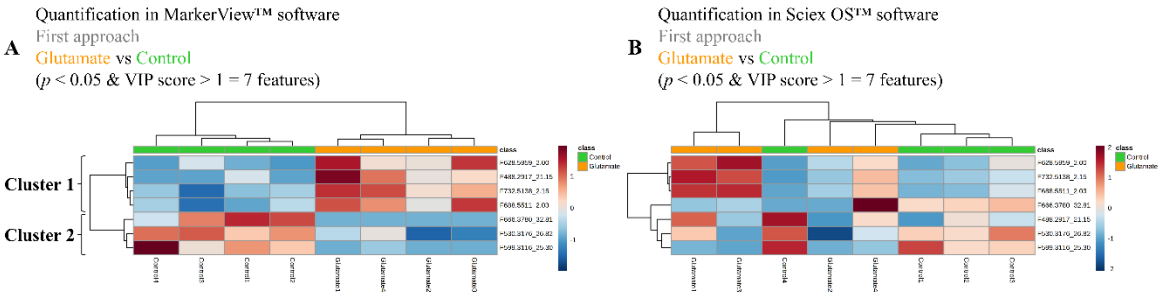

Supplementary Figure 7. Hierarchical clustering heatmaps obtained in the comparison of data acquired by LC-MS/MS for Glutamate and Control groups (n = 4). The data used corresponds to the data of the 7 features with statistically significant differences (*p*-value (*p*) < 0.05) from Mann-Whitney test and variable importance in projection (VIP) score greater than 1 from PLS-DA (first approach) obtained through the quantification performed in MarkerView™ software (A) and through the quantification performed in Sciex OS™ software (B). Increased features are in red and decreased features are in blue. A) The hierarchical clustering analysis (on top) shows the separation into two groups (Glutamate group in yellow and Control group in green). The heatmap shows the formation of two clusters (1 and 2). Cluster 1: features increased in the Glutamate group. Cluster 2: features increased in the Control group. Hierarchical clustering heatmaps were performed in MetaboAnalyst 5.0 using auto scaling and the distance measure Euclidean.

Supplementary Table 2. Metabolites identified in Sciex OS™ software using the LC-MS/MS data of the interesting features selected in each of the two approaches for OGD and Sham groups for the untargeted metabolomics analysis of the primary cultures of cerebrocortical neurons submitted to an OGD insult and a glutamate stimulus, with the respective precursor mass-to-charge ratio (*m/z*) and retention time (RT) used for identification. M+Na: sodium adduct.

	Feature (*m/z*_RT)	
Metabolite	**Precursor *m/z***	**RT (min)**
Tyrosine	182.0777	4.56
Tryptophan	205.0920	7.66
Diaveridine	261.0833	2.09
Methylthioadenosine	298.0923	7.89
Sphinganine	302.3012	26.03
Maltose/Sucrose, M+Na	365.1004	2.88
Helvolic acid	569.3028	25.17

Supplementary Table 3. Interesting features of OGD and Sham groups (first thirty-one lines of the table) and of Glutamate and Control groups (last eight lines of the table), selected in each of the two approaches performed for the comparison of the two groups of each insult, for which no identification was obtained in Sciex OS™ software and no annotation was obtained in XCMS™ platform. The features in bold are the ones that presented statistically significant differences (*p*-value smaller than 0.05) between the Sham and OGD groups after quantification in Sciex OS™ software. The data represented were obtained from two models of induced neuronal death based on oxygen and glucose deprivation (OGD) and glutamate excitotoxicity, with the respective controls for each model, performed on primary cultures of cerebrocortical neurons. For each model (OGD vs Sham and Glutamate vs Control), the data obtained after quantification in Sciex OS™ software (mean values of each group, *p*-value, and base-2 logarithm (log) of fold change (FC)) are represented. To compare the OGD and Sham groups was performed a Student's *t*-test and to compare the Glutamate and Control groups was performed a Mann-Whitney test. The FC is the ratio between the two group means. *m/z*: mass-to-charge ratio; RT: retention time; SEM: standard error of the mean.

Untargeted analysis								
	OGD vs Sham				**Glutamate vs Control**			
Feature (*m/z*_RT)	**Sham mean ± SEM**	**OGD mean ± SEM**	***p*-value**	**log_2(FC) (OGD/Sham)**	**Control mean ± SEM**	**Glutamate mean ± SEM**	***p*-value**	**log_2(FC) (Glutamate/Control)**
274.2709_23.91	32.663 ± 14.193	46.143 ± 1.414	0.3981	0.498	37.445 ± 8.172	29.530 ± 6.932	0.6857	-0.343
1143.3370_21.72	0.006 ± 0.001	0.025 ± 0.004	0.0085	2.187	0.007 ± 0.004	0.001 ± 0.000	0.6286	-2.469
1226.8103_25.05	0.014 ± 0.010	0.034 ± 0.001	0.1169	1.292	0.006 ± 0.003	0.010 ± 0.003	0.4857	0.675
520.3333_26.25	0.367 ± 0.091	0.536 ± 0.023	0.1449	0.546	0.641 ± 0.148	1.070 ± 0.448	0.4857	0.740
774.5983_32.87	0.095 ± 0.034	0.150 ± 0.028	0.2813	0.656	0.130 ± 0.028	0.134 ± 0.025	0.8857	0.048
737.5020_26.31	0.061 ± 0.023	0.074 ± 0.006	0.6072	0.283	0.048 ± 0.019	0.046 ± 0.016	0.8857	-0.069
350.2850_17.32	0.065 ± 0.016	0.204 ± 0.007	0.0014	1.661	0.133 ± 0.032	0.057 ± 0.023	0.2000	-1.223

864.4235_2.03	0.063 ± 0.015	0.106 ± 0.015	0.1104	0.751	0.093 ± 0.008	0.161 ± 0.029	0.0571	0.800
290.2648_24.70	0.704 ± 0.233	2.044 ± 0.337	0.0308	1.537	1.007 ± 0.210	0.688 ± 0.150	0.3429	-0.550
930.2606_21.63	0.015 ± 0.002	0.081 ± 0.016	0.0156	2.452	0.023 ± 0.013	0.006 ± 0.004	0.3429	-1.909
346.3270_25.93	0.585 ± 0.159	3.150 ± 0.414	0.0044	2.429	2.713 ± 0.729	0.975 ± 0.410	0.1143	-1.476
390.3528_25.93	0.113 ± 0.033	0.691 ± 0.095	0.0046	2.613	0.493 ± 0.134	0.174 ± 0.082	0.1143	-1.505
1228.8285_24.98	0.011 ± 0.006	0.036 ± 0.004	0.0307	1.681	0.006 ± 0.003	0.005 ± 0.001	>0.9999	-0.444
867.3696_24.45	0.088 ± 0.066	0.156 ± 0.026	0.3881	0.830	0.112 ± 0.036	0.072 ± 0.014	0.4857	-0.630
957.2223_21.63	0.024 ± 0.004	0.067 ± 0.009	0.0121	1.495	0.032 ± 0.012	0.012 ± 0.004	0.1143	-1.386
306.2597_16.94	0.587 ± 0.193	1.312 ± 0.097	0.0285	1.160	0.896 ± 0.208	0.388 ± 0.126	0.2000	-1.207
225.1061_19.54	0.424 ± 0.133	0.842 ± 0.099	0.0655	0.992	0.881 ± 0.238	0.257 ± 0.108	0.0571	-1.778
1389.3965_21.63	0.025 ± 0.005	0.108 ± 0.026	0.0352	2.092	0.032 ± 0.016	0.010 ± 0.003	0.6857	-1.653
768.5407_32.87	0.313 ± 0.075	0.211 ± 0.083	0.4139	-0.568	0.174 ± 0.041	0.286 ± 0.088	0.4857	0.716
919.2678_21.63	0.462 ± 0.089	1.417 ± 0.219	0.0156	1.616	0.501 ± 0.222	0.219 ± 0.058	0.3429	-1.192
330.3319_27.01	0.177 ± 0.037	0.465 ± 0.080	0.0302	1.397	0.835 ± 0.181	0.364 ± 0.197	0.2000	-1.199
496.3348_32.87	0.288 ± 0.098	0.251 ± 0.053	0.7555	-0.199	0.330 ± 0.083	0.551 ± 0.254	0.4857	0.740

941.2497_21.63	0.142 ± 0.030	0.570 ± 0.120	0.0257	2.008	0.225 ± 0.071	0.142 ± 0.069	0.2000	-0.666
599.2575_24.64	0.062 ± 0.025	0.070 ± 0.015	0.7827	0.189	0.102 ± 0.027	0.110 ± 0.051	>0.9999	0.117
699.3737_16.31	0.095 ± 0.024	0.137 ± 0.011	0.1804	0.530	0.114 ± 0.023	0.079 ± 0.018	0.3429	-0.533
1411.3786_21.63	0.008 ± 0.001	0.047 ± 0.011	0.0231	2.534	0.014 ± 0.006	0.007 ± 0.003	0.4857	-1.031
262.2342_16.40	3.312 ± 1.047	6.018 ± 0.577	0.0863	0.862	3.828 ± 0.889	1.965 ± 0.640	0.2000	-0.962
683.5352_29.01	0.195 ± 0.044	0.338 ± 0.096	0.2476	0.795	0.869 ± 0.334	0.726 ± 0.216	>0.9999	-0.260
745.4181_14.50	0.318 ± 0.087	0.354 ± 0.090	0.7863	0.155	0.165 ± 0.050	0.131 ± 0.028	0.8857	-0.333
652.3665_32.90	0.134 ± 0.035	0.160 ± 0.033	0.6177	0.255	0.149 ± 0.013	0.162 ± 0.016	0.8857	0.117
1367.4182_21.63	0.055 ± 0.010	0.190 ± 0.036	0.0233	1.786	0.051 ± 0.027	0.017 ± 0.005	0.4857	-1.574
488.2917_21.15	0.182 ± 0.051	0.514 ± 0.237	0.2433	1.495	0.415 ± 0.107	0.378 ± 0.090	0.8857	-0.134
666.3780_32.81	0.062 ± 0.017	0.088 ± 0.022	0.3991	0.497	0.078 ± 0.006	0.077 ± 0.014	0.6857	-0.009
688.5511_2.03	0.131 ± 0.029	0.200 ± 0.029	0.1647	0.611	0.176 ± 0.017	0.309 ± 0.047	0.0571	0.815
530.3176_26.82	0.282 ± 0.106	0.260 ± 0.108	0.8916	-0.117	0.716 ± 0.053	0.427 ± 0.104	0.1143	-0.744
732.5138_2.15	0.055 ± 0.010	0.090 ± 0.007	0.0505	0.712	0.071 ± 0.007	0.129 ± 0.022	0.1143	0.863
628.5959_2.00	0.125 ± 0.038	0.159 ± 0.005	0.4230	0.344	0.141 ± 0.019	0.251 ± 0.039	0.0571	0.836

766.5345_32.84	0.083 ± 0.030	0.072 ± 0.033	0.8211	-0.202	0.094 ± 0.019	0.129 ± 0.027	0.3429	0.458
525.2805_12.26	2.091 ± 0.466	2.552 ± 0.224	0.4229	0.287	1.941 ± 0.251	2.614 ± 0.193	0.1143	0.429

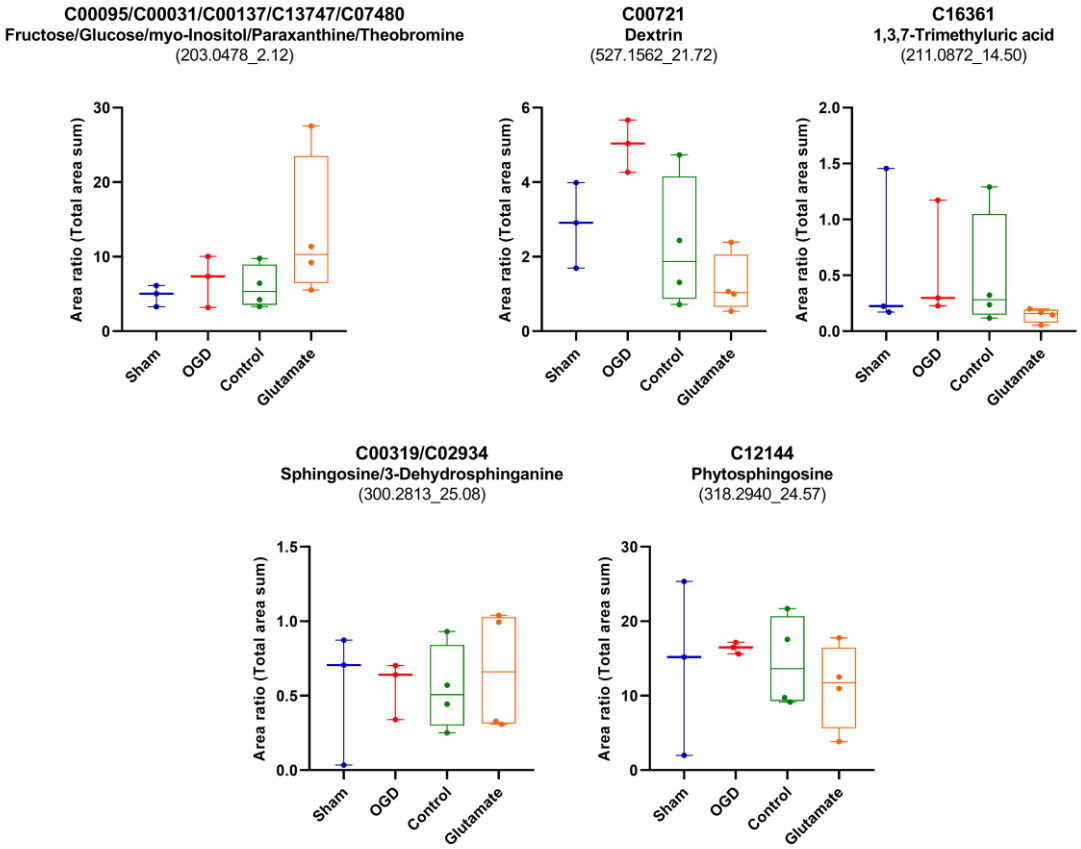

Supplementary Figure 8. Quantification of the KEGG compound entries obtained through the metabolic pathways analysis performed using the LC-MS/MS data of the monoisotopic features of OGD and Sham groups (n = 3). The respective metabolites are represented in bold and the *m/z* value and the retention time used to perform the quantification are represented in brackets (*m/z*_RT). The data represent the area ratio for each sample of each group (Sham, OGD, Control and Glutamate). Area ratio corresponds to the peak area obtained from Sciex OS™ software normalized to the total area sum of all detected features in MarkerView™ software for each sample. The whiskers represent the minimum and maximum area ratio values.

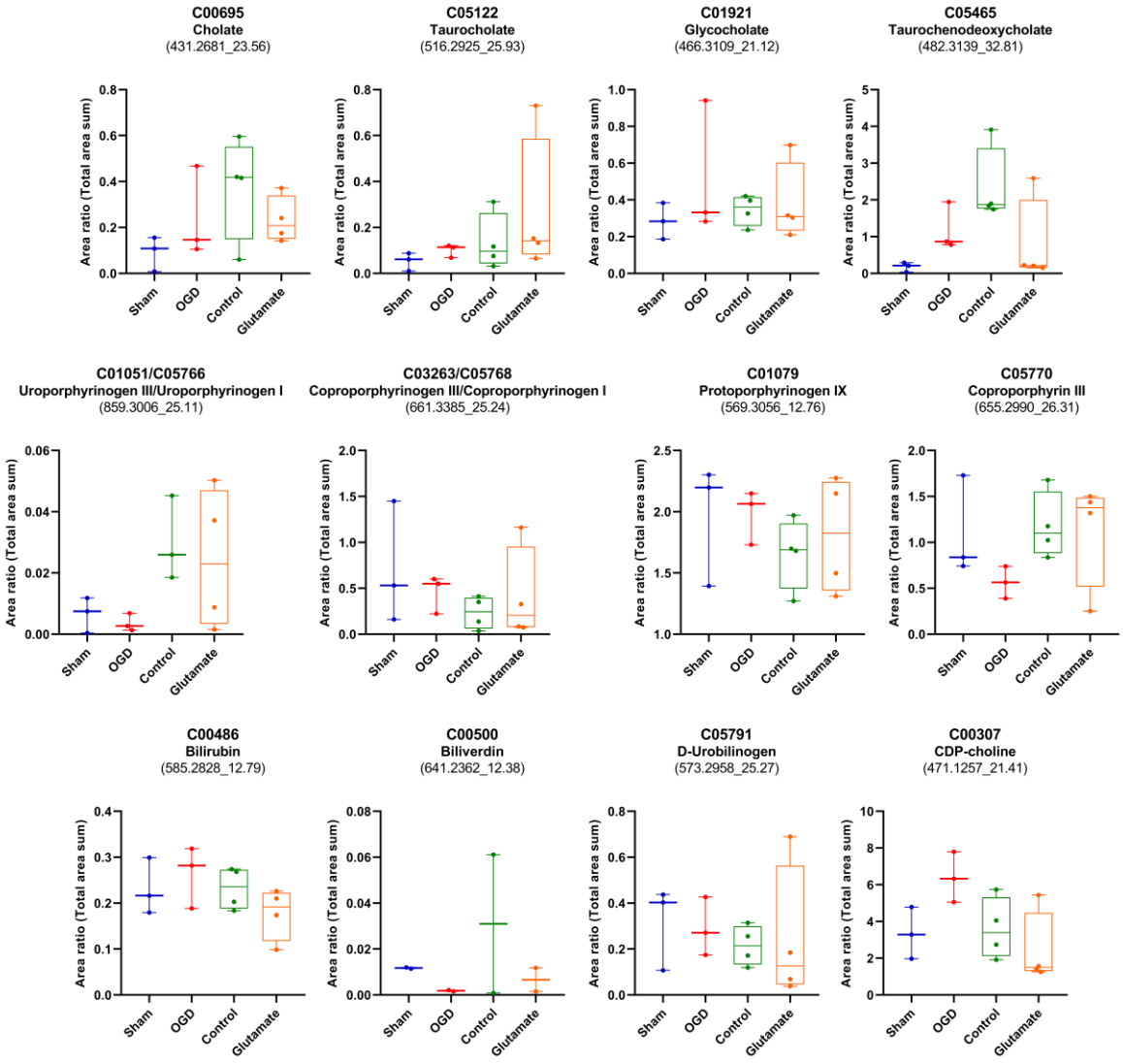

Supplementary Figure 9. Quantification of the KEGG compound entries obtained through the metabolic pathways analysis performed using the LC-MS/MS data of the monoisotopic features of Glutamate and Control groups (n = 4). The respective metabolites are represented in bold and the *m/z* value and the retention time used to perform the quantification are represented in brackets (*m/z*_RT). The data represent the area ratio for each sample of each group (Sham, OGD, Control and Glutamate). Area ratio corresponds to the peak area obtained from Sciex OS™ software normalized to the total area sum of all detected features in MarkerView™ software for each sample. The whiskers represent the minimum and maximum area ratio values. CDP-choline: cytidine 5-diphosphocholine.

Supplementary Table 4. KEGG compound entries obtained for the metabolic pathways analysis performed with the LC-MS/MS data of the monoisotopic features of OGD and Sham groups (first five) and of Glutamate and Control groups (last twelve) using the Mummichog algorithm and *Rattus norvegicus* (rat) library. The data represented were obtained from two models of induced neuronal death based on oxygen and glucose deprivation (OGD) and glutamate excitotoxicity, with the respective controls for each model, performed on primary cultures of cerebrocortical neurons. For each model (OGD vs Sham and Glutamate vs Control), the data obtained after quantification in Sciex OS™ software (mean values of each group, *p*-value, and base-2 logarithm (log) of fold change (FC)) are represented. To compare the OGD and Sham groups was performed a Student's *t*-test and to compare the Glutamate and Control groups was performed a Mann-Whitney test. The FC is the ratio between the two group means. SEM: standard error of the mean.

Metabolic pathways analysis								
	OGD vs Sham				**Glutamate vs Control**			
KEGG compound entries	**Sham mean ± SEM**	**OGD mean ± SEM**	***p*-value**	**log_2(FC) (OGD/Sham)**	**Control mean ± SEM**	**Glutamate mean ± SEM**	***p*-value**	**log_2(FC) (Glutamate/Control)**
C00095/C00031/ C00137/ C13747/C07480	4.821 ± 0.832	6.858 ± 1.994	0.3991	0.508	5.938 ± 1.436	13.417 ± 4.862	0.2000	1.176
C16361	0.617 ± 0.420	0.566 ± 0.304	0.9258	-0.125	0.492 ± 0.269	0.142 ± 0.031	0.2000	-1.791
C00319/C02934	0.538 ± 0.256	0.561 ± 0.112	0.9377	0.061	0.549 ± 0.143	0.667 ± 0.202	0.6857	0.282
C12144	14.176 ± 6.755	16.423 ± 0.446	0.7566	0.212	14.532 ± 3.062	11.267 ± 2.871	0.8857	-0.367
C00721	2.864 ± 0.662	4.991 ± 0.405	0.0518	0.802	2.299 ± 0.885	1.249 ± 0.397	0.3429	-0.881
C00695	0.091 ± 0.043	0.240 ± 0.115	0.2912	1.399	0.373 ± 0.112	0.232 ± 0.051	0.3429	-0.683
C01921	0.285 ± 0.057	0.519 ± 0.212	0.3455	0.866	0.345 ± 0.041	0.382 ± 0.108	0.6857	0.148

C00307	3.350 ± 0.813	6.393 ± 0.793	0.0552	0.932	3.611 ± 0.834	2.419 ± 1.008	0.2000	-0.578
C05465	0.179 ± 0.075	1.196 ± 0.375	0.0565	2.743	2.348 ± 0.522	0.793 ± 0.599	0.2000	-1.565
C05122	0.053 ± 0.023	0.101 ± 0.016	0.1614	0.927	0.134 ± 0.062	0.270 ± 0.155	0.4857	1.011
C01079	1.964 ± 0.287	1.982 ± 0.128	0.9579	0.013	1.655 ± 0.145	1.808 ± 0.238	0.6857	0.128
C05791	0.316 ± 0.105	0.291 ± 0.073	0.8540	-0.120	0.215 ± 0.043	0.245 ± 0.151	0.6857	0.189
C00486	0.232 ± 0.035	0.263 ± 0.039	0.5831	0.183	0.232 ± 0.023	0.177 ± 0.028	0.3429	-0.389
C00500	0.012 ± 0.000	0.002 ± 0.000	0.0014	-2.662	0.031 ± 0.030	0.007 ± 0.005	>0.9999	-2.222
C05770	1.103 ± 0.314	0.564 ± 0.101	0.1780	-0.968	1.179 ± 0.181	1.127 ± 0.294	0.8857	-0.065
C03263/C05768	0.713 ± 0.383	0.458 ± 0.118	0.5588	-0.639	0.234 ± 0.088	0.413 ± 0.257	>0.9999	0.818
C01051/C05766	0.007 ± 0.003	0.004 ± 0.002	0.4722	-0.862	0.030 ± 0.008	0.024 ± 0.012	0.8571	-0.291

8.2. Targeted Analysis

Supplementary Table 5. Metabolites identified and quantified in Sciex OS™ software for the targeted metabolomics analysis of the primary cultures of cerebrocortical neurons submitted to an OGD insult and a glutamate stimulus, with the respective precursor mass-to-charge ratio (*m/z*) used for identification, and fragment *m/z* used for quantification. The retention time (RT) used for identification and quantification is represented. M+Na: sodium adduct; FAD: flavin adenine dinucleotide.

Targeted analysis			
Metabolite	**Precursor *m/z***	**Fragment *m/z***	**RT (min)**
Norvaline	118.08626	72.0828	3.67
Nicotinamide	123.05529	80.0490	4.48
Pipecolic acid	130.08626	84.0823	1.82
Isoleucine/Leucine/Norleucine	132.10191	86.0991	4.65
Lysine	147.11280	84.0789	1.88
Citramalate	149.04445	133.0135	13.89
Cinnamic acid	149.05971	131.0496	5.86
Methionine	150.05833	56.0499	3.74
Phenylalanine	166.08626	120.0840	5.81
Tyrosine	182.08117	91.0557	4.23
Spermine	203.22302	84.0789	1.82
O-Acetylcarnitine	204.12303	85.0299	3.75
Tryptophan	205.09715	188.0698	7.51
N-Acetylphenylalanine	208.09682	120.0821	12.47
Thiamine	265.11176	122.0727	3.28
Adenosine	268.10403	137.0646	4.76
Methylthioadenosine	298.09684	136.0667	7.68
Glutathione reduced	308.09108	76.0205	3.76
Maltose/Sucrose, M+Na	365.10543	203.0533	2.78
Riboflavin	377.14556	243.0900	10.17
S-Adenosylhomocysteine	385.12887	136.0644	4.52
Folate	442.14696	295.0914	8.35
Glycochenodeoxycholate	450.32140	414.3043	24.05
Glycocholate	466.31631	412.2846	20.95
Hesperidin	611.19705	303.0862	13.86
β-Nicotinamide adenine dinucleotide	664.11640	428.0384	3.76
FAD	786.16441	348.0723	8.46

Supplementary Table 6. Metabolites identified and quantified in Sciex OS™ software for the targeted metabolomics analysis that showed no statistically significant differences after quantification. The data represented were obtained from two models of induced neuronal death based on oxygen and glucose deprivation (OGD) and glutamate excitotoxicity, with the respective controls for each model, performed on primary cultures of cerebrocortical neurons. For each model (OGD vs Sham and Glutamate vs Control), the data obtained after quantification in Sciex OS™ software (mean values of each group, *p*-value, and base-2 logarithm (log) of fold change (FC)) are represented. To compare the OGD and Sham groups was performed a Student's *t*-test and to compare the Glutamate and Control groups was performed a Mann-Whitney test. The FC is the ratio between the two group means. SEM: standard error of the mean.

Targeted analysis								
	OGD vs Sham				**Glutamate vs Control**			
Metabolite	**Sham mean ± SEM**	**OGD mean ± SEM**	***p*-value**	**log_2(FC) (OGD/Sham)**	**Control mean ± SEM**	**Glutamate mean ± SEM**	***p*-value**	**log_2(FC) (Glutamate/Control)**
Norvaline	1.442 ± 0.899	1.773 ± 0.060	0.7317	0.298	1.519 ± 0.275	1.464 ± 0.458	0.8857	-0.054
Nicotinamide	0.419 ± 0.182	0.447 ± 0.071	0.8937	0.092	0.463 ± 0.050	0.477 ± 0.083	0.8857	0.042
Pipecolic acid	0.246 ± 0.080	0.183 ± 0.076	0.6012	-0.425	0.222 ± 0.063	0.331 ± 0.100	0.4857	0.577
Isoleucine/Leucine/Norleucine	32.275 ± 9.294	31.512 ± 7.464	0.9520	-0.035	37.211 ± 5.827	59.136 ± 11.140	0.2000	0.668
Lysine	0.242 ± 0.080	0.180 ± 0.075	0.6039	-0.425	0.222 ± 0.061	0.325 ± 0.098	0.4857	0.554
Citramalate	0.200 ± 0.079	0.150 ± 0.028	0.5823	-0.416	0.124 ± 0.022	0.139 ± 0.015	0.6857	0.169
Cinnamic acid	0.044 ± 0.014	0.057 ± 0.014	0.5711	0.350	0.074 ± 0.014	0.067 ± 0.007	0.6857	-0.144
Methionine	0.776 ± 0.345	0.625 ± 0.136	0.7059	-0.311	0.795 ± 0.123	0.975 ± 0.164	0.3429	0.294

Phenylalanine	58.405 ± 15.933	64.196 ± 15.959	0.8100	0.136	78.333 ± 13.080	102.466 ± 15.786	0.4857	0.387
Tyrosine	0.862 ± 0.260	0.620 ± 0.210	0.5085	-0.476	0.882 ± 0.200	1.576 ± 0.477	0.4857	0.837
Spermine	0.006 ± 0.002	0.004 ± 0.001	0.4905	-0.594	0.007 ± 0.001	0.007 ± 0.002	0.8857	0.128
Tryptophan	98.852 ± 30.750	83.439 ± 20.776	0.6992	-0.245	106.394 ± 17.629	157.132 ± 25.213	0.3429	0.563
N-Acetylphenylalanine	0.109 ± 0.057	0.094 ± 0.024	0.8197	-0.215	0.112 ± 0.032	0.063 ± 0.025	0.2000	-0.828
Thiamine	6.698 ± 2.356	8.118 ± 3.941	0.7725	0.277	10.330 ± 2.667	18.206 ± 3.158	0.1143	0.818
Adenosine	0.049 ± 0.016	0.043 ± 0.012	0.7948	-0.173	0.043 ± 0.006	0.077 ± 0.021	0.2000	0.839
Methylthioadenosine	20.686 ± 7.037	18.014 ± 2.473	0.7383	-0.200	36.833 ± 8.897	9.509 ± 4.240	0.0571	-1.954
Glutathione reduced	0.018 ± 0.017	0.011 ± 0.009	0.7384	-0.751	0.009 ± 0.003	N/A	N/A	N/A
Riboflavin	0.236 ± 0.100	0.252 ± 0.107	0.9162	0.097	0.268 ± 0.084	0.441 ± 0.102	0.3429	0.720
S-Adenosylhomocysteine	0.122 ± 0.055	0.088 ± 0.036	0.6375	-0.460	0.186 ± 0.049	0.085 ± 0.020	0.0571	-1.124
Folate	13.290 ± 4.410	14.179 ± 6.062	0.9113	0.093	17.026 ± 4.529	32.597 ± 6.812	0.1143	0.937
Glycochenodeoxycholate	0.236 ± 0.086	0.267 ± 0.100	0.8257	0.178	0.447 ± 0.169	0.693 ± 0.163	0.2000	0.633
Glycocholate	0.579 ± 0.241	0.727 ± 0.301	0.7213	0.327	0.839 ± 0.235	1.548 ± 0.384	0.3429	0.883

Hesperidin	0.062 ± 0.025	0.070 ± 0.021	0.8391	0.157	0.060 ± 0.009	0.052 ± 0.002	>0.9999	-0.201